Transmit Waveform Design for Coexisting Radar and Communications Systems

by

John S. Kota

A Dissertation Presented in Partial Fulfillment
of the Requirements for the Degree
Doctor of Philosophy

Approved April 2016 by the
Graduate Supervisory Committee:

Antonia Papandreou-Suppappola, Chair
Visar Berisha
Daniel Bliss
Narayan Kovvali

ARIZONA STATE UNIVERSITY

May 2016

ABSTRACT

In recent years, there has been an increased interest in sharing available bandwidth to avoid spectrum congestion. With an ever-increasing number of wireless users, it is critical to develop signal processing based spectrum sharing algorithms to achieve cooperative use of the allocated spectrum among multiple systems in order to reduce interference between systems. This work studies the radar and communications systems coexistence problem using two main approaches. The first approach develops methodologies to increase radar target tracking performance under low signal-to-interference-plus-noise ratio (SINR) conditions due to the coexistence of strong communications interference. The second approach jointly optimizes the performance of both systems by co-designing a common transmit waveform.

When concentrating on improving radar tracking performance, a pulsed radar that is tracking a single target coexisting with high powered communications interference is considered. Although the Cramér-Rao lower bound (CRLB) on the covariance of an unbiased estimator of deterministic parameters provides a bound on the estimation mean squared error (MSE), there exists an SINR threshold at which estimator covariance rapidly deviates from the CRLB. After demonstrating that different radar waveforms experience different estimation SINR thresholds using the Barankin bound (BB), a new radar waveform design method is proposed based on predicting the waveform-dependent BB SINR threshold under low SINR operating conditions.

A novel method of predicting the SINR threshold value for maximum likelihood estimation (MLE) is proposed. A relationship is shown to exist between the formulation of the BB kernel and the probability of selecting sidelobes for the MLE. This relationship is demonstrated as an accurate means of threshold prediction for the radar target parameter estimation of frequency, time-delay and angle-of-arrival.

For the co-design radar and communications system problem, the use of a common

transmit waveform for a pulse-Doppler radar and a multiuser communications system is proposed. The signaling scheme for each system is selected from a class of waveforms with nonlinear phase function by optimizing the waveform parameters to minimize interference between the two systems and interference among communications users. Using multi-objective optimization, a trade-off in system performance is demonstrated when selecting waveforms that minimize both system interference and tracking MSE.

ACKNOWLEDGEMENTS

The work presented in this dissertation is the result from years of unyielding focus and dedication that was made possible through various sources of motivation and support. I would be remiss if I failed to acknowledge the individuals whom have been there for help and guidance when I needed it the most.

First, I would like to thank my advisor Prof. Antonia Papandreou-Suppappola who has provided mentoring, support, and guidance for both professional and personal purposes on an uncountable number of situations. Additional thanks goes to Prof. Daniel Bliss whose career advice, help, and mentoring goes far beyond what is required for a committee member. Thank you to Dr. Narayan Kovvali for providing helpful discussions and support for my research ideas throughout my years of study. Thank you to Prof. Visar Berisha for offering support and feedback.

My sincerest thanks to my mother, father, and sister. None of this would have been possible without their patience for understanding the challenges that I had to overcome as well as their motivation, guidance, emotional and financial support. I am forever grateful for their enduring help.

I would like to thank all of the members of the Signal Processing and Adaptive sensing laboratory for providing motivation and useful research discussions. Lastly, I would like to thank my weightlifting coach Giuseppe Micela and teammates at Performance One Advanced Sports Training who have given me numerous non-academic motivations that I have tried to utilize to aid both my research and work ethic in general.

This work was sponsored by the DARPA Shared Spectrum Access for Radar and Communications (SSPARC) program as well as the Ira A. Fulton and Peter E. Crouch Excellence fellowships.

TABLE OF CONTENTS

CHAPTER Page

CHAPTER Page

LIST OF FIGURES

Figure Page

Figure Page

Figure Page

Figure Page

Chapter 1

INTRODUCTION

1.1 Radar and Communications System Coexistence

Radar systems and wireless communications systems have different objectives, both for commercial and government use. However, due to spectrum congestion in some frequency bands, there is an increased interest in having multiple systems coexist and share available bandwidth [1, 2]. Both radar and communications systems currently occupy different regions of most of the available bandwidth below 4 GHz. For the two systems to share the same bandwidth, it is important to develop schemes to maximize the signal-to-interference-plus-noise-ratio (SINR) imposed on each system from the coexistence of the other system.

Recent studies in this area considered joint estimation bounds on the performance of radar and communications coexistence [3–6]. In [7], Guerci, et. al. presented a new theoretical foundation for radar and communications joint design and operation; the framework was based on advanced joint channel estimation and on an adaptive space-time transmit and receive optimization for maximizing forward channel SINR while minimizing co-channel interference. In [3, 5, 8, 9], the authors presented a method for a joint radar and communications system with signaling based on orthogonal frequency division multiplexing (OFDM). The idea of a joint radar and communications systems dates back to 1978 [10] and since then, it is used as an approach for spectrum sharing applications [6, 9, 11–27]. Because of the high throughput of OFDM and current wireless communications designs, the authors in [28] considered a joint system that employed OFDM for the communications system and linear frequency-

Figure 1.1: An Illustration of a Practical Joint Radar and Communications Environment.

modulated (LFM) signaling for the radar and utilizes the fractional Fourier transform for spectrum sharing. In addition to a joint radar and communications system that is based on OFDM, the use of LFMs was also considered in [29–31]. However, these studies did not extend their results to a multi-user communications system, and the model for the radar is not very practical in terms of current systems.

1.2 Radar Waveform Design for High Communications Interference

A general joint spectral environment, with coexisting radar and communications systems, is illustrated in Figure 1.1. Until recently, the two systems are allocated unique spectral bands, and the systems designers consider the physical constraints on the system that are affected by the allocated band. For example, wireless communications systems design the antenna physical size since the size should be smaller as frequency increases [32, 33]. As another example, radar systems design the carrier modulation frequency of the high powered transmit signal since it affects the received target return [34, 35].

Due to the increased demand on the finite amount of spectrum as well as the physical constraints required to stay within a specific spectrum band, systems are now faced with the problem of spectrum congestion. As a result it has become necessary for different systems to consider novel signal processing methods that allow for both systems to occupy the same frequency band [3–9, 11–20, 26–31, 36–43]. One approach toward system coexistence is to develop methodologies to increase radar

target tracking performance under low SINR conditions, when the low SINR is due to the presence of strong communications signals. From the perspective of a radar system, the communications system can be modeled as a random process whose power needs to be reduced at the radar receiver. This approach has been recently considered in [3, 7, 36, 37]. When considering the communications signals as interference for the radar system, it is important to examine performance bounds on the mean squared error (MSE) for estimating unknown target parameters in low SINR. Information on the bounds could lead to methods for predicting and benchmarking system performance for a variety of practical problems such as the estimation of Doppler shifts, time-delays, and angles of arrival.

The Cramér-Rao lower bound (CRLB) provides a lower bound on the MSE performance of unbiased estimators of deterministic parameters [44]. It is a commonly used bound for high SINR, especially since it is simple to compute assuming that the probability density functions (pdfs) involved in the computation do not violate the assumed regularity conditions [44, 45]. For example, the maximum likelihood estimator (MLE) attains the CRLB when the SINR is high or when large data records are available. However, in many nonlinear estimation problems, the MLE can rapidly deviate from the CRLB below a unique SINR value. The MSE region where this deviation is observed is called the SINR threshold region and is associated with side-lobes of the likelihood function exceeding the main-lobe with very high probabilities [33, 45–51]. Note that the CRLB only considers local main-lobe error and does not provide any information about SINR threshold prediction. One possible method for predicting the SINR threshold is the method of interval errors (MIE) [33, 47–50, 52, 53], however it is algorithm/problem dependent and does not always have a simple formulation.

The Barankin bound (BB) was originally formulated in [54] in order to obtain a tighter bound on estimator MSE performance. In [55], P. Swerling was the first

ever to apply the BB [54] to engineering problems. The BB has been applied to many statistical signal processing problems using approximations of the theoretical formulation is that very difficult to implement [56–60].

The various approximations used to compute the BB [46, 56, 58, 61–63] have improved algorithm efficiency in the number of test points required to obtain computationally tractable methods for practical applications. Most approximations for the BB ultimately end up in the form of a Euclidean norm minimization over a finite set of equality constraints for mean unbiasedness [51, 64, 65]. However, extreme care needs to be taken in the selection of these test points [66]. The general challenge experienced amongst researchers who work with the BB for signal processing applications is largely focused on test-point selection and the numerical challenges associated with the bound [51, 67, 68]. Although for many signal processing related estimation problems there exist methods for intelligent test-point selection, such as considering peak side-lobe locations [66, 69], there does not exist a robust method for two-dimensional measurement models such as the ambiguity function. Note, however, that since the BB provides a tighter bound on the MSE estimation, it is promising as a tool for SINR threshold prediction.

1.3 Co-design of Radar and Communications Signaling Schemes

Many joint radar and communications systems addressed the spectrum congestion problem through cooperative means [6, 9, 11–27]. Another approach that can be considered for non-cooperative radar and communications systems is the design for both systems in order to jointly reduce the interference of the two systems with the assumption that information can be shared between the two systems. In [29–31], the authors proposed the use of the LFM for a single user communications system and a pulsed radar. However, they do not consider the case of multiple communications

users. In [3, 5, 8, 9], the authors propose the use of OFDM as a joint radar and communications signaling scheme. However, the cyclostationary properties of OFDM manifest into poor ambiguity function characteristics and do not inherently possess properties that are desired for a transmit radar waveform. The OFDM signaling scheme also suffers from high peak to average power ratio [33].

1.4 Work Contributions

Although many contributions have been made toward spectrum coexistence for radar and communications systems, it still remains a challenging problem. To this end, we propose two main approaches. The first approach focuses on designing radar waveforms for low SINR conditions to improve target tracking performance. The second approach develops a common signaling scheme for both radar and communications systems and considers a multi-objective optimization scheme to trade-off between the performance of the two systems.

1.4.1 SINR Threshold Prediction via Kernel Effective Rank

We develop a novel approach to compute the SINR threshold value for deterministic parameter estimation via the effective rank of the BB kernel. We demonstrate that there exist a relationship between the singular value decomposition of the BB kernel as function of SINR and the probability of side-lobe selection for the MLE. The flexibility and usefulness of this approach for estimating Doppler shift, time-delay, and angle of arrival of a target is demonstrated and compared to other common methods for SINR threshold prediction.

A numerical method is proposed for predicting the MLE SINR threshold by utilizing the inherent relationship between outlier probability and effective rank of the BB kernel. The proposed method is useful for computing the SINR threshold rather

than computing a tighter MSE performance bound. Using the proposed approach there is no need for problem specific test-point selection or complicated probability computations. It is shown that using the effective rank of the BB kernel provides a very accurate prediction and can be considered as a tool for engineers when analyzing system and algorithm benchmark performance.

1.4.2 Radar Waveform Design Using Barankin Bound Predicted SINR Threshold

Under low SINR conditions, the estimation accuracy of an efficient estimator of deterministic parameters, such as the MLE suddenly decreases. In particular, past an SINR threshold value, the estimator covariance rapidly deviates from the CRLB. Knowing when this threshold region occurs can be very useful in selecting transmit waveforms for optimum system performances [70, 71], as it can provide insight into the system's estimation accuracy. An estimate of the SINR threshold value can be obtained using the BB [54, 72–76]. As such, the BB has been used in various applications to estimate time-delay, Doppler frequency, and direction of arrival [73, 77–80].

In this thesis, we propose a waveform design method for low SINR tracking scenarios with an overall objective to improve target tracking performance. We achieve our objective by adaptively selecting SINR threshold regions using the BB. Note that the BB threshold analysis was performed in [71] for a track-before-detect tracking problem by approximating the measurement model using Gaussian point spread functions. We obtain a tighter bound by using instead the BB approximation in [61] for the ambiguity function resolution cell measurement model. Using a dictionary of waveforms with nonlinear time-varying phase functions and varying parameters, we compute the deviation of the BB from the CRLB as a function of the signal parameters. We select the optimal signal for transmission by minimizing the bound deviation. The proposed

waveform selection algorithm is integrated with a track-before-detect tracker for low SINR scenarios. We demonstrate the proposed algorithm by adaptively designing the radar waveform at every transmission in order to minimize the adverse interactions between coexisting radar and communications systems in the S band, ranging from 2 to 4 GHz.

1.4.3 Joint Radar and Communications Waveform Co-Design

We propose the use of a common transmit LFM waveform with amplitude modulation and optimized parameters in a co-design signaling scheme to be jointly used by a ground based pulse-Doppler radar and a multi-user communications system. The signal scheme is designed to reduce interference between the radar and communications systems as well as interference between the multiple users. We demonstrate the feasibility of this signaling design to achieve desirable performance for both systems. We examine the trade-offs in performance for both systems and propose the use of a multi-objective (Pareto) optimization to select radar transmit waveforms that jointly minimize radar MSE performance and interference between the two systems. The proposed scheme first designs the duration of the communications users transmit signal to satisfy some desired gross bit rate and using the bandwidth allocation to both systems. Once the duration is selected, we optimize the LFM rate parameter for each user to minimize multiple access interference (MAI). This is achieved by selecting the LFM parameters such that the user transmit waveforms are approximately orthogonal to each other over their symbol duration, assuming that the users are temporally synchronized.

When not all possible users occupy the given spectrum, we further optimize the LFM rates of the current users by finding the rate combination that minimizes MAI. As the search for the best combination becomes very computationally intensive as the

number of users increase, we use simulated annealing to reduce the computational cost. Once the communications signals are designed, information on the LFM rates and duration are made available to the radar system. Using this information, the radar transmit waveform is selected using multi-objective optimization.

1.5 Thesis Organization

The rest of this thesis is organized as follows. In Chapter 2, we summarize the mathematical framework needed for this work on MSE performance bounds and target tracking under low SINR conditions. In Chapter 3, we investigate the numerical challenges associated with computing the BB in practice and propose the use of singular value decomposition to exploit the effective rank of the BB kernel matrix to predict the SINR threshold. In Chapter 4, we propose a radar transmit waveform design approach that is based on predicting the SINR threshold by optimizing the deviation of the BB from the CRLB for multiple waveforms with varying parameters and nonlinear phase function. In Chapter 5, we propose a co-design signaling scheme for a pulse-Doppler radar and a multiuser communications system. The design selects LFM waveform parameters using a multi-objective optimization that minimizes both the radar MSE performance and the interference between the two systems.

Chapter 2

RADAR AND COMMUNICATIONS COEXISTENCE PROBLEM

2.1 Radar and Communications Systems Spectrum Sharing

In general, different systems, such as radar and wireless communications with entirely different goals of operation may be required to share the same allocated spectrum. The goal of a communications system is to transmit some information and process the noisy received signal to extract the information. As the channel can distort the signal, causing changes such as amplitude fading or multipath delay, the system needs to estimate the transmitted information using any prior channel knowledge [32]. A radar system, however, has a different goal. The radar receiver needs to process the received signal to estimate the effects of the channel in order to extract information on the target from the reflected signal [21, 34, 81]. Despite the difference in their goals, this work considers the problem of radar and wireless communications systems coexisting by sharing the same bandwidth to avoid spectrum congestion and interference [1, 2].

The coexistence of the two systems over a common bandwidth of B_a Hz is demonstrated in Figure 2.1 both for the baseband and passband transmission with a carrier frequency of f_c Hz. Assuming a co-located receiver for both systems, the received signal can be given by

$$z(t) = x_r(t) + x_c(t) + w(t) \tag{2.1}$$

where $x_r(t)$ is due to the radar and $x_c(t)$ is due to the communications. The term $w(t)$ is additive white Gaussian noise (AWGN) due to electrical thermal noise with

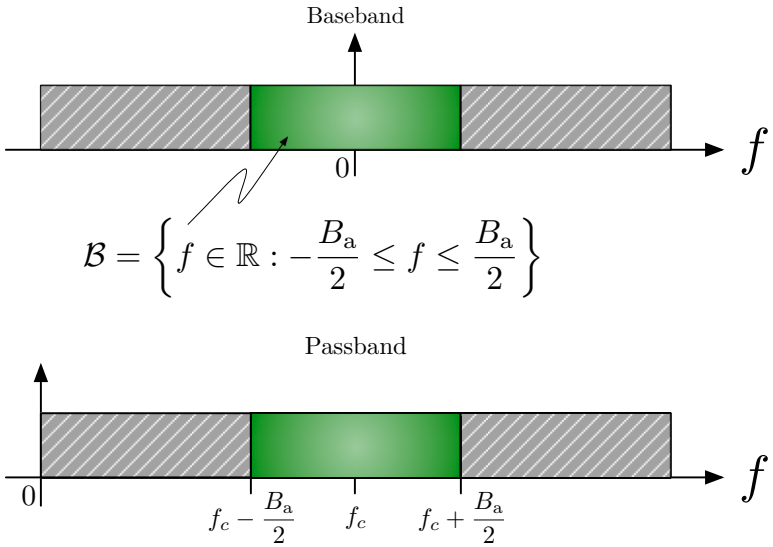

Figure 2.1: Baseband and Passband Illustration of a Radar System and a Communications System Sharing the Same Spectrum.

associated power [33, 34]

$$\sigma_w^2 = k_B T_{\text{eff}} B_a$$

where $k_B = 1.3806488 \times 10^{-23}$ (J/K), T_{eff} is the effective temperature in the electronics system in Kelvin (K) units, and B_a is the available bandwidth in Hertz. The measurement $z(t)$ is assumed to be present at both the communications and radar receivers.

For a single point target, the narrowband radar channel that results in the signal $x_r(t)$ in (2.1) can be described as a linear time-invariant (LTI) system with impulse response [34, 35, 81]

$$h_r(t) = \sqrt{P_\mathrm{r}}\delta(t - \tau_0)e^{-j2\pi\nu_0 t}$$

where τ_0 and ν_0 are the time-delay and frequency shift caused by the reflection of the transmitted radar signal off of the target and P_r is the radar return power [34]. Using the time delay $\tau_0 = 2r_0/c_{\epsilon_0}$, we can obtain the range r_0 of the target from the radar, where $c_{\epsilon_0} = 3 \times 10^8$ m/s is the wave velocity for electromagnetic propagation in free

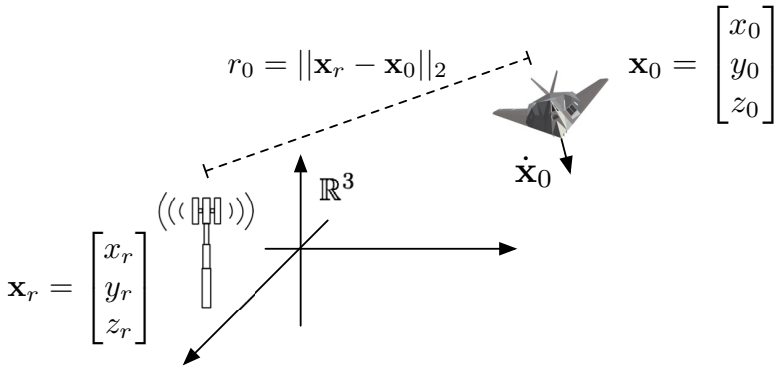

Figure 2.2: Visualization for Modeling Range and Range Rate of a Target with a Ground Based Radar.

space (the speed of light) [33, 34, 81]. The frequency shift $\nu_0 = 2f_c\dot{r}_0/c_{\epsilon_0}$ occurs by nature of the Doppler effect from the motion of the target and it can be utilized to obtain the range rate $\dot{r}_0$ of the target.

As demonstrated in Figure 2.2, we assume that a target is located at the three-dimensional (3-D) Cartesian coordinate (x_0, y_0, z_0) and the location is given by the vector $\mathbf{x}_0 = [x_0\ y_0\ z_0]^T \in \mathbb{R}^3$. We also assume that the target moves at a velocity $\dot{\mathbf{x}}_0 = [\dot{x}_0\ \dot{y}_0\ \dot{z}_0]^T \in \mathbb{R}^3$ where $(\dot{x}_0, \dot{y}_0, \dot{z}_0)$ is the three dimensional Cartesian coordinate of the target velocity. A stationary ground based radar, located at $\mathbf{x}_r = [x_r\ y_r\ z_r]^T \in \mathbb{R}^3$ is used to observe the radar return and to estimate the target's range and range rate which are given by

$$\begin{aligned} r_0 &= ||\mathbf{x}_r - \mathbf{x}_0||_2 \\ \dot{r}_0 &= \frac{\dot{\mathbf{x}}_0^T (\mathbf{x}_r - \mathbf{x}_0)}{||\mathbf{x}_r - \mathbf{x}_0||_2}. \end{aligned} \tag{2.2}$$

Here $\mathbf{x}^T$ denotes vector transpose of the vector $\mathbf{x}$ and $||\mathbf{x}_0||_2^2 = \mathbf{x}_0^T\mathbf{x}_0 = x_0^2 + y_0^2 + z_0^2$ is the Euclidean norm.

The radar return power is given by the radar equation for the monostatic case as [34, 35]

$$P_{\mathrm{r}} = \frac{P_{\mathrm{rt}} G_{\mathrm{rad}}^2 \lambda^2 \sigma_{\mathrm{RCS}}}{64\pi^3 r_0^4}$$

where P_{rt} is the radar transmit power in Watts, G_{rad} is the radar antenna gain, $\lambda = c_{\epsilon_0}/f_c$ is the wavelength of the radar signal, r_0 is the range from the target to the radar from (2.2), and σ_{RCS} is the radar cross section (RCS).

Assuming a frequency selective channel, the communications received signal $x_c(t)$ in (2.1) can be represented as the output of an LTI system with impulse response [32, 33]

$$h_c(t) = \sqrt{P_c} \sum_{l=0}^{L_p-1} \alpha_l \delta(t - \tau_l).$$

Here, we assume L_p multipath components τ_l with corresponding fading coefficients α_l and P_c represents the communications received signal power given by [32, 33]

$$P_c = \frac{P_{\text{ct}} G_{\text{ct}} G_{\text{cr}} \lambda^2}{16\pi^2 r_c^2}$$

where P_{ct} is the transmitter power, G_{ct} and G_{cr} are the transmitter and receiver antenna gains, and r_c is the range from the communications transmitter to the receiver.

2.2 Estimation Bounds of Unknown Deterministic Parameters

2.2.1 Estimation Mean Squared Error and Maximum Likelihood

A deterministic parameter estimation problem involves the estimation of the n_p-dimensional unknown parameter vector $\boldsymbol{\theta}^{(0)} = [\theta_1^{(0)} \ \ldots \ \theta_{n_p}^{(0)}]^T \in \boldsymbol{\Theta}$ where $\boldsymbol{\Theta} \subseteq \mathbb{R}^{n_p}$ is the parameter space and we are given an N_s-dimensional noisy discrete-time observation written as the vector $\mathbf{z} = [z[1] \ \ldots \ z[N_s]]^T \in \mathcal{Z}$, where $\mathcal{Z}$ is the observation space [44]. The observation vector can consist of a signal in AWGN that depends on the parameters

$$\mathbf{z} = \mathbf{s}(\boldsymbol{\theta}^{(0)}) + \mathbf{w} \tag{2.3}$$

where $\mathbf{s}(\boldsymbol{\theta}^{(0)}) = [s[1; \boldsymbol{\theta}^{(0)}] \ \ldots \ s[N_s; \boldsymbol{\theta}^{(0)}]]^T$ and $\mathbf{w} = [w[1] \ \ldots \ w[N_s]]^T$ is a random noise vector that is often assumed to have a normal probability density function [44].

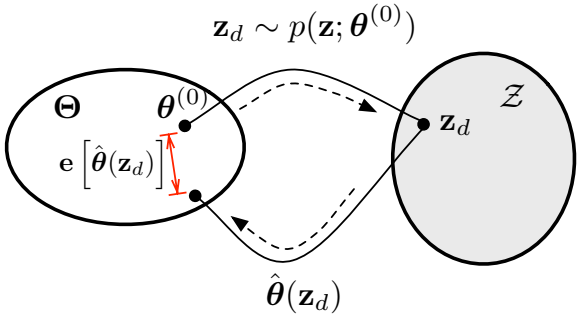

Figure 2.3: Conceptual View of Random Measurements Being Mapped into Observation Space $\mathcal{Z}$ and an Estimator Mapping an Estimate of the True Parameter $\theta^{(0)}$ Back into a Point in the Parameter Space $\boldsymbol{\Theta}$. The Error is the Deviation that the Estimate Has From the True Parameter.

Regardless of the complexity of the observation, we want to estimate the unknown parameters as close to their true values as possible using an optimal and efficient approach. The estimated parameter $\hat{\boldsymbol{\theta}}(\mathbf{z})$ depends on the observation vector $\mathbf{z}$.

Conceptually shown in Figure 2.3 we can see that a draw $\mathbf{z}_d$ from the likelihood function $p(\mathbf{z};\boldsymbol{\theta}^{(0)})$ that characterizes the statistics of the measurement takes us from the parameter space into the observation space. An estimator, $\hat{\boldsymbol{\theta}}(\mathbf{z}_d)$ utilizing this measurement takes us back to observation space, usually to a different location but hopefully close to the true parameter $\boldsymbol{\theta}^{(0)}$. The deviation between the estimate and the true parameter is the error $\mathbf{e}[\hat{\boldsymbol{\theta}}(\mathbf{z}_d)]$ which is a function of the estimator. It is particularly useful to have as small of an error as possible and as such we typically have ways to analyze the error of an estimator so that we can judiciously choose the best one for a given problem. We will be discussing these methods of analysis in the following sections in this chapter.

The mean squared error (MSE) of a parameter estimation can be defined as

$$\begin{aligned}\mathbf{MSE}_{\boldsymbol{\theta}^0}(\hat{\boldsymbol{\theta}}(\mathbf{z})) &= E_{\mathbf{z};\boldsymbol{\theta}^{(0)}}\left\{||\mathbf{e}[\hat{\boldsymbol{\theta}}(\mathbf{z})]||_2^2\right\} \\ &= \int_{\mathbb{R}^{n_z}} \mathbf{e}^T[\hat{\boldsymbol{\theta}}(\mathbf{z})]\mathbf{e}[\hat{\boldsymbol{\theta}}(\mathbf{z})]p(\mathbf{z};\boldsymbol{\theta}^{(0)})d\mathbf{z}. \end{aligned} \tag{2.4}$$

where $\mathbf{e}[\hat{\boldsymbol{\theta}}(\mathbf{z})] = \hat{\boldsymbol{\theta}}(\mathbf{z}) - \boldsymbol{\theta}^{(0)}$ and $p(\mathbf{z};\boldsymbol{\theta}^{(0)})$ is the likelihood function [44].

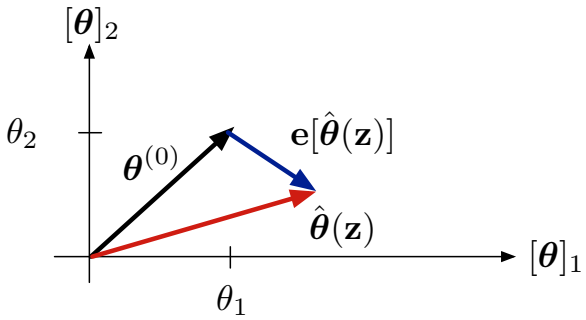

Figure 2.4: Geometric Interpretation of a 2-D Parameter Vector $\boldsymbol{\theta} = [\theta_1 \ \theta_2]^T$ In Terms of its Estimate $\hat{\boldsymbol{\theta}}(\mathbf{z})$, True Value and Error.

The estimator, the true parameter vector, and the error have the geometric interpretation shown in Figure 2.4 for when $\boldsymbol{\theta} \in \mathbb{R}^2$.

The bias of an estimator is defined as [44]

$$\mathbf{b}_{\hat{\boldsymbol{\theta}}(\mathbf{z})} = E_{\mathbf{z};\boldsymbol{\theta}}\left\{\hat{\boldsymbol{\theta}}(\mathbf{z})\right\} - \boldsymbol{\theta}, \ \forall \boldsymbol{\theta} \in \boldsymbol{\Theta}$$

where $E_{\mathbf{z};\boldsymbol{\theta}}\{\cdot\}$ denotes statistical expectation with respect to the likelihood function $p(\mathbf{z};\boldsymbol{\theta})$ [44, 82].

Mean unbiasedness relates the covariance $\boldsymbol{\Sigma}_{\hat{\boldsymbol{\theta}}(\mathbf{z})}$ of an estimator with its MSE as

$$\mathrm{tr}\left\{\mathbf{MSE}_{\boldsymbol{\theta}^0}(\hat{\boldsymbol{\theta}}(\mathbf{z}))\right\} = \mathrm{tr}\left\{\boldsymbol{\Sigma}_{\hat{\boldsymbol{\theta}}(\mathbf{z})}\right\} + ||\mathbf{b}_{\hat{\boldsymbol{\theta}}(\mathbf{z})}||_2^2 \tag{2.5}$$

where if an estimator is unbiased, then its covariance is equal to the MSE. The notation $\mathrm{tr}\{\mathbf{M}\}$ is the trace of the matrix $\mathbf{M}$ which is the sum of the diagonal elements of $\mathbf{M}$. The covariance matrix is computed as

$$\boldsymbol{\Sigma}_{\hat{\boldsymbol{\theta}}(\mathbf{z})} = \int_{\mathbb{R}^{n_z}} \left(\hat{\boldsymbol{\theta}}(\mathbf{z}) - E_{\mathbf{z};\boldsymbol{\theta}}\left\{\hat{\boldsymbol{\theta}}(\mathbf{z})\right\}\right)\left(\hat{\boldsymbol{\theta}}(\mathbf{z}) - E_{\mathbf{z};\boldsymbol{\theta}}\left\{\hat{\boldsymbol{\theta}}(\mathbf{z})\right\}\right)^T p(\mathbf{z};\boldsymbol{\theta})d\mathbf{z} \tag{2.6}$$

From the covariance (2.6) and the relationship in (2.5), an unbiased estimator satisfies

$$E_{\mathbf{z};\boldsymbol{\theta}}\left\{\hat{\boldsymbol{\theta}}(\mathbf{z})\right\} = \boldsymbol{\theta}, \ \forall \boldsymbol{\theta} \in \boldsymbol{\Theta}.$$

For the case of minimum MSE estimation, mean unbiasedness of an estimator is one possible constraint that can be introduced to avoid trivial estimators that

wholly make no sense, viz. consider the estimator $\hat{\theta}(\mathbf{z}) = \theta^{(0)}$ that would result from unconstrained MMSE optimization. In general, mean unbiasedness is part of a general family of expressions of biasedness, known as Lehmann bias [82] which defines bias in terms of the classical cost functions such as hit-or-miss error, absolute error, squared error, and periodic error.

In many applications, the observation vector in (2.3) can be given as a linear model. Specifically,

$$\mathbf{z} = \mathbf{S}\boldsymbol{\theta}^{(0)} + \mathbf{w} \tag{2.7}$$

where $\mathbf{S} \in \mathbb{R}^{n_z \times n_p}$ is a known deterministic, full rank channel matrix and $\mathbf{w}$ can be assumed to be Gaussian with zero mean vector and covariance matrix $\boldsymbol{\Sigma} = \sigma_w \mathbf{I}_{N_s}$ that we can write as $\mathbf{w} \sim \mathcal{N}(\mathbf{0}_{n_z}, \sigma_w^2 \mathbf{I}_{n_z})$. Here, we can compute the likelihood function

$$p(\mathbf{z}; \boldsymbol{\theta}) \propto \exp\left[-\frac{1}{2\sigma_w^2}||\mathbf{z} - \mathbf{S}\boldsymbol{\theta}||_2^2\right].$$

Under the assumption of a high signal-to-interference-plus-noise ratio (SINR) or large data records, the maximum likelihood estimate (MLE) can used to provide efficient estimates of the parameters of interest. The MLE can be computed by maximizing the gradient of the likelihood, or equivalently the log-likelihood function. Performing this calculation for the linear model, we obtain

$$\hat{\boldsymbol{\theta}}_{\mathrm{ML}}(\mathbf{z}) = \left(\mathbf{S}^T\mathbf{S}\right)^{-1}\mathbf{S}^T\mathbf{z}. \tag{2.8}$$

The MLE can be shown to be unbiased since

$$E_{\mathbf{z};\boldsymbol{\theta}}\left\{\left(\mathbf{S}^T\mathbf{S}\right)^{-1}\mathbf{S}^T\mathbf{z}\right\} = \boldsymbol{\theta},\ \forall\boldsymbol{\theta} \in \boldsymbol{\Theta}$$

The MSE can be found to be

$$\mathbf{MSE}_{\boldsymbol{\theta}^0}(\hat{\boldsymbol{\theta}}(\mathbf{z})) = \sigma_w^2\left(\mathbf{S}^T\mathbf{S}\right)^{-1}. \tag{2.9}$$

In this case, the MSE is equivalent to the covariance of the MLE since it is an unbiased estimator.

2.2.2 Estimator Mean Squared Error Bounds

An estimator's performance lower bound is a mathematical inequality that can be derived to provide a limit on the performance in terms of estimator MSE. For a given estimator, the bound can then be used to evaluate the estimator's performance; if the bound is not met then the estimator's MSE is worse than the bound.

For MSE bound analysis, we consider the observation space $\mathcal{Z}$ and the parameter space $\mathbb{R}^{n_p}$ to define the Hilbert space $H_{\mathbf{z};\theta}$. For scalar parameters, this Hilbert space is a vector space with inner product [45, 67, 83, 84]

$$\left\langle g, h \right\rangle_{H_{\mathbf{z};\theta}} = \int_{\mathcal{Z}} g(\mathbf{z}) h(\mathbf{z}) p(\mathbf{z};\theta) d\mathbf{z}$$

where $g(\mathbf{z})$ and $f(\mathbf{z})$ are scalar functions of the observation vector $\mathbf{z}$ in $H_{\mathbf{z};\theta}$, and induced norm given by

$$||g||^2_{H_{\mathbf{z};\theta}} = \langle g, g \rangle_{H_{\mathbf{z};\theta}} = E_{\mathbf{z};\boldsymbol{\theta}} \left\{ g^2 \right\}.$$

Note that for $n_p \geq 1$, the general Hilbert space $H_{\mathbf{z};\theta} \times \cdots \times H_{\mathbf{z};\theta}$ is the product of n_p Hilbert spaces. Using this norm definition, the MSE for estimating the scalar deterministic parameter $\theta^{(0)}$ is given by

$$\mathrm{MSE}_{\boldsymbol{\theta}^0}(\hat{\boldsymbol{\theta}}(\mathbf{z})) = \left|\left|\hat{\theta}(\mathbf{z}) - \theta^{(0)}\right|\right|^2_{H_{\mathbf{z};\theta^{(0)}}}.$$

which is sometimes referred to as the second-order absolute central moment (SACM) at $\theta^{(0)}$ [54]. In this sense, by stating that the estimator error $e[\hat{\theta}(\mathbf{z})] \in H_{\mathbf{z};\theta}$ means that

$$\left|\left|e[\hat{\theta}(\mathbf{z})]\right|\right|^2_{H_{\mathbf{z};\theta}} < \infty$$

and hence this Hilbert space only concerns ourselves with estimators that are convergent in the MSE sense or all functions of the measurements having finite SACMs

with respect to the true likelihood function. We can also state that $\hat{\theta}(\mathbf{z}) \in H_{\mathbf{z};\theta^0}$ since finite affine translations of an estimator do not influence its convergence in the Hilbert space [45, 67, 83, 84].

If $H(K)$ is another Hilbert space, that is a proper Hilbert subspace of $H_{\mathbf{z};\theta}$, then the projection of the error vector onto $H(K)$ provides a geometric interpretation of an estimator's performance bound [45, 67, 83, 85, 86]. The norm of this projection provides a lower bound on the MSE for an estimator, as geometrically interpreted in Figure 2.5. Specifically, for some vector $\mathbf{v}(\mathbf{z}) \in H(K)$, the lower bound on the MSE lower bound on the MSE is given by [45, 67, 83, 84]

$$\mathbf{MSE}_{\boldsymbol{\theta}^0}(\hat{\boldsymbol{\theta}}(\mathbf{z})) \succeq \left|\left|\text{proj}_{\mathbf{v}(\mathbf{z})}\mathbf{e}[\hat{\boldsymbol{\theta}}(\mathbf{z})]\right|\right|^2_{H_{\mathbf{z};\theta^{(0)}}\times\cdots\times H_{\mathbf{z};\theta^{(0)}}} \tag{2.10}$$

where $\text{proj}_{\mathbf{v}(\mathbf{z})}\mathbf{e}[\hat{\boldsymbol{\theta}}(\mathbf{z})]$ denotes the projection of the error vector for some $\mathbf{v}(\mathbf{z})$. It should be noted that by changing $\mathbf{v}(\mathbf{z})$ that different bounds on the MSE can be computed. In particular, any such bound can be represented in terms of the norm of the projection in a linear transformed subspace for all vectors $\mathbf{v}(\mathbf{z})$. Typically these linear transformations are of the form of derivatives and/or sampling operators and can be expressed as integral operators. This type of analysis was first introduced by Emanuel Parzen in [85], was then further elucidated by Duttweiler et. al. in the series of articles published under similar titles to [87] and most recently revitalized by the couple of papers produced by Todros and Tabrikian in [45, 67, 83, 84].

The notation $\mathbf{A} \succeq \mathbf{B}$ in (2.10) is the Loewner partial ordering of matrices $\mathbf{A}, \mathbf{B} \in \mathbb{S}^{n_p}_{++}$ such that $\mathbf{A}-\mathbf{B}$ is a symmetric positive semidefinite matrix. This ordering states that the size of the eigenstructure (spectral radius) of the estimator's MSE matrix is either larger than or equal to the squared norm matrix.

The Hilbert space $H(K)$ is a reproducing Kernel Hilbert space (RKHS) [45, 67, 83–

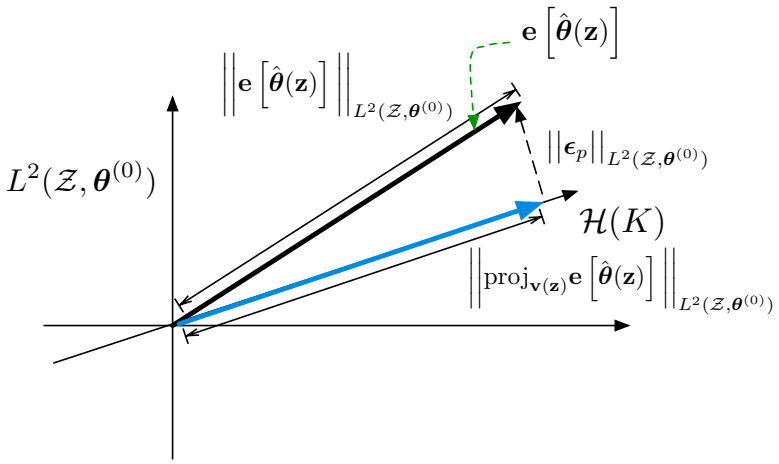

Figure 2.5: Geometric View for Estimator MSE Performance Bounds. A Bound on the MSE Can be Expressed as the Norm of a Projection from $H_{\mathbf{z};\theta}$ onto Vectors $\mathbf{v}(\mathbf{z}) \in H(K)$.

85]. Specifically, if we define the likelihood function ratio (LFR) [54]

$$\pi_{\boldsymbol{\theta}} = \frac{p(\mathbf{z};\boldsymbol{\theta})}{p(\mathbf{z};\boldsymbol{\theta}^{(0)})} \in H(K)$$

then we can define the unique reproducing kernel as

$$K(\boldsymbol{\theta},\boldsymbol{\theta}') = E_{\mathbf{z};\boldsymbol{\theta}^{(0)}}\left\{\pi_{\boldsymbol{\theta}}\pi_{\boldsymbol{\theta}'}\right\} \tag{2.11}$$

$$= \langle \pi_{\boldsymbol{\theta}}, \pi_{\boldsymbol{\theta}'} \rangle_{H_{\mathbf{z};\theta 0}} \tag{2.12}$$

that is symmetric and non-negative [85]. An RKHS is a unique Hilbert space with unique reproducing kernel provided that the following two properties hold [85–87]

$$K(\boldsymbol{\theta},\boldsymbol{\theta}') \in H(K),\ \forall \boldsymbol{\theta}' \in \boldsymbol{\Theta} \tag{2.13}$$

$$\langle \boldsymbol{\alpha}(\boldsymbol{\theta}'), K(\boldsymbol{\theta},\boldsymbol{\theta}') \rangle_{H(K)} = \boldsymbol{\alpha}(\boldsymbol{\theta}),\ \forall \boldsymbol{\theta} \in \boldsymbol{\Theta},\ \forall \boldsymbol{\alpha}(\boldsymbol{\theta}) \in H(K) \tag{2.14}$$

where the second line is known as the reproducing property.

In order to demonstrate that a projection provides a lower bound on the MSE for an unbiased estimator or equivalently, to demonstrate the inequality [45, 67, 83–85]

$$||\mathbf{e}[\hat{\boldsymbol{\theta}}(\mathbf{z})]||^2_{H_{\mathbf{z};\theta}} \geq \left|\left|\text{proj}_{\mathbf{v}(\mathbf{z})}\mathbf{e}[\hat{\boldsymbol{\theta}}(\mathbf{z})]\right|\right|^2_{H_{\mathbf{z};\theta}} \tag{2.15}$$

we first use the LFR $\pi_{\boldsymbol{\theta}}$ to represent the definition of unbiasedness in terms of the true likelihood function as

$$\int_{\mathcal{Z}} \hat{\boldsymbol{\theta}}(\mathbf{z}) \pi_{\boldsymbol{\theta}} p(\mathbf{z}; \boldsymbol{\theta}^{(0)}) d\mathbf{z} = \boldsymbol{\theta}, \ \boldsymbol{\theta} \in \boldsymbol{\Theta}. \tag{2.16}$$

Using (2.16) and the linearity property of integration, it can be shown that

$$\int_{\mathcal{Z}} \left(\hat{\boldsymbol{\theta}}(\mathbf{z}) - \boldsymbol{\theta}^{(0)} \right) \pi_{\boldsymbol{\theta}} p(\mathbf{z}; \boldsymbol{\theta}^{(0)}) d\mathbf{z} = \boldsymbol{\theta} - \boldsymbol{\theta}^{(0)}$$

for $\boldsymbol{\theta} \in \boldsymbol{\Theta}$. If the vector $\mathbf{v}(\mathbf{z})$ in the RKHS is defined as the linear combination

$$\mathbf{v}(\mathbf{z}) = \int_{\boldsymbol{\Theta}} \boldsymbol{\alpha}(\boldsymbol{\theta}) \pi_{\boldsymbol{\theta}} d\boldsymbol{\theta} \in H(K) \tag{2.17}$$

for some coefficients $\boldsymbol{\alpha}(\boldsymbol{\theta})$, then $\mathbf{v}(\mathbf{z})$ can be used in the derivation of general bounds for unbiased deterministic parameter estimators at the true parameter $\boldsymbol{\theta}^{(0)}$. We also note that the projection of the error onto the RKHS $H(K)$ is estimator independent. This is demonstrated by applying the Hilbert projection theorem [45, 67, 83–86] which says that there exists a unique $\mathbf{v}(\mathbf{z}) \in H(K)$ such that

$$\text{proj}_{\mathbf{v}(\mathbf{z})} \mathbf{e}[\hat{\boldsymbol{\theta}}(\mathbf{z})] = \arg \min_{\mathbf{v}(\mathbf{z}) \in H(K)} \left\{ \left|\left| \mathbf{e}[\hat{\boldsymbol{\theta}}(\mathbf{z})] - \mathbf{v}(\mathbf{z}) \right|\right|^2_{H_{\mathbf{z};\theta}} \right\}$$

by expanding the norm, the equivalent objective function to be minimized can be given as

$$\text{proj}_{\mathbf{v}(\mathbf{z})} \mathbf{e}[\hat{\boldsymbol{\theta}}(\mathbf{z})] = \arg \min_{\mathbf{v}(\mathbf{z}) \in H(K)} \left\{ ||\mathbf{v}(\mathbf{z})||^2_{H_{\mathbf{z};\theta}} - 2 \langle \hat{\boldsymbol{\theta}}(\mathbf{z}) - \boldsymbol{\theta}^{(0)}, \mathbf{v}(\mathbf{z}) \rangle_{H_{\mathbf{z};\theta}} \right\}$$

Using (2.16) for the second term we obtain from the linearity of integration

$$\langle \hat{\boldsymbol{\theta}}(\mathbf{z}) - \boldsymbol{\theta}^{(0)}, \mathbf{v}(\mathbf{z}) \rangle_{H_{\mathbf{z};\theta}} = \int_{\boldsymbol{\Theta}} \boldsymbol{\alpha}(\boldsymbol{\theta}) \left(\boldsymbol{\theta} - \boldsymbol{\theta}^{(0)} \right) d\boldsymbol{\theta}$$

demonstrating that the projection does not depend on the estimator $\hat{\boldsymbol{\theta}}(\mathbf{z})$. Note from Figure 2.5 and using the Pythagorean theorem, it can be shown that

$$||\mathbf{e}[\hat{\boldsymbol{\theta}}(\mathbf{z})]||^2_{H_{\mathbf{z};\theta}} = ||\boldsymbol{\epsilon}_p||^2_{H_{\mathbf{z};\theta}} + \left|\left| \text{proj}_{\mathbf{v}(\mathbf{z})} \mathbf{e}[\hat{\boldsymbol{\theta}}(\mathbf{z})] \right|\right|^2_{H_{\mathbf{z};\theta}}$$

which leads to Equation (2.15), $\boldsymbol{\epsilon}_p \perp H(K)$ is the vector representing the projection error and $0 \leq ||\boldsymbol{\epsilon}_p||_{H_{\mathbf{z};\theta}} < \infty$ since $||\mathbf{e}[\hat{\boldsymbol{\theta}}(\mathbf{z})]||^2_{H_{\mathbf{z};\theta}} < \infty$.

2.2.3 The Cramér-Rao Lower Bound

The most noteworthy and fundamental bound in estimation theory is the Cramér-Rao Lower Bound (CRLB) [44]. The CRLB provides a lower bound on the MSE of an unbiased estimator. Mathematically, we can write the relationship

$$\mathbf{MSE}_{\hat{\boldsymbol{\theta}}(\mathbf{z})} \succeq \mathbf{CRLB} \tag{2.18}$$

and equivalently $\text{tr}\left\{\mathbf{MSE}_{\hat{\boldsymbol{\theta}}(\mathbf{z})}\right\} \geq \text{tr}\left\{\mathbf{CRLB}\right\}$.

An estimator whose MSE achieves the CRLB is said to be efficient [44]. In practice, high SINR and/or very large data records will allow for approximate equality between the CRLB and the estimator MSE in (2.18); in such cases the estimator is asymptotically efficient [44].

The CRLB can be derived by using the projection based approach as follows. We assume that $n_p = 1$ and we consider the simple vector from Equation (2.17) in the RKHS $H(K)$

$$\begin{aligned} v_1(\mathbf{z}) &= \pi_{\boldsymbol{\theta}^{(0)}} - \pi_{\boldsymbol{\theta}^{(1)}} \\ &= 1 - \pi_{\boldsymbol{\theta}^{(1)}} \end{aligned}$$

where $\theta^{(1)} \in \Theta$ and the coefficients are $\alpha_0 = 1$ and $\alpha_1 = -1$. Using Equation (2.15) we know that the squared norm of the projection of the error vector $e[\hat{\theta}(\mathbf{z})] = \hat{\theta}(\mathbf{z}) - \theta^{(0)}$ onto $v_1(\mathbf{z})$ provides a bound. Thus, we have a bound that we will denote for now as C that is given by

$$C = \left|\left|\text{proj}_{v_1(\mathbf{z})}\hat{\theta}(\mathbf{z}) - \theta^{(0)}\right|\right|^2_{H(K)} \tag{2.19}$$

$$= \left|\langle \hat{\theta}(\mathbf{z}) - \theta^{(0)}, v_1(\mathbf{z})\rangle_{H_{\mathbf{z};\theta^0}}\right|^2 \tag{2.20}$$

$$= \left|\int_{\mathcal{Z}} \left(\hat{\theta}(\mathbf{z}) - \theta^{(0)}\right) v_1(\mathbf{z}) p(\mathbf{z};\theta^{(0)}) d\mathbf{z}\right|^2. \tag{2.21}$$

Using the Cauchy-Schwartz inequality the bound in (2.19) can be shown to satisfy [88]

$$\left| \int_{\mathcal{Z}} \left(\hat{\theta}(\mathbf{z}) - \theta^{(0)} \right) v_1(\mathbf{z}) p(\mathbf{z}; \theta^{(0)}) d\mathbf{z} \right|^2 \leq \tag{2.22}$$

$$\int_{\mathcal{Z}} \left(\hat{\theta}(\mathbf{z}) - \theta^{(0)} \right)^2 p(\mathbf{z}; \theta^{(0)}) d\mathbf{z} \int_{\mathcal{Z}} v_1^2(\mathbf{z}) p(\mathbf{z}; \theta^{(0)}) d\mathbf{z} \tag{2.23}$$

and $v_1(\mathbf{z})p(\mathbf{z}; \theta^{(0)}) = 1 - p(\mathbf{z}; \theta^{(1)})$. The LFR combined with the unbiased definition in Equation (2.16) can be used to obtain

$$\int_{\mathcal{Z}} (\hat{\theta}(\mathbf{z}) - \theta^{(0)}) \left(\pi_{\theta^{(0)}} - \pi_{\theta^{(1)}} \right) p(\mathbf{z}; \theta^{(0)}) d\mathbf{z} = \theta^{(1)} - \theta^{(0)}$$

which, when substituted into the left-hand side (LHS) in the inequality of (2.22) results in

$$\left(\theta^{(1)} - \theta^{(0)}\right)^2 \leq$$
$$\int_{\mathcal{Z}} \left(\hat{\theta}(\mathbf{z}) - \theta^{(0)} \right)^2 p(\mathbf{z}; \theta^{(0)}) d\mathbf{z} \int_{\mathcal{Z}} v_1^2(\mathbf{z}) p(\mathbf{z}; \theta^{(0)}) d\mathbf{z}.$$

By rearranging terms we obtain in the previous inequality,

$$\int_{\mathcal{Z}} \left(\hat{\theta}(\mathbf{z}) - \theta^{(0)} \right)^2 p(\mathbf{z}; \theta^{(0)}) d\mathbf{z} \geq \frac{\left(\theta^{(1)} - \theta^{(0)}\right)^2}{\int_{\mathcal{Z}} v_1^2(\mathbf{z}) p(\mathbf{z}; \theta^{(0)}) d\mathbf{z}}. \tag{2.24}$$

As can be seen, the LHS of the inequality is the MSE at $\theta^{(0)}$ of an estimator $\hat{\theta}(\mathbf{z})$.

If we let $\theta^{(1)} = \theta^{(0)} + \epsilon$ for some small real-valued $\epsilon > 0$, then as $\epsilon \to 0$, the right-hand side (RHS) of Equation (2.24) results in

$$\mathrm{MSE}_{\hat{\theta}(\mathbf{z})} \geq \lim_{\epsilon \to 0} \frac{\epsilon^2}{\int_{\mathcal{Z}} \left(\frac{p(\mathbf{z}; \theta^{(0)} + \epsilon) - p(\mathbf{z}; \theta^{(0)})}{p(\mathbf{z}; \theta^{(0)})} \right)^2 p(\mathbf{z}; \theta^{(0)}) d\mathbf{z}}. \tag{2.25}$$

The term in the denominator in the RHS of (2.25) can be expressed as

$$\int_{\mathcal{Z}} \left(\frac{1}{p(\mathbf{z}; \theta^{(0)})} \lim_{\epsilon \to 0} \frac{p(\mathbf{z}; \theta^{(0)} + \epsilon) - p(\mathbf{z}; \theta^{(0)})}{\epsilon} \right)^2 p(\mathbf{z}; \theta^{(0)}) d\mathbf{z}$$

which, using the definition of the derivative, corresponds to

$$J = \int_{\mathcal{Z}} \left(\frac{1}{p(\mathbf{z}; \theta^{(0)})} \frac{\partial p(\mathbf{z}; \theta^{(0)})}{\partial \theta} \right)^2 p(\mathbf{z}; \theta^{(0)}) d\mathbf{z}. \tag{2.26}$$

Using the properties of the chain rule for natural logarithm functions, we can write $p^{-1}(\mathbf{z}; \theta^{(0)}) \partial p(\mathbf{z}; \theta^{(0)}) / \partial \theta = \partial \ln p(\mathbf{z}; \theta^{(0)}) / \partial \theta$. We also note that if we just take a general $\theta^{(1)} \in \Theta$ and do not take a limit in Equation (2.25) we obtain what is known as the Hammersley-Chapman-Robbins bound (HChRB) [56, 89].

The inverse of the term in Equation (2.26) provides the CRLB for scalar parameter estimation. Specifically, the CRLB is given by

$$\text{CRLB} \triangleq J^{-1} \tag{2.27}$$

$$= \frac{1}{E_{\mathbf{z};\theta^{(0)}} \left\{ \left(\frac{\partial \ln p(\mathbf{z}; \theta^{(0)})}{\partial \theta} \right)^2 \right\}} \tag{2.28}$$

$$= \frac{1}{\left|\left| \frac{\partial \ln p(\mathbf{z}; \theta^{(0)})}{\partial \theta} \right|\right|^2_{H_{\mathbf{z};\theta}}}. \tag{2.29}$$

Note that J in (2.26), which is the inverse of the CRLB, is the Fisher information (FI) [44]. It is a function that represents the amount of information provided by the measurement $\mathbf{z}$ about the unknown parameter $\boldsymbol{\theta}$. The CRLB can be generalized for estimating the $n_p > 1$ dimensional vector parameter [44]

$$\mathbf{CRLB} = \mathbf{J}^{-1} \in \mathbb{S}^{n_p}_{++}$$

where $\mathbf{J}$ is the Fisher information matrix (FIM) defined as

$$\mathbf{J} \triangleq E_{\mathbf{z};\boldsymbol{\theta}} \left\{ \frac{\partial \ln p(\mathbf{z}; \boldsymbol{\theta})}{\partial \boldsymbol{\theta}} \frac{\partial \ln p(\mathbf{z}; \boldsymbol{\theta})}{\partial \boldsymbol{\theta}}^T \Big|_{\boldsymbol{\theta}=\boldsymbol{\theta}^{(0)}} \right\} \tag{2.30}$$

and $\mathbb{S}^{n_p}_{++}$ defines the set of all n_p-dimensional matrices that are symmetric positive definite.

The CRLB can be shown to exist under certain regularity conditions of the likelihood function. The conditions are [44]: (1) the derivative of the log-likelihood function exists and is finite; and (2) the derivative operation on $\boldsymbol{\theta}$ can be interchanged with the integration on $\mathbf{z}$. The CRLB can be viewed as a measure of the likelihood function's curvature [33, 44]. This is demonstrated using the 1-D measurement $z = s_0\theta + w$, where θ is an unknown parameter, $s_0 = 1$, and w is a Gaussian random variable with zero mean and variance σ_w^2. In this case, the likelihood function and corresponding log-likelihood function are given, respectively, by

$$p(z;\theta) = \frac{1}{\sqrt{2\pi\sigma_w^2}} \exp\left[-\frac{1}{2\sigma_w^2}(z - s_0\theta)^2\right]$$
$$\ln p(z;\theta) = -\ln\sqrt{2\pi\sigma_w^2} - \frac{(z - s_0\theta)^2}{2\sigma_w^2}. \tag{2.31}$$

Following (2.27) to compute the CRLB, the first derivative of the log-likelihood function with respect to θ results in

$$\frac{\partial \ln p(z;\theta)}{\partial\theta} = \frac{h_0}{\sigma_w^2}z - \frac{s_0^2\theta}{\sigma_w^2}.$$

Computing another derivative with respect to θ and inverting the result yields CRLB $= \sigma_w^2/s_0^2$. The effect on the CRLB for a fixed $s_0 = 1$ and different variances for this simple example is shown in Figure 2.6. Here the true parameter value is $\theta^{(0)} = 2$. This figure demonstrates that when the variance of the noise, and thus the CRLB, are low, the likelihood function has a sharper peak.

If we compute the MLE of θ using Equation (2.31), we obtain

$$\hat{\theta}_{\text{MLE}}(z) = \frac{z}{s_0}.$$

The variance of the MLE is plotted in Figure 2.7 using 100 Monte Carlo simulations. As the figure shows, the estimator variance performance increases and the asymptotic variance as the number of simulations increases, averaged over all simulations is approximately equal to the CRLB.

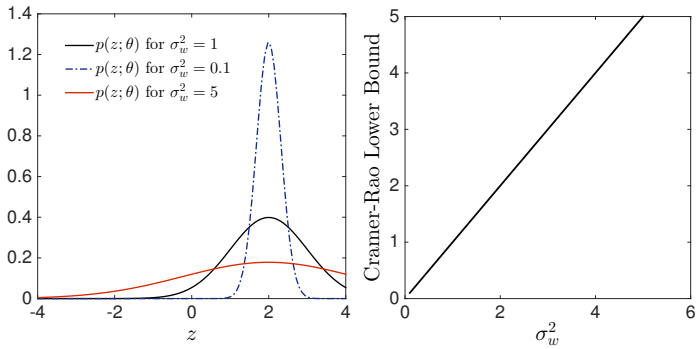

Figure 2.6: Noise Variance Effect on CRLB for Fixed $s_0 = 1$ and $\theta^{(0)} = 2$. (left) Likelihood Function $p(z;\theta)$ for Different Noise Variance Values; (right) CRLB for the Corresponding Cases.

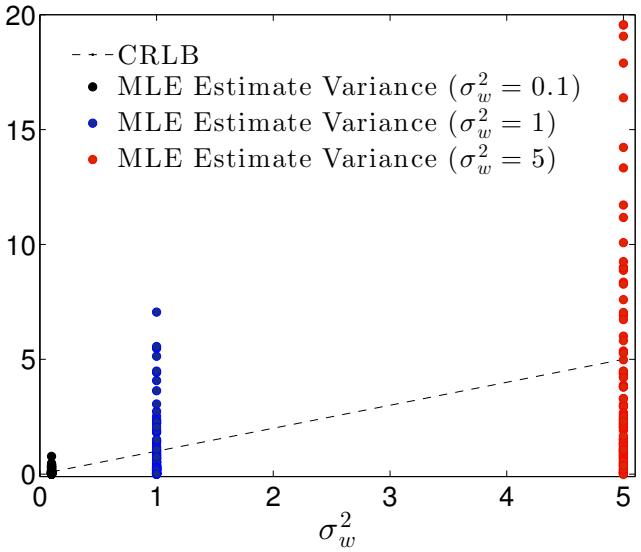

Figure 2.7: Measurement Noise Variance Effect on MLE Estimates with CRLB for Fixed $s_0 = 1$ and $\theta^{(0)} = 2$ for the Different Noise Variance Cases for 100 Trials of the Measurement.

2.2.4 The Barankin Bound

As discussed in the previous section, the CRLB only provides estimator MSE performance information at high SINR and/or large data record lengths. For low SINR and/or small data records, we consider large error bounds as they provide tighter bounds when system operating conditions become poor. For the case of unknown deterministic parameter estimation, the large error bound is the Barankin bound (BB).

It is the tightest estimation bound that can be obtained for an unbiased estimator.

We sometimes refer to the CRLB as a small error bound because of the fact that the CRLB only provides estimator MSE performance information at high SINR and/or large data record lengths. However, it is possible to consider the derivation of estimator performance bounds for the low SINR and/or small data record lengths. These bounds are referred to as large error bounds in the literature as they provide tighter bounds when operating conditions become poor in the system. For the case of unknown deterministic parameter estimation, the BB is the tightest bound one can compute for an unbiased estimator that is best at estimating $\theta^{(0)}$.

The BB is useful as it provides an attempt to characterize the SINR threshold because the large error bounds will actually provide an obvious CRLB departure. In this way, the BB is a useful low SINR tool for assessing how well a particular system will function when conditions become poor.

Computation of the Barankin Bound

We consider an estimator $\hat{\theta}_{\mathrm{B}}(\mathbf{z})$ that satisfies two criteria. The first criterion is that the estimator is unbiased and thus satisfies

$$\int_{\mathcal{Z}} \hat{\theta}_{\mathrm{B}}(\mathbf{z}) p(\mathbf{z};\theta) d\mathbf{z} = \theta, \ \forall \theta \in \Theta.$$

The second criterion is that the estimator is minimum SACM compared to all unbiased estimators at $\theta^{(0)}$ and

$$\left|\left|\hat{\theta}_{\mathrm{B}}(\mathbf{z}) - \theta^{(0)}\right|\right|^2_{H_{\mathbf{z};\theta^{(0)}}} \leq \left|\left|\phi(\mathbf{z}) - \theta^{(0)}\right|\right|^2_{H_{\mathbf{z};\theta^{(0)}}}, \ \forall \phi \in \mathcal{U} \tag{2.32}$$

where $\mathcal{U}$ defines the manifold of $H_{\mathbf{z};\theta^{(0)}}$ of unbiasedness estimators as

$$\mathcal{U} = \left\{ \phi(\mathbf{z}) \in H_{\mathbf{z};\theta^{(0)}} : \int_{\mathcal{Z}} \phi(\mathbf{z}) p(\mathbf{z};\theta) d\mathbf{z} = \theta, \ \forall \theta \in \Theta \right\}. \tag{2.33}$$

This is the problem that was of interest by Edward W. Barankin in his seminal paper [54].

The above two criteria describe the *locally best* unbiased estimator at $\theta^{(0)}$. Note that the term locally is used in this context to emphasize that the parameter is assumed to be deterministic.

Returning to the original problem for local estimation, we can say that the estimator $\hat{\theta}_{\mathrm{B}}(\mathbf{z})$ satisfying both (2.32) and (2.33) is then said to be the locally best unbiased estimator, the quantity

$$B = \left|\left|\hat{\theta}_{\mathrm{B}}(\mathbf{z}) - \theta^{(0)}\right|\right|^2_{H_{\mathbf{z};\theta^{(0)}}} \tag{2.34}$$

is essentially providing a lower bound for the MSE of all unbiased estimators. This is because, by construction no other estimator can have better MSE than $\hat{\theta}_{\mathrm{B}}(\mathbf{z})$. In Section 2.2.2, we noted that all bounds on the MSE are projections onto a RKHS. Thus, the bound B can be given as

$$\left|\left|\hat{\theta}_{\mathrm{B}}(\mathbf{z}) - \theta^{(0)}\right|\right|^2_{H_{\mathbf{z};\theta^{(0)}}} = \left|\left|\mathrm{proj}_{v(\mathbf{z})}\left(\hat{\theta}(\mathbf{z}) - \theta^{(0)}\right)\right|\right|^2_{H_{\mathbf{z};\theta^{(0)}}}$$

where $v(\mathbf{z}) \in H(K)$ and $\hat{\theta}(\mathbf{z})$ is any estimator satisfying $\mathcal{U}$. If we let

$$v(\mathbf{z}) = \int_{\Theta} \alpha(\theta)\pi_\theta d\theta$$

and project any estimator satisfying $\mathcal{U}$ onto this vector, we obtain the following

$$\mathrm{proj}_{v(\mathbf{z})}\left(\hat{\theta}(\mathbf{z}) - \theta^{(0)}\right) = \frac{\langle \hat{\theta}(\mathbf{z}) - \theta^{(0)}, v(\mathbf{z})\rangle_{H_{\mathbf{z};\theta^{(0)}}} v(\mathbf{z})}{||v(\mathbf{z})||^2_{H_{\mathbf{z};\theta^{(0)}}}}.$$

Hence,

$$\begin{aligned}
&\left|\left|\mathrm{proj}_{v(\mathbf{z})}\left(\hat{\theta}(\mathbf{z}) - \theta^{(0)}\right)\right|\right|^2_{H_{\mathbf{z};\theta^{(0)}}} \\
&= \left|\langle \hat{\theta}(\mathbf{z}) - \theta^{(0)}, v(\mathbf{z})\rangle_{H_{\mathbf{z};\theta^{(0)}}}\right|^2 \\
&= \left|\int_{\mathcal{Z}} \left(\hat{\theta}(\mathbf{z}) - \theta^{(0)}\right)\left(\int_{\Theta} \alpha(\theta)\pi_\theta d\theta\right) p(\mathbf{z};\theta^{(0)}) d\mathbf{z}\right|^2.
\end{aligned}$$

Once again, using the Cauchy-Schwartz inequality, we obtain

$$\left| \int_{\mathcal{Z}} \left(\hat{\theta}(\mathbf{z}) - \theta^{(0)} \right) \int_{\Theta} \alpha(\theta) \pi_{\theta^{(0)}}(\theta) d\theta p(\mathbf{z}; \theta^{(0)}) d\mathbf{z} \right|^2 \leq \tag{2.35}$$
$$\int_{\mathcal{Z}} \left(\hat{\theta}(\mathbf{z}) - \theta^{(0)} \right)^2 p(\mathbf{z}; \theta^{(0)}) d\mathbf{z} \int_{\mathcal{Z}} \left(\int_{\Theta} \alpha(\theta) \pi_{\theta} d\theta \right)^2 p(\mathbf{z}; \theta^{(0)}) d\mathbf{z}.$$

Similar to the steps used to derive the CRLB in Section 2.2.3, we apply the unbiased definition to the LHS of (2.35) to obtain

$$\left| \int_{\mathcal{Z}} \left(\hat{\theta}(\mathbf{z}) - \theta^{(0)} \right) \int_{\Theta} \alpha(\theta) \pi_{\theta} d\theta p(\mathbf{z}; \theta^{(0)}) d\mathbf{z} \right|^2 = \left[\int_{\Theta} \alpha(\theta) \left(\theta - \theta^{(0)} \right) d\theta \right]^2.$$

Rearranging the terms, we can obtain the inequality

$$\int_{\mathcal{Z}} \left(\hat{\theta}(\mathbf{z}) - \theta^{(0)} \right)^2 p(\mathbf{z}; \theta^{(0)}) d\mathbf{z} \geq \frac{\left[\int_{\Theta} \alpha(\theta) \left(\theta - \theta^{(0)} \right) d\theta \right]^2}{\int_{\mathcal{Z}} \left(\int_{\Theta} \alpha(\theta) \pi_{\theta} d\theta \right)^2 p(\mathbf{z}; \theta^{(0)}) d\mathbf{z}}$$

From this inequality, a lower bound for all unbiased estimators of the true parameter $\theta^{(0)}$ is given by

$$B \triangleq \sup_{\alpha(\theta) \neq 0} \frac{\left[\int_{\Theta} \alpha(\theta) \left(\theta - \theta^{(0)} \right) d\theta \right]^2}{\left|\left| \int_{\Theta} \alpha(\theta) \pi_{\theta} d\theta \right|\right|^2} = \left|\left| \hat{\theta}_{\mathrm{B}}(\mathbf{z}) - \theta^{(0)} \right|\right|^2_{H_{\mathbf{z};\theta^{(0)}}} \tag{2.36}$$

where the least upper bound is taken so that the LHS of the inequality is as tight as possible and that it equals the SACM of $\hat{\theta}_{\mathrm{B}}(\mathbf{z})$ at $\theta^{(0)}$. Equivalently, this is the minimum possible MSE for all unbiased estimators of $\theta^{(0)}$.

One might note here that the optimization is looking for an optimal solution vector $v^*(\mathbf{z})$ that maximizes the projection [84] further facilitating it's fundamental relationship with the RKHS integral equation and projection theorem interpretation from above [85]. This occurs when the orthogonality principle for estimation theory holds or equivalently the projection that makes the projection error vector orthogonal to $H(K)$. This is also a corollary of the Hilbert projection theorem and it occurs when the norm in the denominator is minimum. This is therefore a minimum norm problem.

If the measure for the integral in Equation (2.36) of the vector is the counting measure and equality is obtained almost everywhere, then the resulting bound is that obtained by Edward W. Barankin [54] and is given by

$$\mathrm{BB} \triangleq \limsup_{\substack{L\to\infty \\ \alpha_1,\ldots,\alpha_L \\ \theta^{(1)},\ldots,\theta^{(L)}}} \frac{\left(\sum_{l=1}^{L} \alpha_l(\theta^{(l)} - \theta^{(0)})\right)^2}{E_{\mathbf{z};\boldsymbol{\theta}^{(0)}}\left\{\left(\sum_{l=1}^{L} \alpha_l \pi_\theta^{(l)}\right)^2\right\}} \tag{2.37}$$

Here, $\theta^{(l)}$, $1,\ldots,L$ is the lth test-point used for computing the BB. The optimization problem in this form becomes a convex quadratic program (QP) with a theoretically infinite number of linear equality constraints.

Both the CRLB and the BB can be expressed in terms of the reproducing kernel function $K(\theta,\theta')$ in (2.11). In particular, if the error is projected onto some vector $\tilde{v}(\mathbf{z}) = \int_\Theta \tilde{\alpha}(\theta)\pi_\theta d\theta$ then the bound in (2.37) can be written as

$$B = ||\tilde{v}(\mathbf{z})||^2_{H_{\mathbf{z};\theta^0}}$$

where

$$||\tilde{v}(\mathbf{z})||^2_{H_{\mathbf{z};\theta^0}} = \int_{\mathcal{Z}}\int_\Theta \tilde{\alpha}(\theta)\pi_\theta d\theta \int_\Theta \tilde{\alpha}(\theta')\pi_{\theta'} d\theta p(\mathbf{z};\theta^{(0)})d\mathbf{z} \tag{2.38}$$

$$= \int_\Theta\int_\Theta \tilde{\alpha}(\theta)\tilde{\alpha}(\theta')\int_{\mathcal{Z}} \pi_\theta\pi_{\theta'} p(\mathbf{z};\theta^{(0)})d\mathbf{z}d\theta d\theta' \tag{2.39}$$

$$= \int_\Theta\int_\Theta \tilde{\alpha}(\theta)\tilde{\alpha}(\theta')K(\theta,\theta')d\theta d\theta'. \tag{2.40}$$

This norm represents a bound and can be simplified to the CRLB by expressing an integral transform of π_θ [45, 67, 83] and rewriting the norm of linear combinations of this integral transform in the subspace that π_θ has been mapped into. Using Equation (2.38), the BB can be shown to be in a quadratic form in the kernel. Specifically, using the Hilbert projection theorem, the optimal projection is one in which the error

vector $\epsilon_p \perp H(K)$ so that [67, 83]

$$\langle \tilde{v}(\mathbf{z}) - e[\hat{\theta}(\mathbf{z})], v(\mathbf{z}) \rangle_{H_{\mathbf{z};\theta^0}} = 0, \ \forall v(\mathbf{z}) \in H(K), \text{ or} \tag{2.41}$$

$$\langle \tilde{v}(\mathbf{z}), v(\mathbf{z}) \rangle_{H_{\mathbf{z};\theta^0}} = \langle e[\hat{\theta}(\mathbf{z})], v(\mathbf{z}) \rangle_{H_{\mathbf{z};\theta^0}} \tag{2.42}$$

$$\langle \tilde{v}(\mathbf{z}), v(\mathbf{z}) \rangle_{H_{\mathbf{z};\theta^0}} = \int_\Theta \alpha(\theta)(\theta - \theta^{(0)}) d\theta \tag{2.43}$$

$$\int_\Theta \int_\Theta \tilde{\alpha}(\theta')\alpha(\theta) \int_\mathcal{Z} \pi_\theta \pi_{\theta'} p(\mathbf{z}; \theta^{(0)}) d\mathbf{z} d\theta d\theta' = \int_\Theta \alpha(\theta)(\theta - \theta^{(0)}) d\theta \tag{2.44}$$

$$\int_\Theta \alpha(\theta) \int_\Theta \tilde{\alpha}(\theta') K(\theta, \theta') d\theta' d\theta = \int_\Theta \alpha(\theta)(\theta - \theta^{(0)}) d\theta, \ \forall \theta \in \Theta. \tag{2.45}$$

We note that the only way equality can occur in the last line in Equation (2.41) is if

$$\int_\Theta \tilde{\alpha}(\theta') K(\theta, \theta') d\theta' = \theta - \theta^{(0)}, \ \forall \theta \in \Theta.$$

In this way the coefficients $\tilde{\alpha}(\theta')$ can be viewed as the coefficients that expand $h(\theta) = \theta - \theta^{(0)}$ into the set of functionals $\Phi_K = \overline{\text{span}} \{K(\theta, \theta')\}_{\theta' \in \Theta}$. We also note that the integral equation described above can be recognized to be in the form of Fredholm integral equation of the first kind [87]. The BB formulation in this way this further elucidates the fact that

$$\text{BB} = ||\theta - \theta^{(0)}||^2_{H(K)}$$

as an equivalent interpretation of the BB, as noted by both Parzen and later by Albuquerque in [85, 86] and also further solidifies the RKHS concept. We can also state that the estimator that achieves this MSE is then [51]

$$\hat{\theta}_\text{B}(\mathbf{z}) = \int_\Theta \tilde{\alpha}(\theta) \pi_\theta d\theta.$$

It is now the case that the BB is easily seen to be a quadratic form in the kernel $K(\theta, \theta')$. This will match later analysis in the approximations introduced in the following section.

The kernel representation of the BB for the general case of $n_p \geq 1$ parameters is the quadratic form [45, 67, 83, 84]

$$\mathbf{BB} \triangleq \int_{\boldsymbol{\Theta}} \int_{\boldsymbol{\Theta}} \boldsymbol{\alpha}(\boldsymbol{\theta}) \boldsymbol{\alpha}^T(\boldsymbol{\theta}') K(\boldsymbol{\theta}, \boldsymbol{\theta}') d\boldsymbol{\theta}' d\boldsymbol{\theta}$$

where $\boldsymbol{\alpha} : \boldsymbol{\Theta} \rightarrow \mathbb{R}^{n_p}$ is the coefficients that solve the linear equations

$$\int_{\boldsymbol{\Theta}} \boldsymbol{\alpha}(\boldsymbol{\theta}') K(\boldsymbol{\theta}, \boldsymbol{\theta}') d\boldsymbol{\theta}' = \boldsymbol{\theta} - \boldsymbol{\theta}^{(0)}, \ \forall \boldsymbol{\theta} \in \boldsymbol{\Theta}.$$

or in other words, the coefficients that assert the reproducing property for the Kernel $K(\boldsymbol{\theta}, \boldsymbol{\theta}')$ [85, 86]. The minimum norm solution to these linear equations yields the tightest bound on the MSE. The problem here is that both the Barankin optimization problem and the Fredholm integral equation are difficult to solve in a closed form and in some cases impossible. As a result, the BB usually is computed using approximations for non-trivial problems.

Barankin Bound Approximation

The BB has been applied to many statistical signal processing problems in the form of an approximation rather than working with the theoretical expressions derived in the previous section [56–60]. In [55], P. Swerling was the first ever to apply the Barankin works [54] to engineering problems.

The BB approximations to solve for the BB that have appeared in the literature [56, 58, 61–63] and have largely acted as improvements in the sense of the efficiency of the number of test points L that are required resulting in computationally tractable methods to compute the BB for practical problem analysis without the need for an infinite number of test points. Most approximations for the BB are in the form of a Euclidean norm minimization over a set of L equality constraints for unbiasedness [51, 64, 65]. Here the norm is the MSE defined in the same way as in the previous sections. The minimum MSE is then considered to approximate the MSE of

the minimum MSE locally best estimator and the argument of the minimum is then $\hat{\theta}_{\mathrm{B}}(\mathbf{z})$.

Thus we can obtain the minimum MSE subject to $L+1$ test-point unbiasedness constraints as

$$\text{minimize } ||\hat{\theta}(\mathbf{z}) - \theta^{(0)}||^2_{H_{\mathbf{z};\theta^0}} \tag{2.46}$$

$$\text{subject to } \langle \hat{\theta}(\mathbf{z}) - \theta^{(0)}, \pi_{\theta^l} \rangle_{H_{\mathbf{z};\theta^0}} = \theta^{(l)} - \theta^{(0)},\ l = 0, 1, ..., L. \tag{2.47}$$

The solution to (2.46) can be obtained using the equality constrained minimum norm lemma given by [51]

$$\text{minimize } ||\mathbf{x}||^2$$

$$\text{subject to } \mathbf{G}\mathbf{x} = \mathbf{h}.$$

This lemma can be solved by Lagrange multipliers [51] to obtain the solution $||\mathbf{x}^*||^2 = \mathbf{h}^T\mathbf{K}^{-1}\mathbf{h}$ with $\mathbf{K} = \mathbf{G}\mathbf{G}^T$. Thus, the optimal solution lies in the space which is orthogonal to the null space of $\mathbf{G}$, $\mathbf{x}^* \perp \text{Null}(\mathbf{G})$.

Applying the lemma to (2.46) the solution to the optimization problem is given by

$$||\hat{\theta}(\mathbf{z}) - \theta^{(0)}||^2_{H_{\mathbf{z};\theta^0}} = \mathbf{h}^T_{\mathrm{MS}}\mathbf{K}^{-1}_{\mathrm{MS}}\mathbf{h}_{\mathrm{MS}}$$

where

$$\mathbf{h}_{\mathrm{MS}} = [\theta^{(0)} - \theta^{(0)} ... \theta^{(L)} - \theta^{(0)}]^T,$$

$$[\mathbf{K}^{-1}_{\mathrm{MS}}]_{l,l'} = K(\theta^{(l)}, \theta^{(l')}) - 1,\ \text{for } l, l' \in \{0, 1, ..., L\}.$$

This solution, which is commonly used [56, 58, 59, 61, 63, 88] is known as the McCaulay-Seidman (MS) approximation of the BB. For $n_p > 1$, the MS approximation has the quadratic form

$$\mathbf{BB}_{\mathrm{MS}} \triangleq \mathbf{H}^T_{\mathrm{MS}}\mathbf{K}^{-1}_{\mathrm{MS}}\mathbf{H}_{\mathrm{MS}}$$

where $\mathbf{H}_{\text{MS}} = [\boldsymbol{\theta}^{(0)} - \boldsymbol{\theta}^{(0)} \ \ldots \ \boldsymbol{\theta}^{(L)} - \boldsymbol{\theta}^{(0)}]^T$ and the l, l'th element of the inverse of the matrix $\mathbf{K}_{\text{MS}}$ is given by $[\mathbf{K}_{\text{MS}}^{-1}]_{l,l'} = K(\boldsymbol{\theta}^{(l)}, \boldsymbol{\theta}^{(l')}) - 1$, $l, l' = 0, 1, \ldots, L$. This results in a matrix $\mathbf{BB}_{\text{MS}} \in \mathbb{S}_{++}^{n_p}$. Note that the quadratic form given by the equality constrained minimum norm solution yields the same solution as discretizing the integral equation (IE) form of the BB discussed in the previous section.

A new BB approximation was proposed in [51], that provides a tighter approximation in terms of predicting the SINR threshold region of the MLE MSE when compared to the commonly used MS approximation [56, 61]. This is referred to as the Quinlan-Chaumette-Larzabal (QCL) approximation [45]. The parameter space in the QCL approximation is divided into finite sub-intervals for which the likelihood function is assumed to satisfy the CRLB regularity conditions allowing for a first order Taylor series expansion to be applied in each sub-interval. For simplicity, the authors in [51] take a first order Taylor expansion at $\theta^{(l)}$ of the likelihood function $p(\mathbf{z}; \theta)$ to obtain

$$p(\mathbf{z}; \theta) \approx p(\mathbf{z}; \theta^{(l)}) + \frac{\partial p(\mathbf{z}; \theta^{(l)})}{\partial \theta}.$$

This means that condition of unbiasedness of the estimator $\hat{\theta}(\mathbf{z})$ at $\theta^{(l)}$ can be approximately expressed locally as

$$\int_{\mathcal{Z}} \hat{\theta}(\mathbf{z}) \left(p(\mathbf{z}; \theta^{(l)}) + \frac{\partial p(\mathbf{z}; \theta^{(l)})}{\partial \theta} \right) d\mathbf{z} = \theta^{(l)} + 1, \ \forall \theta^{(l)} \in \Theta.$$

This equation can be further expanded into a meaningful integral in $H_{\mathbf{z};\theta^{(0)}}$ by carefully rewriting the LHS of the above equation as

$$\int_{\mathcal{Z}} \hat{\theta}(\mathbf{z}) \left(\frac{p(\mathbf{z}; \theta^{(l)})}{p(\mathbf{z}; \theta^{(0)})} \right) p(\mathbf{z}; \theta^{(0)}) d\mathbf{z} + \int_{\mathcal{Z}} \hat{\theta}(\mathbf{z}) \left(\frac{1}{p(\mathbf{z}; \theta^{(0)})} \frac{\partial p(\mathbf{z}; \theta^{(l)})}{\partial \theta} \right) p(\mathbf{z}; \theta^{(0)}) d\mathbf{z}.$$

In compact form using the LFR, this can be rewritten as

$$\langle \hat{\theta}(\mathbf{z}), \pi_{\theta^l} \rangle_{H_{\mathbf{z};\theta^0}} + \left\langle \hat{\theta}(\mathbf{z}), \frac{\partial \pi_{\theta^{(0)}}(\theta^{(l)})}{\partial \theta^{(l)}} \right\rangle_{H_{\mathbf{z};\theta^0}}. \tag{2.48}$$

Note that the first term in (2.48) is the equality constraint for the MS minimum norm problem that defines unbiasedness in the Barankin sense, as the second term is essentially defining unbiasedness of the score function for the likelihood [85].

The QCL approximation uses the second term in (2.48) as an additional optimization constraint. The optimization problem is then stated as the following minimum norm formulation

$$\begin{aligned} &\text{minimize} && ||\hat{\theta}(\mathbf{z}) - \theta^{(0)}||^2_{H_{\mathbf{z};\theta^0}} \\ &\text{subject to} && \langle \hat{\theta}(\mathbf{z}) - \theta^{(0)}, \pi_{\theta^{(l)}} \rangle_{H_{\mathbf{z};\theta^0}} = \theta^{(l)} - \theta^{(0)},\ l = 0, 1, ..., L. \\ & && \left\langle \hat{\theta}(\mathbf{z}) - \theta^{(0)}, \frac{\partial \pi_{\theta^{(l)}}}{\partial \theta^{(l)}} \right\rangle_{H_{\mathbf{z};\theta^0}} = \frac{\partial \left(\theta^{(l)} - \theta^{(0)}\right)}{\partial \theta^{(l)}},\ l = 0, 1, ..., L \end{aligned}$$

where we note that the additional constraint has added a sense of unbiasedness to the score function or informant of the likelihood. Also note that for the estimation problem of particular interest here, the term $\partial \left(\theta^{(l)} - \theta^{(0)}\right) / \partial \theta^{(l)} = 1$, $\forall l = 0, 1, \ldots, L$ since we are assuming estimation of the parameters directly and not a function of the parameters.

This results in the minimum norm solution of the form

$$||\hat{\theta}(\mathbf{z}) - \theta^{(0)}||^2_{H_{\mathbf{z};\theta^0}} = \mathbf{H}^T_{\text{QCL}} \mathbf{K}^{-1}_{\text{QCL}} \mathbf{H}_{\text{QCL}},$$

that includes higher order constraints for the unbiasedness constraint discussed in the previous section [65]. The QCL approximation can ultimately be written in a similar form to the MS approximation for $n_p \geq 1$ as

$$\mathbf{BB}_{\text{QCL}} \triangleq \mathbf{H}^T_{\text{QCL}} \mathbf{K}^{-1}_{\text{QCL}} \mathbf{H}_{\text{QCL}} \tag{2.49}$$

where

$$\mathbf{H}_{\mathrm{QCL}} = \left[\boldsymbol{\theta}^{(0)} - \boldsymbol{\theta}^{(0)} \;\; \boldsymbol{\theta}^{(1)} - \boldsymbol{\theta}^{(0)} \;\; \cdots \;\; \boldsymbol{\theta}^{(L)} - \boldsymbol{\theta}^{(0)} \;\; \mathbf{I}_{n_p} \cdots \mathbf{I}_{n_p}\right]^T$$

$$\mathbf{K}_{\mathrm{QCL}} = \begin{bmatrix} \mathbf{K}_{\mathrm{MS}} & \mathbf{U}^T \\ \mathbf{U} & \mathbf{E} \end{bmatrix}$$

where $\mathbf{H}_{\mathrm{QCL}} \in \mathbb{R}^{(n_p+1)(L+1)\times n_p}$, $\mathbf{K}_{\mathrm{MS}} \in \mathbb{R}^{(L+1)\times(L+1)}$, $\mathbf{E} \in \mathbb{R}^{n_p(L+1)\times n_p(L+1)}$ extends the FIM to incorporate L test points $\boldsymbol{\theta}^{(l)} \in \boldsymbol{\Theta}$, $l = 1, \ldots, L$, beyond the true parameter $\boldsymbol{\theta}^{(0)}$ and the $\mathbf{U} \in \mathbb{R}^{n_p(L+1)\times(L+1)}$ contains a cross terms between the entries of the $\mathbf{K}_{\mathrm{MS}}$ and $\mathbf{E}$ matrices. The resulting bound is a matrix $\mathbf{BB}_{\mathrm{QCL}} \in \mathbb{S}^{n_p}_{++}$. The individual structure of these three matrices, demonstrating the dependence on the test points $\boldsymbol{\theta}^{(l)}$, are given by

$$\mathbf{K}_{\mathrm{MS}} = \begin{bmatrix} K(\boldsymbol{\theta}^{(0)}, \boldsymbol{\theta}^{(0)}) & \cdots & K(\boldsymbol{\theta}^{(0)}, \boldsymbol{\theta}^{(L)}) \\ \vdots & \ddots & \vdots \\ K(\boldsymbol{\theta}^{(L)}, \boldsymbol{\theta}^{(0)}) & \cdots & K(\boldsymbol{\theta}^{(L)}, \boldsymbol{\theta}^{(L)}) \end{bmatrix}, \tag{2.50}$$

$$\mathbf{U} = \begin{bmatrix} \mathbf{u}(\boldsymbol{\theta}^{(0)}, \boldsymbol{\theta}^{(0)}) & \cdots & \mathbf{u}(\boldsymbol{\theta}^{(0)}, \boldsymbol{\theta}^{(L)}) \\ \vdots & \ddots & \vdots \\ \mathbf{u}(\boldsymbol{\theta}^{(L)}, \boldsymbol{\theta}^{(0)}) & \cdots & \mathbf{u}(\boldsymbol{\theta}^{(L)}, \boldsymbol{\theta}^{(L)}) \end{bmatrix}, \text{ and} \tag{2.51}$$

$$\mathbf{E} = \begin{bmatrix} \mathbf{E}(\boldsymbol{\theta}^{(0)}, \boldsymbol{\theta}^{(0)}) & \cdots & \mathbf{E}(\boldsymbol{\theta}^{(0)}, \boldsymbol{\theta}^{(L)}) \\ \vdots & \ddots & \vdots \\ \mathbf{E}(\boldsymbol{\theta}^{(L)}, \boldsymbol{\theta}^{(0)}) & \cdots & \mathbf{E}(\boldsymbol{\theta}^{(L)}, \boldsymbol{\theta}^{(L)}) \end{bmatrix}. \tag{2.52}$$

Note that the sub-block elements of these matrices have the dimensions $K(\boldsymbol{\theta}^{(m)}, \boldsymbol{\theta}^{(n)}) \in \mathbb{R}_{++}$, $\mathbf{u}(\boldsymbol{\theta}^{(m)}, \boldsymbol{\theta}^{(n)}) \in \mathbb{R}^{N_p}$, and $\mathbf{E}(\boldsymbol{\theta}^{(m)}, \boldsymbol{\theta}^{(n)}) \in \mathbb{R}^{N_p \times N_p}$, and $m, n \in \{0, 1, \ldots, L\}$ are indexed up to the maximum number of test points L (including the true parameter $\boldsymbol{\theta}^{(0)}$). Also note that n_p is the dimension of the vector of deterministic parameters $\boldsymbol{\theta}$ to be estimated.

If this BB approximation is applied to the signal model

$$\mathbf{z} = \sqrt{P}\mathbf{s}(\boldsymbol{\theta}^{(0)}) + \mathbf{w}$$

where $\mathbf{s} : \mathbb{R}^{n_p} \to \mathbb{C}^{n_z}$ is a known deterministic nonlinear function and is complex Gaussian with zero mean and covariance matrix $\sigma_w^2 \mathbf{I}_{N_s}$, then the sub-matrices in the block matrices $\mathbf{K}_{\text{MS}}$, $\mathbf{U}$, and $\mathbf{E}$ in Equation (2.49) as [51]

$$K(\boldsymbol{\theta}^{(l)}, \boldsymbol{\theta}^{(l')}) = \exp\left[\frac{P}{\sigma_w^2}(n_1(\boldsymbol{\theta}^{(l)}, \boldsymbol{\theta}^{(l)'}) - n_2(\boldsymbol{\theta}^{(l)}, \boldsymbol{\theta}^{(l)'}))\right] \tag{2.53}$$

$$n_1(\boldsymbol{\theta}^{(l)}, \boldsymbol{\theta}^{(l)'}) = ||\mathbf{s}(\boldsymbol{\theta}^{(l)}) + \mathbf{s}(\boldsymbol{\theta}^{(l')}) - \mathbf{s}(\boldsymbol{\theta}^{(0)})||_2^2$$

$$n_2(\boldsymbol{\theta}^{(l)}, \boldsymbol{\theta}^{(l)'}) = ||\mathbf{s}(\boldsymbol{\theta}^{(l)})||_2^2 + ||\mathbf{s}(\boldsymbol{\theta}^{(l')})||_2^2 - ||\mathbf{s}(\boldsymbol{\theta}^{(0)})||_2^2$$

$$[\mathbf{u}(\boldsymbol{\theta}^{(l)}, \boldsymbol{\theta}^{(l')})]_i = \frac{P}{\sigma_w^2} K(\boldsymbol{\theta}^{(l)}, \boldsymbol{\theta}^{(l')}) \left\langle \mathbf{s}(\boldsymbol{\theta}^{(l')}) - \mathbf{s}(\boldsymbol{\theta}^{(0)}), \frac{\partial \mathbf{s}(\boldsymbol{\theta}^{(l)})}{\partial [\boldsymbol{\theta}]_i} \right\rangle \tag{2.54}$$

$$[\mathbf{E}(\boldsymbol{\theta}^{(l)}, \boldsymbol{\theta}^{(l')})]_{i,l} = \frac{P}{\sigma_w^2} K(\boldsymbol{\theta}^{(l)}, \boldsymbol{\theta}^{(l')}) \left\{ \left\langle \frac{\partial \mathbf{s}(\boldsymbol{\theta}^{(l')})}{\partial [\boldsymbol{\theta}]_i}, \frac{\partial \mathbf{s}(\boldsymbol{\theta}^{(l)})}{\partial [\boldsymbol{\theta}]_j} \right\rangle + \right. \tag{2.55}$$

$$\left. \frac{P}{\sigma_w^2} \left\langle \mathbf{s}(\boldsymbol{\theta}^{(l')}) - \mathbf{s}(\boldsymbol{\theta}^{(0)}), \frac{\partial \mathbf{s}(\boldsymbol{\theta}^{(l)})}{\partial [\boldsymbol{\theta}]_i} \right\rangle \cdot \left\langle \mathbf{s}(\boldsymbol{\theta}^{(l)}) - \mathbf{s}(\boldsymbol{\theta}^{(0)}), \frac{\partial \mathbf{s}(\boldsymbol{\theta}^{(l')})}{\partial [\boldsymbol{\theta}]_j} \right\rangle \right\} \tag{2.56}$$

where $\mathbf{s}(\boldsymbol{\theta}^{(l)})$ is the evaluation of the nonlinear function at the test point $\boldsymbol{\theta}^{(l)}$ and $\langle \mathbf{u}, \mathbf{v} \rangle = \mathbf{v}^T \mathbf{u}$ is the standard inner product for vectors $\mathbf{u}, \mathbf{v} \in \mathbb{R}^N$. In (2.53)-(2.56), we see the dependence on the SINR $= P/\sigma_w^2$ and $i, j \in \{1, \ldots, n_p\}$. For the frequency estimation problem the parameter to be estimated is a scalar ($n_p = 1$) and $\theta^{(l)} = f_l$ for $f_l \in (-1/2, 1/2)$.

Note that for $L = 1$, $\mathbf{BB}_1 = \mathbf{HChRB}$, is the Hammersley-Chapman-Robbins bound (HChRB) [51, 59] and for $L = 0$, the CRLB is given by

$$\mathbf{CRLB} = [\mathbf{E}]_{1,1}^{-1} = \mathbf{E}(\boldsymbol{\theta}^{(0)}, \boldsymbol{\theta}^{(0)})^{-1}.$$

Barankin Bound Test Point Selection

The selection of test points $\boldsymbol{\theta}^{(l)}$ is an important step for computing the BB. In general, as long as $\boldsymbol{\theta}^{(l)} \in \boldsymbol{\Theta}$ a bound can be obtained. However, not all test points provide the tightest bound possible and not all test points provide a convergent bound [66]. As such, the BB approximation in the previous section needs an additional attention given to both how the test points are selected and also to how many test points should be considered.

In theory, as the number of test points L increases, the tightness of the bound also increases [89]. However, this also increases the computational complexity since the dimension of the matrix $\mathbf{K}_{\text{QCL}}$, that needs to be inverted, becomes very large, especially when there are a number of parameters to be estimated.

Consider the MS approximation of the BB given by $\text{BB}_{\text{MS}} = \mathbf{h}_{\text{MS}}^T \mathbf{K}_{\text{MS}}^{-1} \mathbf{h}_{\text{MS}}$ where the inverse of the kernel matrix was defined to have elements

$$[\mathbf{K}_{\text{MS}}]_{l,l'} = K(\theta^{(l)}, \theta^{(l)}) - 1, \; l, l' \in \{1, \ldots, L\}$$

and $\mathbf{h}_{\text{MS}} = [\theta^{(1)} - \theta^{(0)} \ldots \; \theta^{(L)} - \theta^{(0)}]^T$. Here, we can conceptually note of ways to make this quantity as large (make the bound tighter) as possible using simple mathematics. Essentially, we either require $p(\mathbf{z}; \theta^{(l)})$ to approximate $p(\mathbf{z}; \theta^{(0)})$ as best as possible so that $\mathbf{K}_{\text{MS}} \approx \mathbf{0}_{L \times L}$ or that the deviations $\theta^{(l)} - \theta^{(0)}$ be as large as possible [62].

As it turns out this can sometimes have a nice relationship to the problem of interest. For example, it was pointed out in [69] that for time-delay of arrival, the best test-points tend to be ones that correspond to peaks in the matched filter output, normally called sidelobes and for some signals these are integer multiples of the period. In this case the test-point selection can be optimally done given knowledge of the problem but in general this is not the case.

In addition to the computational complexity required to compute the large in-

version of either $\mathbf{K}_{\mathrm{MS}}$ or $\mathbf{K}_{\mathrm{QCL}}$, test-point selection is one of the largest drawbacks that adds to the difficult effort of computing large-error bounds. Comparing what is required for the BB to that of the CRLB, which has a rather pedestrian calculation, forces the practical computation for large-error bounds to continue to be an area of active research [45, 51, 67, 83]. Furthermore, the selected test-points need to be carefully chosen for the problem so as to avoid a violation of the underlying assumptions for unbiased estimation [66] otherwise divergent bounds can be accidentally computed and SINR threshold predictions may be inaccurate and actually make no sense.

2.3 Sequential Bayesian Filtering

When the unknown parameters to be estimated vary with time, then sequential Bayesian filtering methods are used to estimate the unknown probability density function of the parameters given measurements over time. This method uses two equation: a transition equation that relates the unknown parameter or state values at the current time step with the corresponding values at the previous time step; and a measurement equation that relates the unknown state values with observation values that evolve over time. The two equations are provided by a state space representation (SSR) and are given by

$$\mathbf{x}_k = \mathbf{f}_k(\mathbf{x}_{k-1}, \mathbf{g}_{k-1}) \tag{2.57}$$

$$\mathbf{z}_k = \mathbf{h}_k(\mathbf{x}_k, \mathbf{v}_k) \tag{2.58}$$

where $\mathbf{x}_k \in \mathbb{R}^{n_x}$ is the state vector at discrete time step k, $\mathbf{f}_k : \mathbb{R}^{n_x} \times \mathbb{R}^{n_g} \to \mathbb{R}^{n_x}$ is a possibly nonlinear time-varying function of the state at the previous time step $k-1$, $\mathbf{z}_k \in \mathbb{R}^m$ is the measurement vector, $\mathbf{h}_k : \mathbb{R}^{n_x} \times \mathbb{R}^{n_v} \to \mathbb{R}^{n_z}$ is a possibly nonlinear time-varying function of the state, and $\mathbf{g}_k \in \mathbb{R}^{n_g}$ and $\mathbf{v}_k \in \mathbb{R}^{n_v}$ is the state process and measurement noise, respectively [90].

A solution to recursively compute the optimal state estimates for the aforementioned SSR model in Equations (2.57) and (2.58) in the Bayesian sense is to iteratively compute the posterior density function of the state in a two step process of state prediction and measurement update. This approach is called recursive Bayesian filtering (RBF) as current values are estimated from past values and current observations [90]. The method assumes a known initial prior distribution $p(\mathbf{x})$ state $\mathbf{x}_0$ at time step $k = 0$ that represents some information that may be available on the initial values of the unknown parameters. In general, if we assume that at time $k-1$ we have the posterior distribution $p(\mathbf{x}_{k-1}|\mathbf{z}_0, \ldots, \mathbf{z}_{k-1})$, then we can compute a *prediction* of the state using the Chapman-Kolmogorov equation by evaluating [90]

$$p(\mathbf{x}_k|\mathbf{Z}_{0:k-1}) = \int_{\mathbb{R}^{n_x}} p(\mathbf{x}_k|\mathbf{x}_{k-1}) p(\mathbf{x}_{k-1}|\mathbf{Z}_{0:k-1}) d\mathbf{x}_{k-1} \tag{2.59}$$

where $\mathbf{Z}_{0:k-1} = \{\mathbf{z}_0, \ldots, \mathbf{z}_{k-1}\}$ represents the sequence of measurements received up to time step $k-1$. When the new measurement $\mathbf{z}_k$ is received, then it can be used to can compute an *update* on the posterior using Bayes' rule

$$p(\mathbf{x}_k|\mathbf{Z}_{0:k}) \propto p(\mathbf{z}_k|\mathbf{x}_k) p(\mathbf{x}_k|\mathbf{Z}_{0:k-1}). \tag{2.60}$$

Using (2.60), an estimate of the state at time step k is computed as

$$\hat{\mathbf{x}}_{k|k} = \int_{\mathbb{R}^{n_x}} \mathbf{x}_k p(\mathbf{x}_k|\mathbf{Z}_{0:k}) d\mathbf{x}_k \tag{2.61}$$

which corresponds to the mean of the posterior distribution $p(\mathbf{x}_k|\mathbf{Z}_{0:k})$. The covariance of this estimate can be similarly computed as

$$\mathbf{P}_{k|k} = \int_{\mathbb{R}^{n_x}} \left(\mathbf{x}_k - \hat{\mathbf{x}}_{k|k}\right) \left(\mathbf{x}_k - \hat{\mathbf{x}}_{k|k}\right)^T p(\mathbf{x}_k|\mathbf{Z}_{0:k}) d\mathbf{x}_k. \tag{2.62}$$

This process of prediction and update is Bayes' optimal, and it provides the minimum mean squared error (MMSE) estimate. The integrals in Equations (2.59)-(2.62)

can be computed explicitly in closed form when the state and measurement models are both linear and the statistics of the process and measurement noise are Gaussian. In this case, the MMSE recursion reduces to the Kalman filter [90]. However, in practice, it is difficult to evaluate these integrals as they usually do not have a closed form.

2.3.1 Particle Filtering

When the assumptions of Gaussian distributed noise model processes and/or non-linear state transition or measurement models cannot be made, then sequential Monte Carlo (SMC) numerical techniques can be used [90]. With the increasing computational power of computers, SMC methods have become common in practice. SMC relies on the ability to draw a large amount of samples from a distribution and propagate them recursively. Integrations can then be performed used finite summations and expectations can be easily computed numerically for a large number of samples and can be shown to converge to the true expectation if enough samples are used [90]. A commonly used SMC algorithm is particle filtering (PF) that draws $N_d >> 1$ samples from a proposal distribution $\pi(\mathbf{x}_k|\mathbf{x}_{0:k-1}^{(i)}, \mathbf{z}_{0:k-1})$, $\mathbf{x}_k^{(i)}$, $i = 1, \ldots, N_d$. At time step $k-1$, each drawn sample $\mathbf{x}_{k-1}^{(i)}$ is assumed to be weighted by an associated set of uniform weights $w_{k-1}^{(i)} = 1/N_d$, $i = 1, \ldots, N_d$. Using the likelihood distribution $p(\mathbf{z}_k|\mathbf{x}_k^{(i)})$, a weight is assigned to each of these samples so that the outlier samples, compared to the measurements $\mathbf{z}_k$, are assigned relatively low values and those that are close are assigned a high value. This overall process is called sequential importance sampling (SIS) and it computes the updated weights at time step k (up to a normalizing constant) as

$$w_k^{(i)} = w_{k-1}^{(i)} \frac{p(\mathbf{z}_k|\mathbf{x}_k^{(i)}) p(\mathbf{x}_k^{(i)}|\mathbf{x}_{k-1}^{(i)})}{\pi(\mathbf{x}_k|\mathbf{x}_{0:k-1}^{(i)}, \mathbf{z}_{0:k-1})} \tag{2.63}$$

for $i = 1, \ldots, N_d$.

Studies demonstrated the applicability of various proposal distributions for different dynamical conditions [90]. However, a commonly used proposal distribution is the transitional prior $p(\mathbf{x}_k^{(i)}|\mathbf{x}_{k-1}^{(i)})$ for the modeling we are concerned with. In this case, the weight update calculation in (2.63) simplifies

$$w_k^{(i)} = w_{k-1}^{(i)} p(\mathbf{z}_k|\mathbf{x}_k^{(i)}). \tag{2.64}$$

Using the samples $\mathbf{x}_k^{(i)}$ and associated weights $w_k^{(i)}$, we can now approximate the posterior distribution $p(\mathbf{x}_k|\mathbf{Z}_{0:k})$ as the probability mass function (pmf)

$$p(\mathbf{x}_k|\mathbf{Z}_{0:k}) \approx \sum_{i=1}^{N_d} w_k^{(i)} \delta(\mathbf{x}_k - \mathbf{x}_k^{(i)}) \tag{2.65}$$

where $\delta(\mathbf{x}_k)$ is the Kronecker delta [90]. It can be shown that as $N_d \to \infty$, the posterior distribution in (2.65) converges to

$$\sum_{i=1}^{N_d} w_k^{(i)} \delta(\mathbf{x}_k - \mathbf{x}_k^{(i)}) \to p(\mathbf{x}_k|\mathbf{Z}_{1:k})$$

almost surely. Using the PF algorithm, computationally intractable expectations can be computed as finite sums. Specifically, given a function $\phi(\mathbf{x}_k)$ of the state, the expected value of the function can be approximated as

$$E_{\mathbf{x}_k|\mathbf{z}_{0:k}} \{\phi(\mathbf{x}_k)\} \approx \sum_{i=1}^{N_d} w_k^{(i)} \phi(\mathbf{x}_k^{(i)}).$$

The estimate of the state vector using the PF, together with the covariance of the estimate at every time step k are given, respectively, by

$$\hat{\mathbf{x}}_{k|k} = \sum_{i=1}^{N_d} w_k^{(i)} \mathbf{x}_k^{(i)}$$

$$\mathbf{P}_{k|k} = \sum_{i=1}^{N_d} w_k^{(i)} (\hat{\mathbf{x}}_{k|k} - \mathbf{x}_k^{(i)})(\hat{\mathbf{x}}_{k|k} - \mathbf{x}_k^{(i)})^T.$$

reducing the integrals in (2.61) and (2.62) to finite sums.

The PF is a powerful method because it allows us to recursively compute estimates for dynamically changing parameters in SSR models with general distributions and nonlinear relationships for the state and measurement functions. The PF described above is known in the literature as the SIS [90] PF. The steps of the SIS-PF algorithm is summarized in Algorithm 1 below.

Algorithm 1 Sequential Importance Sampling (SIS) Algorithm

$\left\{\mathbf{x}_k, \mathbf{x}_k^{(i)}, w_k^{(i)}\right\}_{i=1}^{N_d} = \mathbf{SIS}\left(\left\{\mathbf{x}_{k-1}^{(i)}, w_{k-1}^{(i)}\right\}_{i=1}^{N_d}, \mathbf{z}_k\right)$

for $i = 1$ to N_d **do**

Draw $\mathbf{x}_k^{(i)} \sim p(\mathbf{x}_k|\mathbf{x}_{k-1}^{(i)})$

Update Weights $w_k^{(i)} = w_{k-1}^{(i)} p(\mathbf{z}_k|\mathbf{x}_k^{(i)})$

end for

Calculate $s = \sum_{i=1}^{N_d} w_k^{(i)}$

for $i = 1$ to N_d **do**

Normalize Weights $w_k^{(i)} = s^{-1} w_k^{*(i)}$

end for

Estimate State $\hat{\mathbf{x}}_{k|k} = \sum_{i=1}^{N_d} w_k^{(i)} \mathbf{x}_k^{(i)}$

return

Ths SIS PF suffers from a problem known as degeneracy [90, 91]. After a few iterations, only a small set of the SIS PF weights $w_k^{(i)}$, $i = 1, \ldots, N_d$ have large values and most of them are close to zero. This violates the assumptions required for the Bayes' recursion as the small number of particles can no longer approximate a valid pdf.

The resampling process for the SIS PF consists of computing the cumulative distribution function (CDF) from the weights [90, 91]. Using the CDF, particles with

low probability are reassigned to particles with high probability. This process ensures that the particles always propagate towards the estimated mean at every time step. As the particles with very small probability are discarded, the PF maintains N_d particles in order to avoid degeneracy. The resampling algorithm is listed in Algorithm 2. After resampling, all of the weights are reset back to uniform, $w_k^{(i)} = N_d^{-1},\ \forall i$. When

Algorithm 2 Resampling Algorithm

$\left\{\mathbf{x}_k^{*(j)}, \tilde{w}_k^{(j)}\right\}_{j=1}^{N_d} = \textbf{Resample}\left(\left\{\mathbf{x}_k^{(i)}, w_k^{(i)}\right\}_{i=1}^{N_d}\right)$

Let $c_1 = w_k^{(1)}$

for $i = 2$ to N_d **do**

$c_i = c_{i-1} + w_k^i$

end for

Let $m = 1$

Draw $u_1 \sim \mathcal{U}(0, N_d^{-1})$

for $j = 1$ to N_d **do**

$u_j = u_1 + (j-1)N_d^{-1}$

while $u_j > c_m$ **do**

$m = m + 1$

end while

$x_k^{*(j)} = x_k^{(m)}$

$\tilde{w}_k^{(j)} = N_d^{-1}$

end for

return

the resampling algorithm is combined with the SIS algorithm, the result is commonly referred to as the sequential importance resampling (SIR) PF.

2.3.2 Track-Before-Detect Filtering

Track-Before-Detect Algorithm

The track-before-detect (TBD) algorithm is a batch measurement processing method that integrates unthresholded measurements over time about a possible estimate of an unknown object. The TBD is useful when the measurement as low SINR or an object is embedded in high clutter or interference. The TBD algorithm can be solved using the Bayes' recursion. However, an additional step needs to be implemented to allow for a varying probability of object detection at each time step k. The object existence is characterized using a two-state Markov chain. Specifically, we let $E_k =$ denote the presence of the object and $E_k = 0$ denote the absence of the object. This gives rise to the probability of object birth P_b and death P_d intuitively computed as [90]

$$P_b = \Pr\left(E_k = 1 | E_{k-1} = 0\right)$$

$$P_d = \Pr\left(E_k = 0 | E_{k-1} = 1\right).$$

These two probabilities can be accurately described as a two state Markov chain this is demonstrated in Figure 2.8. If the object is not present, then its state parameter is considered undefined, and it is not transitioned to the next time step for prediction. We can also write this in the form of a stochastic matrix representing the transition probabilities as

$$\mathbf{\Pi}_{\mathrm{BD}} = \begin{bmatrix} 1 - P_b & P_b \\ P_d & 1 - P_d \end{bmatrix} \tag{2.66}$$

In this case, the received signal model has two hypothesis: hypothesis H_0 corresponds to the case when $E_k = 0$ and hypothesis H_1 corresponds to the case when $E_k = 1$.

The Bayes' optimal estimate for the TBD algorithm can be recursively computed using the Chapman-Kolmogorov equations with the additional bookkeeping required

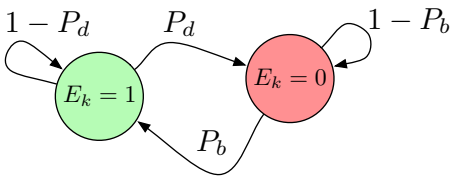

Figure 2.8: Birth and Death Two-State Markov chain of Order One that Describes Object Existence $E_k \in \{0, 1\}$ From Time Step $k-1$ to k with a Probability of Birth P_b and Death P_d

for the probability of a target not being present. The prediction step is now given by

$$\begin{aligned} p(\mathbf{x}_k, E_k = 1|\mathbf{Z}_{1:k-1}) = &\int_{\mathbb{R}^{n_x}} p(\mathbf{x}_{k-1}, E_{k-1} = 1|\mathbf{Z}_{1:k-1}) \cdot \\ &p(\mathbf{x}_k, E_k = 1|\mathbf{x}_{k-1}, E_{k-1} = 1) d\mathbf{x}_{k-1} + \\ &\int_{\mathbb{R}^{n_x}} p(\mathbf{x}_{k-1}, E_{k-1} = 0|\mathbf{Z}_{1:k-1}) \cdot \\ &p(\mathbf{x}_k, E_k = 1|\mathbf{x}_{k-1}, E_{k-1} = 0) d\mathbf{x}_{k-1} \end{aligned}$$

where

$$\begin{aligned} p(\mathbf{x}_k, E_k = 1|\mathbf{x}_{k-1}, E_{k-1} = 1) &= p(\mathbf{x}_k|\mathbf{x}_{k-1}, E_k = 1, E_{k-1} = 1) \cdot \qquad (2.67) \\ &\quad \Pr(E_k = 1|E_{k-1} = 1) \\ &= p(\mathbf{x}_k|\mathbf{x}_{k-1})(1 - P_d) \qquad (2.68) \\ p(\mathbf{x}_k, E_k = 1|\mathbf{x}_{k-1}, E_{k-1} = 0) &= p(\mathbf{x}_k|\mathbf{x}_{k-1}, E_k = 1, E_{k-1} = 0) \cdot \qquad (2.69) \\ &\quad \Pr(E_k = 1|E_{k-1} = 0) \\ &= \pi_b(\mathbf{x}_k) P_b \qquad (2.70) \end{aligned}$$

where $p(\mathbf{x}_k|\mathbf{x}_{k-1})$ is the kinematic transitional prior, and $\pi_b(\mathbf{x}_k)$ is the birth pdf. The update can be computed using Bayes' rule giving

$$p(\mathbf{x}_k, E_k = 1|\mathbf{Z}_{1:k}) \propto p(\mathbf{z}_k|\mathbf{x}_k, E_k = 1) p(\mathbf{x}_k, E_k = 1|\mathbf{Z}_{1:k-1}).$$

The estimate of the state at time step k, when the target is present, is computed

as the expectation over the posterior distribution

$$\hat{\mathbf{x}}_{k|k} = \int_{\mathbb{R}^{n_x}} \mathbf{x}_k p(\mathbf{x}_k, E_k = 1|\mathbf{Z}_{1:k}) d\mathbf{x}_k \tag{2.71}$$

and the covariance of this estimate can be similarly computed as

$$\mathbf{P}_{k|k} = \int_{\mathbb{R}^{n_x}} \left(\mathbf{x}_k - \hat{\mathbf{x}}_{k|k}\right)\left(\mathbf{x}_k - \hat{\mathbf{x}}_{k|k}\right)^T p(\mathbf{x}_k, E_k = 1|\mathbf{Z}_{1:k}) d\mathbf{x}_k. \tag{2.72}$$

Implementation of TBD Using Particle Filtering

The TBD algorithm can be implemented using an SMC PF method as follows. We first define a set of particles for the state and existence with corresponding weights as

$$\mathcal{P}_k = \left\{\mathbf{x}_k^{(i)}, E_k^{(i)}, w_k^{(i)}\right\}_{i=1}^{N_d}$$

where we can approximate the posterior distribution as the probability mass function (pmf)

$$p(\mathbf{x}_k, E_k = 1|\mathbf{Z}_{1:k}) \approx \sum_{i \in \mathcal{E}_k} w_k^{(i)} \delta(\mathbf{x}_k - \mathbf{x}_k^{(i)}) \tag{2.73}$$

with $\mathcal{E}_k = \left\{i \in \mathbb{Z} : E_k^{(i)} = 1\right\} \subseteq \{1, \ldots, N_d\}$ representing an indexed set corresponding to the particles that remain present. We assume that the existence particles, $E_k^{(i)}$ all follow the two state birth and death Markov chain in (2.66). Specifically, each existence particle has the distribution

$$E_k^{(i)} \sim \mathbf{\Pi}_{\text{BD}}, \ i = 1, \ldots, N_d$$

The state particles $\mathbf{x}_k^{(i)} = [x_k^{(i)}, y_k^{(i)}, \dot{x}_k^{(i)}, \dot{y}_k^{(i)}]^T$ for $i = 1, \ldots, N_d$ are drawn from the following distributions depending upon particle existence

$$p(\mathbf{x}_k, E_k = 1|\mathbf{x}_{k-1}, E_{k-1} = 1) = p(\mathbf{x}_k|\mathbf{x}_{k-1})$$

$$p(\mathbf{x}_k, E_k = 1|\mathbf{x}_{k-1}, E_{k-1} = 0) = \pi_b(\mathbf{x}_k)$$

When a particle represents an object that is not present, the particle state is set to $\mathbf{x}_k^{(i)} = \emptyset$.

The overall measurement likelihood function for both the RF and bearing measurements combined can be computed as

$$p(\mathbf{z}_k|\mathbf{x}_k^{(i)}) = \frac{p(\mathbf{z}_k|\mathbf{x}_k^{(i)}, H_1)}{p(\mathbf{z}_k, H_0)}$$

Note that the likelihood ratio is used as it is not known whether or not the object is present.

Chapter 3

BARANKIN KERNEL EFFECTIVE RANK THRESHOLD REGION PREDICTION

3.1 Signal-to-Interference-Plus-Noise Ratio Threshold Estimation

The Crámer-Rao lower bound (CRLB), presented in Section 2.2.3, for estimating unknown deterministic parameters can be shown to be equal to the mean squared error (MSE) estimator performance when the observation is related linearly to the unknown parameters [60]. This is demonstrated using the following linear model example. We consider the observation given by

$$\mathbf{z} = \mathbf{S}\boldsymbol{\theta} + \mathbf{w} \tag{3.1}$$

where $\mathbf{z} \in \mathbb{R}^{N_s}$, $\mathbf{S} \in \mathbb{R}^{N_s \times n_p}$, $\boldsymbol{\theta} \in \mathbb{R}^{n_p}$, and $\mathbf{w}$ is a zero-mean additive white Gaussian noise (AWGN) random vector with covariance matrix $\sigma_w^2 \mathbf{I}_{N_s}$. The CRLB for estimating $\boldsymbol{\theta}$ can be computed in closed form using Equation (2.30) to obtain

$$\mathbf{CRLB} = \sigma_w^2 \left(\mathbf{S}^T \mathbf{S}\right)^{-1}.$$

The MSE for the same problem was computed in Equation (2.9) to be exactly equal to the CRLB. A simple example of a linear model was also provided in Section 2.2.3.

When the observation model is nonlinear, the MSE can be shown to asymptotically approach the CRLB at high signal-to-interference-plus-noise ratio (SINR) values or for large data records. To demonstrate this, we consider an observation of a noisy sinusoid with unknown frequency $f^{(0)}$. Specifically, we consider the noisy measurement $\mathbf{z}$ given by

$$\mathbf{z} = \sqrt{P}\mathbf{s}\left(f^{(0)}\right) + \mathbf{w} \tag{3.2}$$

where P is the signal power, $\mathbf{s}(f^{(0)}) = [1 \; e^{j2\pi f^{(0)}} \; \ldots \; e^{j2\pi f^{(0)}(N_s-1)}]^T \in \mathbb{C}^{N_s}$ and $\mathbf{w}$ is a zero-mean circularly-symmetric complex AWGN random vector with covariance matrix $\sigma_w^2 \mathbf{I}_{N_s}$. Here, we define the SINR to be P/σ_w^2. In this particular case, the maximum likelihood estimate (MLE) can be computed as

$$\hat{f}_{\mathrm{ML}}(\mathbf{z}) = \arg \max_{f \in (-\frac{1}{2}, \frac{1}{2})} \left\{ -\frac{1}{2\sigma_w^2} \left|\left| \mathbf{z} - \sqrt{P}\mathbf{s}(f) \right|\right|_2^2 \right\} \tag{3.3}$$

that requires a search of the maximum norm between the received measurement and the transmit sinusoid over the normalized frequency range. As a specific example, consider $N_s = 10$, $\sigma_w^2 = 1$, and $f^{(0)} = 0$ in Equation (3.2). Using simulations, we plot the MSE of the frequency MLE for various SINR values in Figure 3.1. The figure also shows the CRLB for varying SINRs.

As it can be seen, the CRLB is equal to the MSE of the MLE estimator for high SINRs, that is, for $P/\sigma_w^2 >> 1$. As the SINR decreases, the estimator MSE deviates from the CRLB resulting in a large increase in MSE for a small change in SINR. Note that the CRLB was computed in closed form as [44, 51]

$$\begin{aligned} \mathrm{CRLB} &= \frac{\sigma_w^2}{P \left|\left| \frac{\partial \mathbf{s}(f^{(0)})}{\partial f} \right|\right|_2^2} \\ &= \frac{3\sigma_w^2}{4\pi^2 P N_s (N_s - 1)(2N_s - 1)} . \end{aligned}$$

The deviation from the CRLB in Figure 3.1 occurred at about 4.4 dB SINR. This deviation is known as the SINR threshold effect, and it is exhibited by general non-linear estimation problems [51, 57]. For this example, the MLE MSE at low SINRs is not adequate since the worst error is bounded by $|\hat{f}(\mathbf{z}) - 1/2|^2$ due to the bounded parameter space. If the parameter space was theoretically the entire real number line, then the MLE MSE would tend to positive infinity. However, in most practical cases, the parameter space can be bounded given some *a priori* knowledge.

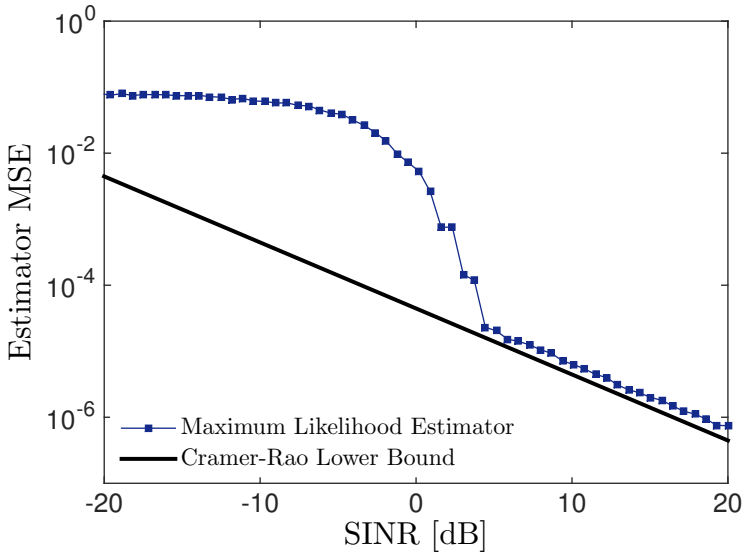

Figure 3.1: MLE Variance for the Frequency Estimation Problem and the Corresponding CRLB.

One method for determining the SINR threshold in based on the method of interval errors (MIE) approximation to the MSE [92]. Using the MIE approximation, MSE is expressed as the convex combination [33, 52, 53]

$$\mathrm{MSE}_{\hat{\theta}(\mathbf{z})} \approx \Pr\left(\hat{\theta}(\mathbf{z}) = \theta^{(0)}\right) \mathrm{CRLB} + \Pr\left(\hat{\theta}(\mathbf{z}) \neq \theta^{(0)}\right) \mathrm{MSE}_{\mathrm{thr}}$$

where $\Pr\left(\hat{\theta}(\mathbf{z}) = \theta^{(0)}\right) = 1 - \Pr\left(\hat{\theta}(\mathbf{z}) \neq \theta^{(0)}\right)$ denotes the probability of the estimator selecting the correct value $\theta^{(0)}$ and $\mathrm{MSE}_{\mathrm{thr}}$ is an approximation of the MSE deviation from the CRLB. Note, however, that the MIE requires good approximations for $\Pr\left(\hat{\theta}(\mathbf{z}) = \theta^{(0)}\right)$ and $\mathrm{MSE}_{\mathrm{thr}}$ for which there is no general approach and it is problem/algorithm dependent. Nevertheless, if it is possible to compute the MIE for a given problem, it is shown to provide quite accurate results for computing the SINR threshold [47–50, 92]. For the frequency estimation problem in (3.1), the symmetry of the parameter space can be used to approximate the threshold region probability of error as a uniform distribution [92]. A detailed MIE derivation for MIE is provided in [33, 52, 53] for estimating direction of arrival in vector arrays.

For the frequency estimation example in (3.2), the MIE formulation in [33, 52, 53] results in

$$\mathrm{MSE}_{f^{(0)}}(\hat{f}(\mathbf{z})) \approx \left[1 - \Pr\left(\hat{f}(\mathbf{z}) \neq f^{(0)}\right)\right] \frac{3\sigma_w^2}{4\pi^2 P N_s (N_s - 1)(2N_s - 1)} + \Pr\left(\hat{f}(\mathbf{z}) \neq f^{(0)}\right) \left(f^{(0)} - 0.5\right)^2.$$

The probability of an interval error occurring is given by [33, 50, 52, 53]

$$\Pr\left(\hat{f}(\mathbf{z}) \neq f^{(0)}\right) = \frac{1}{2}\Big[1 - Q_M\left(a_1, b_1\right) + Q_M\left(b_1, a_1\right)\Big]$$

where

$$a_1 = \sqrt{\frac{PN_s}{2\sigma_w^2}\left(1 + \sqrt{1 - |\rho_0|^2}\right)}$$

$$b_1 = \sqrt{\frac{PN_s}{2\sigma_w^2}\left(1 - \sqrt{1 - |\rho_0|^2}\right)}$$

$$\rho_0 = \frac{1}{N_s}\mathbf{s}^H(f^{(0)})\,\mathbf{s}(0.5)$$

and $Q_M(\cdot)$ is the Marcum Q-function.

3.2 Barankin Bound Kernel

In Section 2.2.4, we presented the Barankin bound (BB) as the lower bound for the MSE of all unbiased estimators of the deterministic parameter $\theta^0 \in \Theta$, where $\Theta \subseteq \mathbb{R}$ is an associated parameter space. We are particularly interested in the problem where we observe a vector of measurements $\mathbf{z} \in \mathbb{C}^{N_s}$ that is, in general, a nonlinear function of the true parameter that gives rise to an SINR threshold at which estimator performance rapidly deviates from the CRLB. Such a model arises ubiquitously in the estimation problem of parameters such as frequency, time-delay and angle-of-arrival. We consider the analysis used in Section 2.2.2 that is based on the estimation

theoretic construction based on inner product spaces [45, 67, 83–85]. For two functions $f, g \in H_{\mathbf{z};\theta^0}$ we have that

$$\langle f, g \rangle_{H_{\mathbf{z};\theta^0}} = \int f(\mathbf{z}) g(\mathbf{z}) p(\mathbf{z}; \theta^o) d\mu(\mathbf{z})$$

and $||g||^2_{H_{\mathbf{z};\theta^0}} = \langle g, g \rangle_{H_{\mathbf{z};\theta^0}}$ is the induced norm. We denote by $\hat{\theta}(\mathbf{z}) : \mathcal{Z} \to \Theta$ any estimator of $\theta^0 \in \Theta$. Then, if the estimation error is $e[\hat{\theta}(\mathbf{z})] = \hat{\theta}(\mathbf{z}) - \theta^0$, then the MSE or second absolute central moment (SACM) at θ^0 is given by [45, 54]

$$\mathrm{MSE}_{\theta^0}(\hat{\theta}(\mathbf{z})) = ||e||^2_{H_{\mathbf{z};\theta^0}} = \int e(\mathbf{z})^2 p(\mathbf{z}; \theta^0) d\mathbf{z}.$$

The estimator mean-biasedness can be found by considering $\pi_\theta = p(\mathbf{z}; \theta)/p(\mathbf{z}; \theta^0)$ and the inner product

$$b_{\hat{\theta}(\mathbf{z})} = \langle \hat{\theta}(\mathbf{z}) - \theta, \pi_\theta \rangle_{H_{\mathbf{z};\theta^0}}, \ \forall \theta \in \Theta$$

for which it can be seen that π_θ simply reassigns the measure of the integral to the distribution associated with the parameter θ. An estimator is said to be unbiased (in the mean) if $b_{\hat{\theta}(\mathbf{z})} = 0, \forall \theta \in \Theta$. The BB estimator can be found by considering [51, 54]

$$\hat{\theta}_{\mathrm{B}}(\mathbf{z}) = \arg \inf_{\phi \in \mathcal{U}} \left\{ ||\phi(\mathbf{z})||^2_{H_{\mathbf{z};\theta^0}} \right\} \tag{3.4}$$

where $\mathcal{U}$ is a manifold of the Hilbert space $H_{\mathbf{z};\theta^0}$ containing all estimators satisfying $b_{\phi(\mathbf{z})} = \theta - \theta^0, \ \forall \theta \in \Theta$. In [54], conditions were considered to find a unique BB estimator, assuming it exists, and utilize it as a bound on MSE. Given the openness of the formulation in (3.4), it should be evident that this problem is enormously challenging.

An approach considered to somewhat simplify the optimization problem of (3.4) is to consider L discrete test-points $\theta^l \in \Theta$ for $l = 1, \ldots, L$, and then solve [51, 64, 65]

$$\begin{aligned} &\text{minimize } ||\phi(\mathbf{z})||^2_{H_{\mathbf{z};\theta^0}} \\ &\text{subject to } \langle \phi(\mathbf{z}), \pi_{\theta^l} \rangle_{H_{\mathbf{z};\theta^0}} = \theta^l - \theta^0, \ l = 1, \ldots, L. \end{aligned}$$

This minimization is known to have a solution of the form [51, 64, 65]

$$\min \ ||\phi(\mathbf{z})||^2_{H_{\mathbf{z};\theta^0}} = \mathbf{h}^T \left(\mathbf{K}_B - \mathbf{1}\mathbf{1}^T\right)^{-1} \mathbf{h} \tag{3.5}$$

where $[\mathbf{K}_B]_{l,l'} = \langle \pi_{\theta^l}, \pi_{\theta^{l'}} \rangle_{H_{\mathbf{z};\theta^0}}$ and $[\mathbf{h}]_l = \theta^l - \theta^0$. The kernel associated with the matrix $\mathbf{K}_B$ is given $K(\theta, \theta')$ in (2.11).

We consider the specific measurement model case of $\mathbf{z} = \sqrt{\eta}\,\mathbf{s}(\theta) + \mathbf{w}$ where $\mathbf{w}$ is a complex Gaussian random vector with zero-mean and identity covariance matrix. Here, η is the SINR of the measurement. In this particular case, the elements of the kernel matrix can be computed in closed form as [45, 51, 58, 65]

$$\begin{aligned}
[\mathbf{K}_B(\eta)]_{l,l'} &= \int \frac{p(\mathbf{z};\theta^l)p(\mathbf{z};\theta^{l'})}{p(\mathbf{z};\theta^0)} d\mathbf{z} \\
&= \exp\left[2\eta\, \Re e\left\{(\mathbf{s}(\theta^l) - \mathbf{s}(\theta^0))^H (\mathbf{s}(\theta^{l'}) - \mathbf{s}(\theta^0))\right\}\right] \\
&= \exp\,(2\eta)^{\rho_{l,l'}}
\end{aligned}$$

where $\rho_{l,l'} \triangleq \Re e\left\{(\mathbf{s}(\theta^l) - \mathbf{s}(\theta^0))^H (\mathbf{s}(\theta^{l'}) - \mathbf{s}(\theta^0))\right\}$, $\Re e\left\{z\right\} = (z + z^*)/2$ is the real part of a complex value z, and z^* denotes the conjugate of z.

Note that the SINR parameter η only affects the BB kernel matrix $\mathbf{K}_B(\eta)$ in Equation (3.5). The vector $\mathbf{h}$ only depends on the deviation of the test-points from the true parameter. If $\mathbf{K}_B(\eta) \in \mathbb{R}^{L\times L}$ we can express the BB kernel in terms of its singular value decomposition (SVD) as

$$\mathbf{K}_B(\eta) = \mathbf{U}(\eta)\mathbf{\Sigma}(\eta)\mathbf{V}^H(\eta) \tag{3.6}$$

Here $\mathbf{U}(\eta)$ and $\mathbf{V}(\eta) \in \mathbb{R}^{L\times L}$ are matrices with rank L whose columns and rows represent the left and right singular vectors of $\mathbf{K}_B(\eta)$, respectively. The diagonal matrix of singular values $\mathbf{\Sigma}(\eta) \in \mathbb{R}^{L\times L}$ has diagonal entries given by the values

$$\sigma_1(\eta) \geq \sigma_2(\eta) \geq \cdots \geq \sigma_L(\eta) \geq 0.$$

Theoretically the rank of the BB kernel is given by the index corresponding to the smallest singular value that is strictly positive.

The matrix $\mathbf{K}_B(\eta)$ in (3.6) represents a full rank invertible Gramian matrix. Numerically, however, $\mathbf{K}_B(\eta)$ can have challenges and in fact depending on the evaluation can result in an ill-conditioned matrix. As a result, although theoretically $\mathbf{K}_B(\eta)$ has rank L, in practice, the effective rank may not be L, due to finite numerical precision computations that begin to become a factor as SINR increases.

3.3 Effective Rank of the BB Kernel

The rank of a matrix is defined as the difference between the largest dimension of any matrix $\mathbf{M} \in \mathbb{F}^{N\times M}$ where $\mathbb{F}$ is any field (typically $\mathbb{F} = \mathbb{R}$ or $\mathbb{F} = \mathbb{C}$) and the number of non-trivial orthogonal vectors $\mathbf{x}$ such that $\mathbf{Mx} = \mathbf{0}$ [93]. The *effective rank* in numerical computations can be computed using SVD where for a particular machine epsilon ϵ the effective rank is defined as [94]

$$\epsilon\text{rank } \mathbf{M} = |\,\{i : \sigma_i > \max(M, N) \cdot \epsilon(\sigma_1)\}\,|$$

where $\epsilon(\sigma_1)$ is the distance from the largest singular value σ_1 to the next largest number in the same precision, and $|\mathcal{S}|$ denotes set cardinality. For the kernel $\mathbf{K}_B(\eta)$, the ϵrank $\mathbf{K}_B(\eta)$ also depends on the SINR parameter.

The columns (and rows) of $\mathbf{K}_B(\eta)$ are orthogonal in theory. However, if we evaluate the l, l'th entry of the kernel matrix as

$$[\mathbf{K}_B(\eta)]_{l,l'} = \left\langle \frac{p(\mathbf{z};\theta^l,\eta)}{p(\mathbf{z};\theta^0,\eta)}, \frac{p(\mathbf{z};\theta^{l'},\eta)}{p(\mathbf{z};\theta^0,\eta)} \right\rangle_{H_{\mathbf{z};\theta^0}}, \tag{3.7}$$

then the likelihood function ratios (LFRs) in (3.7) approach arbitarly small positive numbers for some threshold SINR η_{thr} when evaluated at the lth parameter θ^l that is distant from the true parameter θ^0. This is a natural correspondence that is

witnessed precisely in the computation of the MLE where at some low SINR η that the probability that the measurement came from some outlier parameter θ^l will become large. The understanding of this phenomenon is known as the threshold effect and is used as the basis for formulating the MIE that is used to predict η_{thr} [33, 47–50, 52, 53].

The BB effective rank ϵrank $\mathbf{K}_B(\eta)$ can thus be utilized to predict the SINR threshold for a given problem. This is because, at some point of evaluation, the effective rank of $\mathbf{K}_B(\eta)$ starts to rapidly decrease as the SINR η increases since the probability that the measurement came from an outlier becomes arbitrarily small. In other words, full effective rank of the kernel corresponds to *absolute ambiguity in the estimation problem* and low effective rank corresponds to *absolute definiteness in the estimation problem*. We thus propose to use the effective rank to predict the SINR threshold and to evaluate it under the assumption of uniform sampling of L test-points over the parameter space Θ.

In general, the MLE $\hat{\theta}(\mathbf{z})$ resulting from a nonlinear estimation problem has a threshold region that is associated with selecting sidelobes as the maximum peak over the mainlobe with high probability. For a given set of measurements $\mathbf{z}$ and corresponding likelihood function $p(\mathbf{z};\theta^0)$, and a given SINR η, this sidelobe probability can be represented as [33, 47–50, 52, 53]

$$\begin{aligned} P_{\text{sl}}(\theta,\eta) &= \Pr\left(\max_{\theta\neq\theta^0\in\Theta}\{p(\mathbf{z};\theta)\} > p(\mathbf{z};\theta^0)\right) \\ &= \Pr\left(\max_{\theta\neq\theta^0\in\Theta}\left\{\frac{p(\mathbf{z};\theta)}{p(\mathbf{z};\theta^0)}\right\} > 1\right) \\ &= \Pr\left(\max_{\theta\neq\theta^0\in\Theta}\{\pi_\theta\} > 1\right). \end{aligned}$$

For the signal model in (3.2), this can be solved to obtain [33, 52, 53]

$$P_{\text{sl}}(\theta,\eta) = \frac{1}{2}\Big[1 - Q_M\left(a_1,b_1\right) + Q_M\left(b_1,a_1\right)\Big]$$

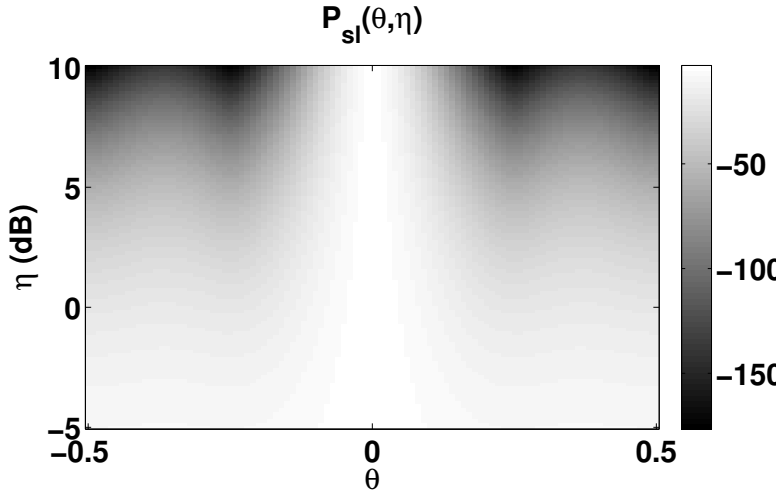

Figure 3.2: Selection of a Sidelobe Probability as a Function of Parameter Space and SINR Parameter η for Estimating Frequency.

where

$$a_1 = \sqrt{\eta N_s \left(1 + \sqrt{1 - |\rho_0|^2}\right)}$$

$$b_1 = \sqrt{\eta N_s \left(1 - \sqrt{1 - |\rho_0|^2}\right)}$$

$$\rho_0 = \frac{1}{N_s} \mathbf{s}^H(f^{(0)})\, \mathbf{s}(0.5)$$

and $Q_M(\cdot)$ is the Marcum Q-function. The sidelobe probability is plotted in Figure 3.2 using the complex sinusoid model with $[\mathbf{s}(\theta)]_n = e^{j2\pi\theta(n-1)}$, $\Theta = (-0.5, 0.5)$, $\theta^0 = 0$ and $N_s = 4$. From the figure, it can be seen that the probability of confusing a sidelobe for a given SINR η falls off exponentially towards a small positive value.

Note that the elements of the BB kernel matrix $\mathbf{K}_B(\eta)$ are correlations of the likelihood function ratios (LFRs) π_{θ^l} at the various sidelobe values in the parameter space as shown in (3.7). The sidelobe probability approaches a exponentially small positive number $\epsilon > 0$. However, the singular vectors associated with $\mathbf{K}_B(\eta)$ are associated with these LFRs with singular values $\sigma_1(\eta) \geq \cdots \geq \sigma_L(\eta) \geq 0$. These singular values fall off rapidly near the SINR threshold as shown in Figure 3.3 and

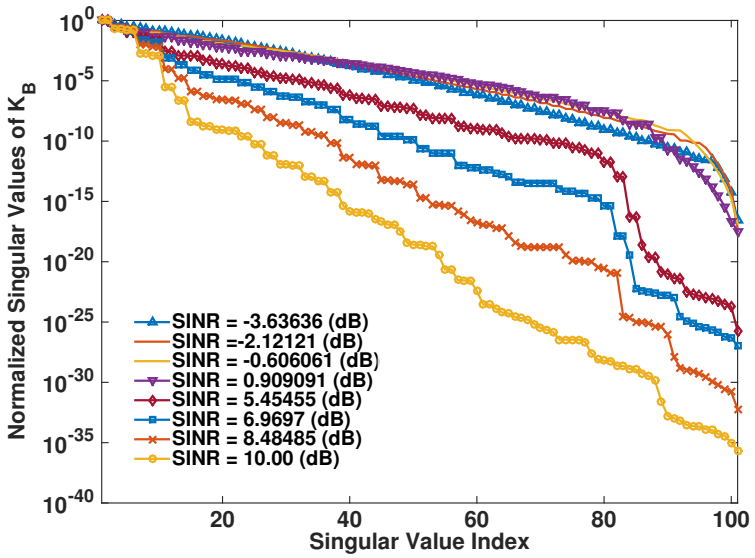

Figure 3.3: Plot of the Normalized SVD Singular Values for $\mathbf{K}_B(\eta)$ for a Range of SINRs for Frequency Estimation.

thus cause the effective rank to decrease rapidly. The proposed method to obtain the predicted SINR threshold η_{thr} using the effective rank of the kernel is given by

$$\eta_{\text{thr}} = \arg\min_{\eta} \left\{ \frac{\partial r_\epsilon(\eta)}{\partial \eta} \right\} = \arg\max_{\eta} \left\{ \frac{\partial^2 r_\epsilon(\eta)}{\partial^2 \eta} \right\} \tag{3.8}$$

where $r_\epsilon(\eta) = \epsilon\text{rank}\ \mathbf{K}_B(\eta)$.

3.4 Simulation Results

In all of the following examples, the numerical computations were obtained in MATLAB using double precision accuracy.

3.4.1 Frequency Estimation

We consider the observation model $\mathbf{z} = \sqrt{\eta}\,\mathbf{s}(\theta) + \mathbf{w}$, where $\mathbf{w}$ is complex Gaussian noise with zero mean and identity covariance matrix and $\mathbf{z} \in \mathbb{C}^{N_s}$. The transmit signal is given by

$$[\mathbf{s}(\theta)]_n = e^{j2\pi\theta(n-1)},$$

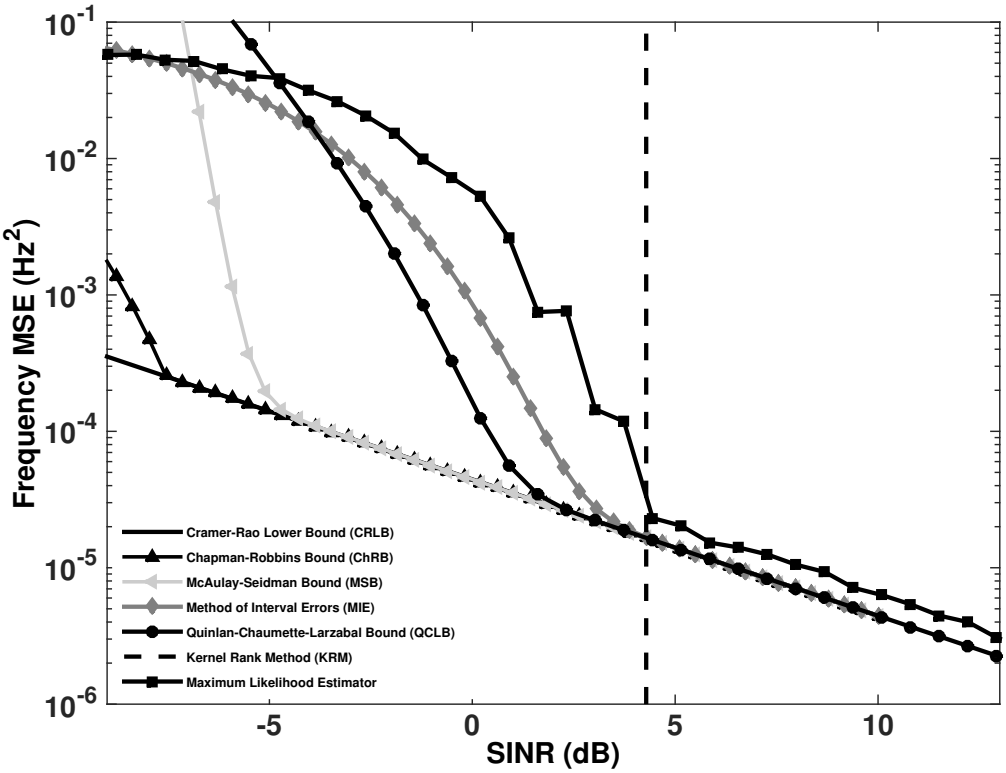

Figure 3.4: Performance for Frequency Estimation.

where $\theta^{(0)} = f^{(0)}$ is the unknown (normalized) frequency. We also assume that $\Theta = (-0.5, 0.5)$, $N_s = 10$, $\theta^0 = 0$, and the SINR is given by η. In Figure 3.4, we compare the Monte-Carlo (MC) MLE estimator performance using $N_{\text{MC}} = 10,000$ number of Monte Carlo trials to the CRLB, the MIE, the Chapmann-Robbins bound (ChRB), McCaulay-Seidman bound (MSB) BB approximation, and the Quinlan-Chaumette-Larzabal bound (QCLB) BB approximation. The figure shows that the other MSE bounds are tighter than the CRLB, but they are not inherently accurate at predicting the true MLE SINR threshold. In this example, the kernel effective rank method, plotted in Figure 3.5, provides the most accurate prediction, followed by the MIE.

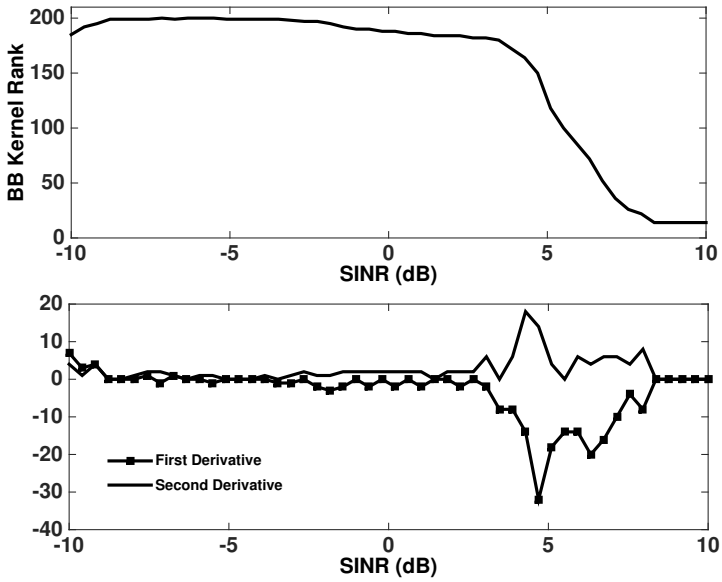

Figure 3.5: Rank of Kernel Matrix as a Function of SINR for Frequency Estimation.

3.4.2 Angle of Arrival Estimation

In this case, we assume an observation model for a uniform linear array (ULA) with Nyquist spatial sampling along the $y-$axis. Thus,

$$[\mathbf{s}(\theta)]_n = e^{j2\pi(n-1)\sin(\theta)}$$

where θ is the unknown angle of arrival with possible values in $\Theta = [\pi/18, 4\pi/9]$. Here, the number of array elements is $N_s = 5$, and the SINR is again given by η. The true angle of the narrowband source is assumed to be $\theta^{(0)} = \pi/4$. In this example, we plot the performance of the MLE, MIE, CRLB and the kernel effective rank method in Figure 3.6. In Figure 3.7, we see that the effective rank of the Barankin kernel provides the most accurate prediction. In this example, we only compare the MC MLE, with $N_{\text{MC}} = 10,000$ trials, to the CRLB and MIE.

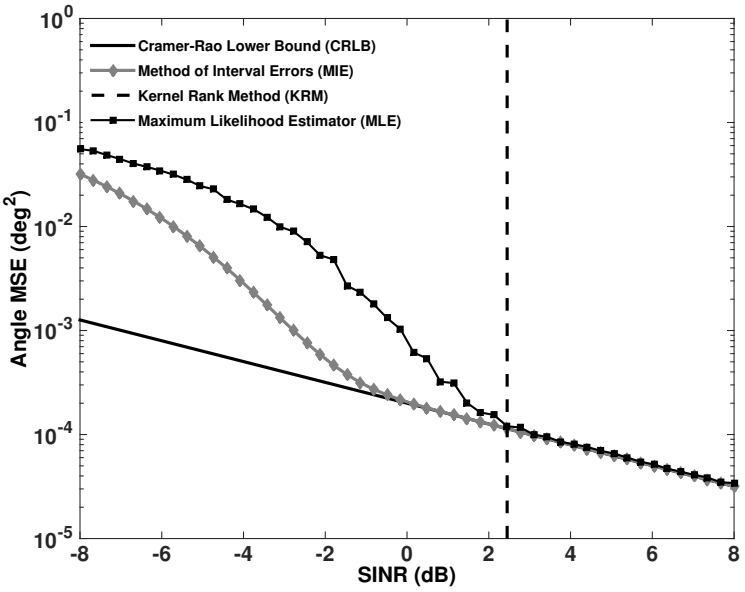

Figure 3.6: Performance for Angle Estimation.

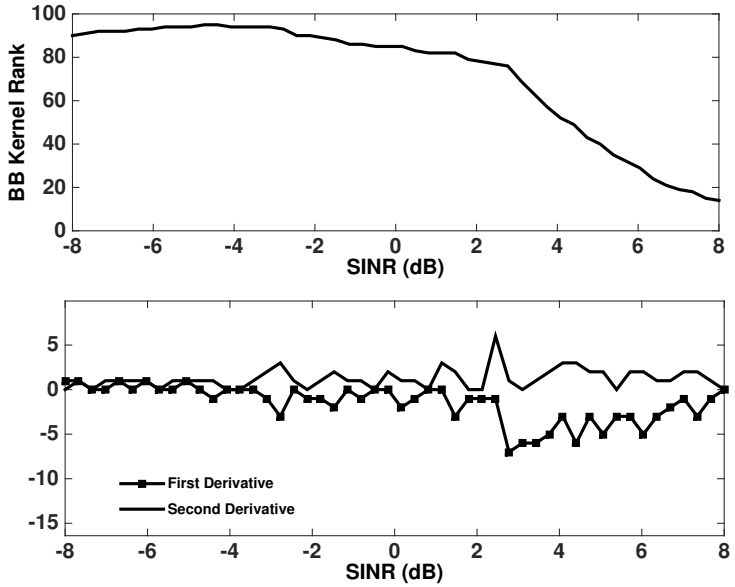

Figure 3.7: Rank of Kernel Matrix as a Function of SINR for Angle of Arrival Estimation.

3.4.3 Time Delay Estimation

In this example, we assume that the transmit signal is an linear frequency-modulated (LFM) chirp with frequency modulation (FM) rate b and pulse duration T. The LFM

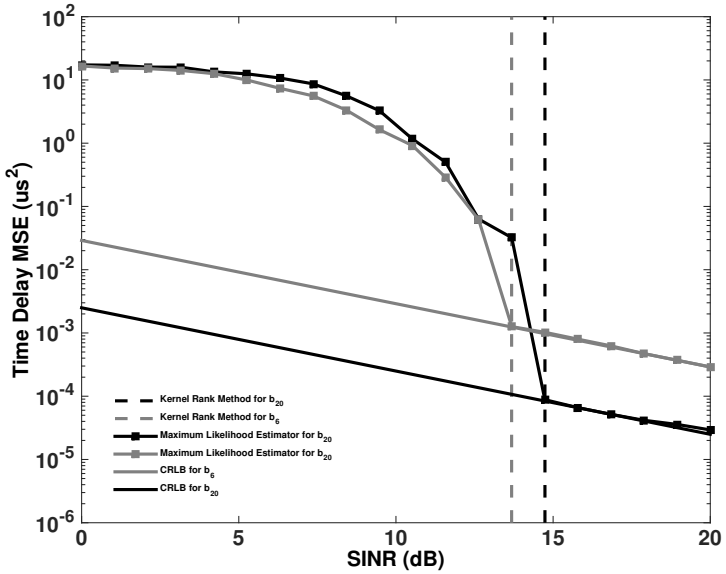

Figure 3.8: Performance for Time-Delay Estimation.

$x(t)$ is received after an unknown time delay θ. The received signal samples are then processed as

$$[\mathbf{s}(\theta)]_n = s(nT_s)$$

where $s(t) = x(t-\theta) = \sqrt{2(t-\theta)}e^{j2\pi b(t-\theta)^2}p_T(t-\theta)$ and $p_T(t) = 1,\ \forall t \in (0,T)$ and zero otherwise. Here we assume that $\Theta = [-2T, 2T]$, $N_s = 320$, $F_s = 1/T_s = 20$ MHz, $\theta^{(0)} = 0$ and that $||\mathbf{s}(\theta)||_2^2 = 1$. In this example, we consider two waveforms with equal duration $T = 4$ μs but with different FM rates $b_1 = 1.25$ GHz/s and $b_2 = 0.6214$ GHz/s. For both waveforms, the performance of the asymptotic time-delay estimation using both MC MLE with $N_{\text{MC}} = 100,000$ and CRLB depends on the bandwidth $B = 2bT$ of the waveform. Generally, the larger the bandwidth, the lower the CRLB. However, in Figure 3.8, we see a trade-off that occurs between asymptotic MSE and SINR threshold for the two different waveforms.

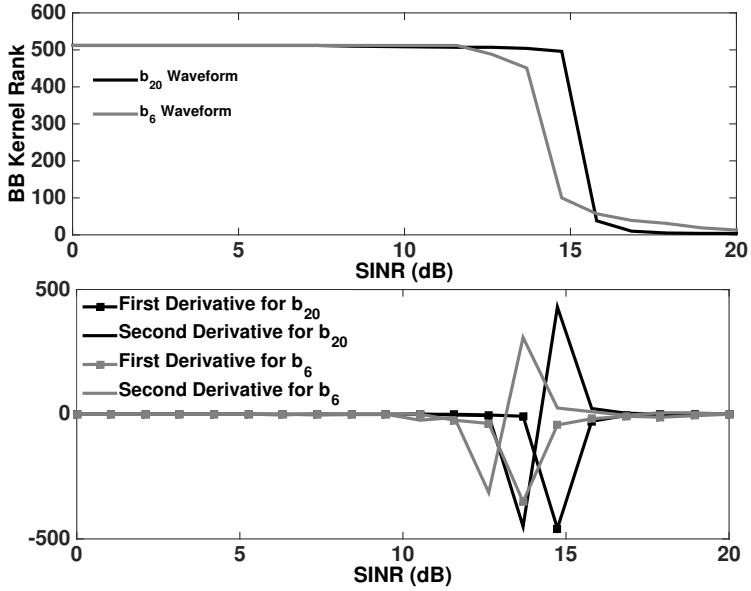

Figure 3.9: Rank of Kernel Matrix as a Function of SINR for Time-Delay Estimation.

Chapter 4

LOW SINR RADAR WAVEFORM DESIGN BASED ON BARANKIN BOUND

4.1 Radar Target Tracking Measurement Model

When a radar system coexists with a wireless communications system by sharing bandwidth, the radar target tracking performance is expected to decrease. The co-existence problem between the two systems is discussed in Section 2.1. Assuming a co-located receiver for both systems, the joint received waveform is a linear combination of the target return signal $x_r(t)$, the wireless communications signal $x_c(t)$, and additive white Gaussian noise (AWGN) $w(t)$. At the radar receiver, the unknown target parameters need to be estimated from the target return signal $x_r(t)$ and the communications signal $x_c(t)$ is seen as high power interference. As a result, the main objective of the radar receiver is to increase the target tracking performance under low signal-to-interference-plus-noise ratio (SINR) conditions.

We consider a pulse-Doppler radar receiver tracking a target in the presence of strong interference from an long term evolution (LTE) time division duplex (TDD) communications system. Assuming that a target is present under the given SINR operating conditions, the noisy complex baseband radar received signal is given by

$$r(t) = \sqrt{P_r}\, s(t-\tau;\mathbf{p})\; e^{-j2\pi\nu t} + v(t),\; t \in T_d \tag{4.1}$$

where $s(t;\mathbf{p})$ is the transmit signal that varies according to the parameter vector $\mathbf{p}$, T_d is the observation time window, and P_r is the power of the radar return. Assuming continuous multiple-user LTE TDD transmissions for both downlink and uplink, the zero-mean additive complex white Gaussian process $v(t)$ is the result of both the

measurement noise and the communications interference. The unknown target parameter vector $\boldsymbol{\theta} = [\tau \ \nu]^T$ consists of the target time delay τ and Doppler shift ν on the transmit signal $s(t; \mathbf{p})$, where T denotes vector transpose.

The radar receiver processing involves detecting the presence of a target and estimating its the unknown parameter vector $\boldsymbol{\theta}$. At high SINR, this estimation processing is performed using the ambiguity function (AF). The cross AF between the received signal $r(t)$ and the transmit signal $s(t)$ is defined as [81, 95]

$$A_{rs}(\tau, \nu; \mathbf{p}) = \int_{\mathbb{R}} r(t) s^*(t - \tau; \mathbf{p}) e^{j2\pi\nu t} dt \,. \tag{4.2}$$

The cross AF can be viewed as the inner product of the received signal $r(t)$ with the signal $s(t - \tau; \mathbf{p})e^{j2\pi\nu t}$ over a range of time delay and Doppler shifted for some $\tau \in [\tau_1, \tau_2]$ and $\nu \in [\nu_1, \nu_2]$, respectively. The auto AF, $A_s(\tau, \nu; \mathbf{p})$, is computed by letting $r(t) = s(t)$ in (4.2). An important property of the auto AF is that its maximum value always occurs at the origin of the (τ, ν) plane. Specifically,

$$|A_s(\tau, \nu; \mathbf{p})|^2 \leq |A_s(0, 0; \mathbf{p})|^2.$$

It is this property of the AF that is used to obtain maximum likelihood estimates (MLEs) of the range and range-rate. This is because, at high SINR, the MLEs of the time-delay and Doppler target parameters are obtained by maximizing the AF. In order to obtain the MLEs, we first expand the cross AF in (4.2) to obtain

$$\begin{aligned} A_{rs}(\tau, \nu; \mathbf{p}) = &= \int_{\mathbb{R}} \left(\sqrt{P_r}\, s(t - \tau_0; \mathbf{p})\, e^{-j2\pi\nu_0 t} + v(t) \right) s(t - \tau; \mathbf{p})\, e^{-j2\pi\nu t} dt \\ &= \int_{\mathbb{R}} \sqrt{P_r}\, s^*(t - \tau_0; \mathbf{p})\, e^{-j2\pi\nu_0 t} s^*(t - \tau; \mathbf{p})\, e^{-j2\pi\nu t} dt + v(\tau, \nu)\,, \end{aligned}$$

where the term $v(\tau, \nu)$ is a random process formed by the cross AF of $x_r(t)$ and $v(t)$. The first term corresponds to the AF of the transmitted signal, so the cross AF can

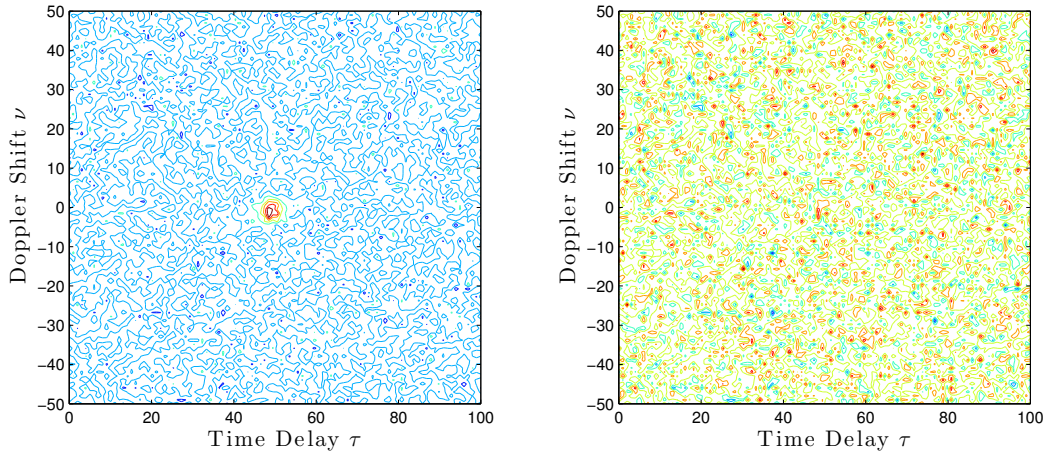

Figure 4.1: Example Measurement of $z(\tau, \nu)$ in (4.3) When the SINR is (left) 20 dB and (right) -10 dB.

be written as

$$z(\tau, \nu) = A_{rs}(\tau, \nu; \mathbf{p}) = \sqrt{P_r} A_s(\tau - \tau_0, \nu - \nu_0; \mathbf{p}) + v(\tau, \nu)\,. \tag{4.3}$$

If we maximize (4.3) over all τ and ν, we obtain

$$\{\tau_0, \nu_0\} = \arg \max_{\tau, \nu} A_{rs}(\tau, \nu; \mathbf{p})\,.$$

This follows from the fact that the peak of $A_s(\tau - \tau_0, \nu - \nu_0; \mathbf{p})$ in (4.3) occurs at $\tau = \tau_0$ and $\nu = \nu_0$ [81].

When the SINR is low, it is very difficult to locate the AF peak due to the high power of the communications interference. This is demonstrated in Figure 4.1 that provides the AF of measurement with 20 dB SINR (plot on the left) and -10 dB SINR (plot on the right). As it can be seen, it is not possible to locate the peak of the AF when the SINR is -10 dB, and a large estimation error is expected if the AF is used to obtain the time delay and Doppler MLEs.

Under low SINR conditions, unthresholded measurements in the form of an AF resolution cell measurement model are used for processing [59, 96]. This model is formed by computing the AF in (4.3) numerically as follows. Using sampling period T_s, we

obtain the discrete-time signal $s[n;\mathbf{p}] = s(nT_s;\mathbf{p})$, $n = 1,\ldots,N_s$, where N_s is the number of signal samples. We consider discrete time-delay bins $i\,\Delta_\tau$, $i = 1,\ldots,N_\tau$, and discrete Doppler bins $l\,\Delta_\nu$, $l \in \mathcal{D}$, $l = 1,\ldots,N_\nu$, where Δ_τ and Δ_ν correspond to the time-delay and Doppler shift values between consecutive bins, respectively, and N_τ and N_ν are the number of time-delay and Doppler shift bins, respectively. This AF measurement model $z(\tau,\nu)$ in (4.3), assuming a signal transmission at each time step k, is thus given in discrete form by

$$z_k[i,l] = z_k(i\,\Delta_\tau, l\,\Delta_\nu) = \sqrt{P_r}A_s(i\,\Delta_\tau - \tau_k, l\,\Delta_\nu - \nu_k;\mathbf{p}_k) + v(i\,\Delta_\tau, l\,\Delta_\nu)\,, \tag{4.4}$$

where τ_k and ν_k are the time-delay and Doppler shift unknown parameters at time step k. The discrete measurement model can also be written in matrix form as

$$\mathbf{Z}_k = \sqrt{P_r}\,\mathbf{A}(\boldsymbol{\theta}_k;\mathbf{p}_k) + \mathbf{V}_k \tag{4.5}$$

where the $(i\,l)$th element of $\mathbf{A}(\boldsymbol{\theta}_k;\mathbf{p}_k) \in \mathbb{C}^{N_\tau \times N_\nu}$ is the AF $A_s(i\,\Delta_\tau - \tau_k, l\,\Delta_\nu - \nu_k;\mathbf{p}_k)$ in (4.4) and the unknown parameter vector $\boldsymbol{\theta}_k = [\tau_k\ \nu_k]^T$ needs to be estimated to obtain the range and range rate of the target at each time step k. The $(i\,l)$th element of $\mathbf{V} \in \mathbb{C}^{N_\tau \times N_\nu}$ is $v(i\,\Delta_\tau, l\,\Delta_\nu)$ in (4.4); it is modeled as discrete AGWN with total power P_v. In vector form, (4.5) can be written as

$$\mathbf{z}_k = \sqrt{P_r}\,\mathbf{a}_{\boldsymbol{\theta}_k;\mathbf{p}_k} + \mathbf{v}_k \tag{4.6}$$

where $\mathbf{a}_{\boldsymbol{\theta}_k;\mathbf{p}_k} = \mathrm{vec}(\mathbf{A}(\boldsymbol{\theta}_k;\mathbf{p}_k))$ is obtained by concatenating the matrix columns of $\mathbf{A}(\boldsymbol{\theta}_k;\mathbf{p}_k)$; similarly, $\mathbf{z}_k = \mathrm{vec}(\mathbf{Z}_k)$ and $\mathbf{v}_k = \mathrm{vec}(\mathbf{V}_k)$.

4.2 Prediction of SINR Threshold for Radar Waveforms

4.2.1 SINR Threshold and Barankin Bound

The SINR threshold effect, presented in Chapter 2, is an important aspect for system design as it provides information on the SINR value at which a particular

estimation problem shows a sudden decrease in MSE performance. The MSE performance of an unbiased estimator depends on the SINR as well as on the transmit waveform and corresponding measurement model. For a given waveform, when the SINR decreases, the low SINR conditions cause a decrease in the probability of target detection and thus in the parameter estimation accuracy. The SINR threshold of a general, possibly nonlinear, estimate $\hat{\boldsymbol{\theta}}(\mathbf{z})$ of an unknown deterministic parameter $\boldsymbol{\theta}^{(0)}$ is defined conceptually as the value $\mathrm{SINR}_{\mathrm{thr}}$ at which the MSE of the estimator rapidly deviates from the CRLB. Specifically, the SINR threshold is a system parameter dependent SINR value at which the covariance of the estimator becomes very large and cannot be predicted using the CRLB.

In Chapter 3, we demonstrate the use of the BB effective rank matrix in predicting the SINR threshold. However, as the effective rank is computed using singular value decomposition (SVD) of the BB kernel, we cannot obtain it for all possible signals. We thus want to examine a different approach that directly uses the BB in order to predict the SINR threshold. In order to relate the SINR threshold with the BB, we compute various BB approximations for the frequency estimation problem from Section 3.1 and compare them to the MLE MSE and the CRLB. We thus consider the estimation of the unknown frequency $\theta^{(0)} = f^{(0)}$ using the noisy measurement

$$\mathbf{z} = \sqrt{P}\,\mathbf{s}\left(f^{(0)}\right) + \mathbf{w}$$

where $\mathbf{z} \in \mathbb{C}^{N_s}$, $\mathbf{s}(f^{(0)}) = [1 \; e^{j2\pi f^{(0)}} \; \ldots \; e^{j2\pi f^{(0)}(N_s-1)}]^T \in \mathbb{C}^{N_s}$ is the complex sinusoid vector, $\mathbf{w}$ is the circularly-symmetric complex AWGN vector with zero mean and covariance $\sigma_w^2\,\mathbf{I}_{N_s}$, and the measurement SINR is computed as P/σ_w^2. The MLE $\hat{f}_{\mathrm{ML}}$ of the unknown frequency is given in Equation (3.3). Also, when the actual frequency was $f^{(0)} = 0$, we showed in Section 3.1 that the MLE MSE deviated from the CRLB at around 4.44 dB SINR . In order to examine the effect of the BB for the same

problem, we computed the corresponding QCL BB approximation using $L = 2$ test points, the MS BB approximation using $L = 200$ test points, and the sampled integral equation (SIE) of the BB using 200 points uniformly sampled on the parameter space. These BB approximations are shown in Figure 4.2 for varying SINR values. It can be seen that the QCL BB approximation is much tighter than the MS and SIE BB approximations. The QCL BB is also much more computationally affordable for computing the MSE bound as it only uses 2 test points. When comparing the BB with the CRLB in the same figure, we see that both the BB and MLE start to deviate from the CRLB near the same SINR value. However, the BB provides a noticeably tighter bound than the MLE MSE in the threshold region. As such, the BB provides a better approach that the MLE in predicting the SINR threshold. We also notice that at high SINR, the relationship between the estimator MSE, BB, and CRLB is given by

$$\mathrm{MSE}_{\hat{f}_{\mathrm{ML}}(\mathbf{z})} \geq \mathrm{BB} \geq \mathrm{CRLB}$$

with approximate equality when SINR$\rightarrow \infty$.

In general, we can define three main estimation operating regions: the asymptotic region, the threshold region, and the no information region. This is visualized in Figure 4.3. It is not usually feasible for most problems to compute the SINR threshold from the MLE covariance. This is because to compute an accurate performance curve for the MLE, we normally require to use Monte Carlo methods as a function of SINR. As a result, we propose to use the BB as a method for computing the SINR threshold region.

For a general estimation problem with MSE matrix $\mathbf{MSE}_{\hat{\boldsymbol{\theta}}(\mathbf{z})}$ of a parameter estimate $\hat{\boldsymbol{\theta}}(\mathbf{z})$, the relationships between the bounds are given by

$$\mathbf{MSE}_{\hat{\boldsymbol{\theta}}(\mathbf{z})} \succeq \mathbf{BB} \succeq \mathbf{CRLB}\,.$$

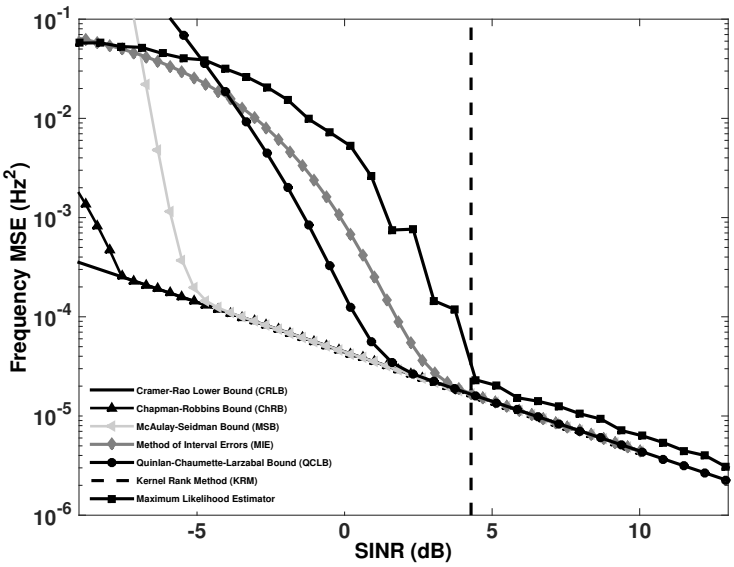

Figure 4.2: QCL BB Approximation with $L = 2$ Test Points Beyond the True Parameter Value with the Corresponding CRLB and MLE Estimator Variance for the Frequency Estimation Problem.

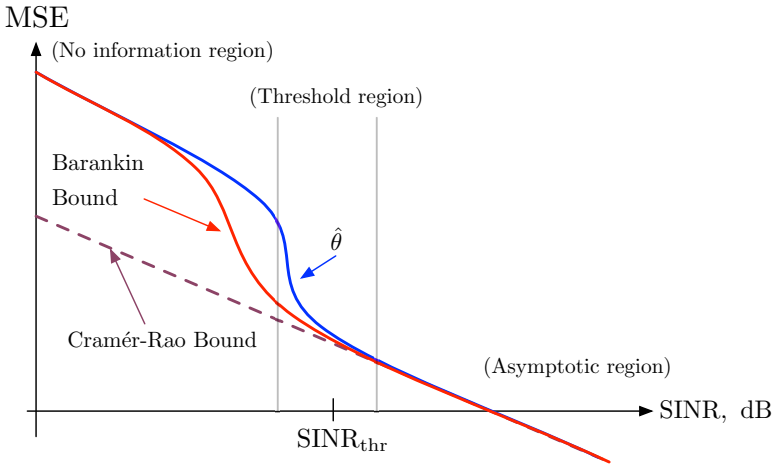

Figure 4.3: General Estimator and Bound Performance Curves, Demonstrating Three Estimation Operating Regions: Asymptotic Region, Threshold Region, and No Information Region.

The equality is achievable asymptotically at high SINR and/or large data record lengths. We can utilize this relationship to approximate the SINR threshold for an estimator by computing the deviation of the BB from the CRLB and finding the SINR value at which this deviation starts to increase (or equivalently, when the deviation

exceeds some $\epsilon > 0$). We define the deviation as a function of SINR as

$$\rho(\text{SINR}) = \frac{\text{tr}\left\{\mathbf{BB} - \mathbf{CRLB}\right\}}{\text{tr}\left\{\mathbf{CRLB}\right\}}.$$

We also define the set that defines the interval at which the deviation $\rho(\text{SINR})$ is less than some small constant ϵ as

$$\mathcal{A}_\epsilon = \left\{\text{SINR} \in \mathbb{R}_{++} : \rho(\text{SINR}) \leq \epsilon\right\}.$$

We then consider the SINR threshold value to be approximated as

$$\text{SINR}_{\text{thr}} = \arg \max_{\text{SINR} \in \mathcal{A}_\epsilon} \rho(\text{SINR})$$

which corresponds to the smallest SINR for which the BB starts to deviate from the CRLB. We demonstrate this using the frequency estimation example by plotting the deviation $\rho(\text{SINR})$ for $\epsilon = 0.01$; the value of ϵ was obtained empirically from simulations. The resulting plot is shown in Figure 4.4. We found that the SINR threshold using the BB based approach was 2.8 dB, which is comparable to the 4.44 dB threshold region obtained using the MLE.

4.2.2 Barankin Bound for Ambiguity Function Measurement Model

Considering the radar tracking problem discussed in Section 4.1, low SINR conditions are expected to reduce both the probability of target detection and parameter estimation accuracy. We thus want to predict the BB SINR threshold region in order to assess the estimation performance accuracy [45, 54, 84]. From the different BB approximations presented in Chapter 2, we use the QCL BB approximation as it results in a tighter bound than the other approximations and thus provides a more accurate estimate of the SINR threshold. Note that, even though the QCL BB approximation was presented in [51] for multiple unknown parameters in vector form, the example

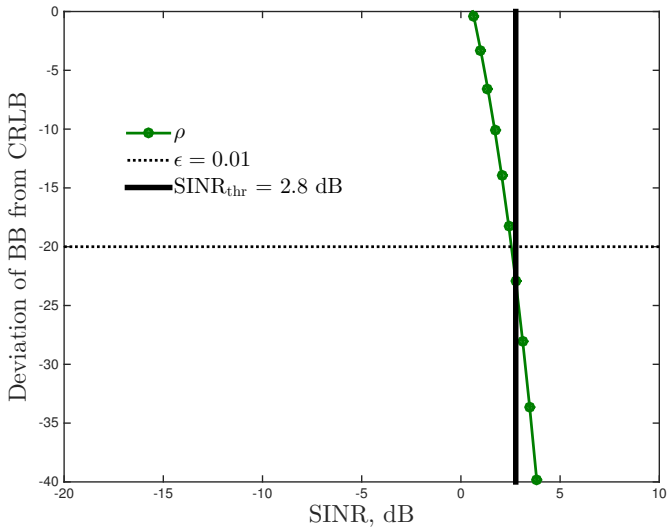

Figure 4.4: Characterization of SINR Threshold Value Using the Deviation of the BB From the CRLB with $\epsilon = 0.01$.

provided was for a single unknown frequency. We propose to compute the QCL BB approximation for the unknown target parameter vector $\boldsymbol{\theta}_k = \boldsymbol{\theta}$ in the radar problem, using the two-dimensional (2-D) AF resolution cell measurement model $\mathbf{a}_{\boldsymbol{\theta},\mathbf{p}}$ in Equation (4.6). Note that, to the best of our knowledge, an example of the QCL BB approximation has not been demonstrated before for an unknown parameter vector. For notational simplicity, we drop the dependence on the time step k.

BB Computation

Using Equation (4.6) and considering a set of L test points, $\{\boldsymbol{\theta}^{(1)}, \boldsymbol{\theta}^{(2)}, \ldots, \boldsymbol{\theta}^{(L)}\}$, where $\boldsymbol{\theta}^{(l)} = [\tau^{(l)}\ \nu^{(l)}]^T$, $l = 1, \ldots, L$, and $n_p = 2$, the BB $\in \mathbb{S}_{++}^{n_p}$ is given by [51]

$$\text{BB}_{\boldsymbol{\Theta},\eta,\,\mathbf{a}_{\boldsymbol{\theta},\mathbf{p}}} = \mathbf{H}_{\boldsymbol{\Theta}}^T\, \mathbf{K}_{\boldsymbol{\Theta},\eta,\,\mathbf{a}_{\boldsymbol{\theta},\mathbf{p}}}^{-1}\, \mathbf{H}_{\boldsymbol{\Theta}}\,. \tag{4.7}$$

Note that the subscript in the BB formulation in (4.7) emphasizes the dependence of BB on the AF $\mathbf{a}_{\boldsymbol{\theta},\mathbf{p}}$ in (4.6), the waveform parameter vector $\mathbf{p}$, the unknown target parameter vector $\boldsymbol{\theta}$, the test point set $\boldsymbol{\Theta} = \{\boldsymbol{\theta}^{(0)}, \boldsymbol{\theta}^{(1)}, \boldsymbol{\theta}^{(2)}, \ldots, \boldsymbol{\theta}^{(L)}\}$, and the SINR value η. Here, $\boldsymbol{\theta}^{(0)}$ is a particular $\boldsymbol{\theta}$ value and $\eta = P_r/\sigma_v^2$ is the SINR value. The

$3(L+1)\times 3(L+1)$ matrix $\mathbf{K}_{\boldsymbol{\Theta},\eta,\,\mathbf{a}(\boldsymbol{\theta};\mathbf{p})}$ in (4.7) is given by [70]

$$\mathbf{K}_{\boldsymbol{\Theta},\eta,\,\mathbf{a}_{\boldsymbol{\theta},\mathbf{p}}} = \begin{bmatrix} \mathbf{M}_{\boldsymbol{\Theta},\eta,\,\mathbf{a}_{\boldsymbol{\theta},\mathbf{p}}} & \mathbf{U}^T_{\boldsymbol{\Theta},\eta,\,\mathbf{a}_{\boldsymbol{\theta},\mathbf{p}}} \\ \mathbf{U}_{\boldsymbol{\Theta},\eta,\,\mathbf{a}_{\boldsymbol{\theta},\mathbf{p}}} & \mathbf{E}_{\boldsymbol{\Theta},\eta,\,\mathbf{a}_{\boldsymbol{\theta},\mathbf{p}}} \end{bmatrix}.$$

The dimensions of the sub-matrices $\mathbf{M}$, $\mathbf{U}$, and $\mathbf{E}$ are $(L+1)\times(L+1)$, $2(L+1)\times(L+1)$ and $2(L+1)\times 2(L+1)$, respectively. The $l\,l'$th element, $l,l'=1,\ldots,L$, of the reproducing kernel matrix $\mathbf{M}$ is [54]

$$[\mathbf{M}_{\boldsymbol{\Theta},\eta,\,\mathbf{a}_{\boldsymbol{\theta},\mathbf{p}}}]_{l\,l'} = \exp\left\{\eta\left(||\mathbf{a}_{\boldsymbol{\theta}^{(l)},\mathbf{p}} + \mathbf{a}_{\boldsymbol{\theta}^{(l')},\mathbf{p}} - \mathbf{a}_{\boldsymbol{\theta}^{(0)},\mathbf{p}})||_2^2 \right.\right. \\ \left.\left. -||\mathbf{a}_{\boldsymbol{\theta}^{(l)},\mathbf{p}}||_2^2 - ||\mathbf{a}_{\boldsymbol{\theta}^{(l')},\mathbf{p}}||_2^2 + ||\mathbf{a}_{\boldsymbol{\theta}^{(0)},\mathbf{p}}||_2^2\right)\right\},$$

where $||\mathbf{u}||_2^2 = \langle \mathbf{u},\mathbf{u}\rangle$ and $\langle \mathbf{u},\mathbf{v}\rangle = \mathbf{u}^T\mathbf{v}$ is the inner product between vectors $\mathbf{u}$ and $\mathbf{v}$. Matrix $\mathbf{E}$ extends the Fisher information matrix [44] to incorporate the L test points beyond the particular value $\boldsymbol{\theta}^{(0)}$. Its $l\,l'$th element, $l,l'=1,\ldots,L$, is also a matrix, with i,jth element, $i,j=1,\ldots,L$, given by

$$[\,[\mathbf{E}_{\boldsymbol{\Theta},\eta,\,\mathbf{a}_{\boldsymbol{\theta},\mathbf{p}}}]_{l\,l'}\,]_{i,j} = \eta\,[\mathbf{M}_{\boldsymbol{\Theta},\eta,\,\mathbf{a}_{\boldsymbol{\theta},\mathbf{p}}}]_{l\,l'}\left(\left\langle \frac{\partial\,\mathbf{a}_{\boldsymbol{\theta}^{(l')},\mathbf{p}}}{\partial\boldsymbol{\theta}^{(i)}}, \frac{\partial\,\mathbf{a}_{\boldsymbol{\theta}^{(l)},\mathbf{p}}}{\partial\boldsymbol{\theta}^{(j)}}\right\rangle + \right. \\ \eta\left\langle (\mathbf{a}_{\boldsymbol{\theta}^{(l')},\mathbf{p}} - \mathbf{a}_{\boldsymbol{\theta}^{(0)},\mathbf{p}}), \frac{\partial\,\mathbf{a}_{\boldsymbol{\theta}^{(l)},\mathbf{p}}}{\partial\boldsymbol{\theta}^{(i)}}\right\rangle \\ \left.\left\langle (\mathbf{a}_{\boldsymbol{\theta}^{(l)},\mathbf{p}} - \mathbf{a}_{\boldsymbol{\theta}^{(0)},\mathbf{p}}), \frac{\partial\,\mathbf{a}_{\boldsymbol{\theta}^{(l')},\mathbf{p}}}{\partial\boldsymbol{\theta}^{(j)}}\right\rangle\right).$$

Matrix $\mathbf{U}$ contains cross terms between the entries of $\mathbf{M}$ and $\mathbf{E}$; its $l\,l'$th element, $l,l'=1,\ldots,L$, is a vector with ith element, $i=1,\ldots,L$, given by

$$[\,[\mathbf{U}_{\boldsymbol{\Theta},\eta,\,\mathbf{a}_{\boldsymbol{\theta},\mathbf{p}}}]_{l\,l'}\,]_i = \eta\,[\mathbf{M}_{\boldsymbol{\Theta},\eta,\,\mathbf{a}_{\boldsymbol{\theta},\mathbf{p}}}]_{l\,l'}\left\langle (\mathbf{a}_{\boldsymbol{\theta}^{(l')},\mathbf{p}} - \mathbf{a}_{\boldsymbol{\theta}^{(0)},\mathbf{p}}), \frac{\partial\,\mathbf{a}_{\boldsymbol{\theta}^{(l)},\mathbf{p}}}{\partial\boldsymbol{\theta}^{(i)}}\right\rangle.$$

The $3(L+1)\times 2$ matrix $\mathbf{H}_{\boldsymbol{\Theta}}$ in (4.7) is given by

$$\mathbf{H}_{\boldsymbol{\Theta}} = \left.\begin{bmatrix} (\boldsymbol{\theta}^{(0)} - \boldsymbol{\theta}^{(0)})^T \\ (\boldsymbol{\theta}^{(1)} - \boldsymbol{\theta}^{(0)})^T \\ \vdots \\ (\boldsymbol{\theta}^{(L)} - \boldsymbol{\theta}^{(0)})^T \\ \mathbf{I}_2 \\ \vdots \\ \mathbf{I}_2 \end{bmatrix}\right\} (L+1) \text{ times}$$

where $\mathbf{I}_2$ is the identity matrix of dimension 2.

Test Point Selection

The tightness of the BB bound depends on the selection of the test points $\boldsymbol{\theta}^{(l)} = [\tau^{(l)}\ \nu^{(l)}]^T$, $l = 1, \ldots, L$, as well as the number L of test points [66, 74]. Although any set of test points inside the parameter space can be selected [51, 70, 73], we select points at the boundary corners of the support $[-\tau_b, \tau_b]\times[-\nu_b, \nu_b]$ of the AF resolution cell. These boundary points were found to maximize the BB as they reflect maximum outliers in the parameter space. In our computation, we continue to increase the number of points L until there is no significant gain in the tightness of the bound [80]. Note that L affects the dimensionality of matrix $\mathbf{K}$ in (4.7). As this matrix needs to be inverted, increasing L also increases the computational cost of the BB.

4.2.3 Radar Waveform SINR Threshold Prediction

Computation of SINR Threshold

As the BB is the greatest lower bound of the MSE of any unbiased estimator of

deterministic parameters, over all possible values of $\boldsymbol{\theta}$, it can be shown that

$$\mathrm{MSE}_{\hat{\boldsymbol{\theta}},\eta,\mathbf{a}_{\boldsymbol{\theta},\mathbf{p}}} \succeq \mathrm{BB}_{\boldsymbol{\Theta},\eta,\,\mathbf{a}_{\boldsymbol{\theta},\mathbf{p}}} \succeq \mathrm{CRLB}_{\eta,\mathbf{a}_{\boldsymbol{\theta},\mathbf{p}}} \tag{4.8}$$

where $\hat{\boldsymbol{\theta}}$ is an unbiased estimate of $\boldsymbol{\theta}$. Given the AF resolution cell measurement model $\mathbf{a}_{\boldsymbol{\theta},\mathbf{p}}$ at SINR value η, the CRLB in (4.8) is computed as the inverse of the Fisher information matrix. The MSE is obtained as

$$\mathrm{MSE}_{\hat{\boldsymbol{\theta}},\eta,\mathbf{a}_{\boldsymbol{\theta},\mathbf{p}}} = \int_{\mathbf{z}} (\hat{\boldsymbol{\theta}} - \boldsymbol{\theta}^{(0)})(\hat{\boldsymbol{\theta}} - \boldsymbol{\theta}^{(0)})^T p(\mathbf{z};\boldsymbol{\theta}^{(0)})\; d\mathbf{z}\,,$$

where $p(\mathbf{z};\boldsymbol{\theta}^{(0)})$ is the probability density function of the measurement $\mathbf{z}$ in (4.6) for fixed SINR value η and particular parameter value $\boldsymbol{\theta}^{(0)}$.

The MSE in (4.8) achieves the CRLB only under asymptotic conditions, such as high SINR or large data records. Under these conditions, the unbiased estimator is characterized by three different operating regions: asymptotic, threshold , and no information regions (shown in Figure 4.3). From these regions, it is important to be able to estimate an SINR threshold of a particular waveform in order to obtain information on the waveform's expected MSE performance. We propose to approximate an SINR threshold using the BB and the CRLB, following the relation in (4.8). We first compute the deviation of the BB from the CRLB for a waveform with fixed parameter vector $\mathbf{p}$ as

$$\rho_{\eta,\mathbf{a}_{\boldsymbol{\theta},\mathbf{p}}} = \frac{\mathrm{tr}\{\mathrm{BB}_{\boldsymbol{\Theta},\eta,\,\mathbf{a}_{\boldsymbol{\theta},\mathbf{p}}} - \mathrm{CRLB}_{\eta,\mathbf{a}_{\boldsymbol{\theta},\mathbf{p}}}\}}{\mathrm{tr}\{\mathrm{CRLB}_{\eta,\mathbf{a}_{\boldsymbol{\theta},\mathbf{p}}}\}}\,, \tag{4.9}$$

where $\mathrm{tr}\{\cdot\}$ denotes the trace of a matrix. The SINR threshold is selected as the SINR value $\eta \in \mathcal{A}_\epsilon$ at which the deviation is as small as possible. We thus set $\rho_{\eta,\mathbf{a}_{\boldsymbol{\theta},\mathbf{p}}} \leq \epsilon$, for small $\epsilon > 0$, and obtain the SINR threshold η_{thr} as

$$\eta_{\mathrm{thr}}(\mathbf{p}) = \arg\max_{\eta\in\mathcal{A}_\epsilon} \rho_{\eta,\mathbf{a}_{\boldsymbol{\theta},\mathbf{p}}}\,, \tag{4.10}$$

which corresponds to the smallest SINR value at which the BB starts to depart from the CRLB. An example of computing the deviation for a sinusoid signal with $\epsilon = 0.01$ is depicted in Figure 4.4.

Radar Transmit Waveform and SINR Threshold

We assume that the radar transmit signal in (4.1) at time step k is a nonstationary signal with nonlinear time-varying phase function $\xi_k(t/t_r)$ and given by [95]

$$s(t; \mathbf{p}_k) = \psi(t)\, e^{j2\pi b_k\, \xi_k(t/t_r)},\ t \in (0, \lambda_k)\,. \tag{4.11}$$

Here, $t_r > 0$ is a reference time and $\psi(t)$ is a (possibly) time-varying amplitude modulation (AM) that is selected such that the signal has unit energy. The parameter vector $\mathbf{p}_k = [\lambda_k\ b_k]^T$ consists of the signal duration λ_k and the frequency modulation (FM) rate b_k at time step k.

We computed the SINR threshold in (4.10) for two waveforms with nonlinear phase function $\xi(t/t_r)$ in (4.11). Specifically, we considered the linear frequency-modulated (LFM) waveform with quadratic phase function $\xi(t/t_r) = (t/t_r)^2$ and the hyperbolic frequency-modulated (HFM) waveform with logarithmic phase function $\xi(t/t_r) = \ln(t/t_r)$. The unit energy LFM waveform, with Gaussian window AM, is given by

$$s(t; \mathbf{p}) = (2\pi\lambda)^{-0.5}\, e^{-(t/t_r)^2/(2\lambda^2)}\ e^{j2\pi b(t/t_r)^2}\,, \tag{4.12}$$

and the HFM, with rectangular window AM, is given by

$$s(t; \mathbf{p}) = e^{j2\pi b \ln(t/t_r)}, \quad t \in (0, \lambda)\,. \tag{4.13}$$

An example of a noisy LFM radar signal embedded in high-power communications interference with 2.2 dB SINR is demonstrated in Figure 4.5. As shown, both the

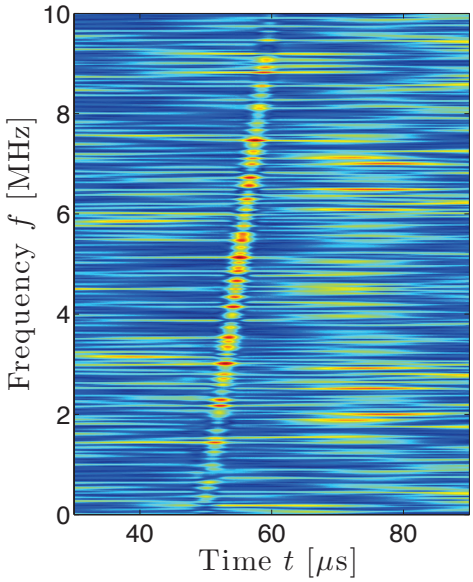

Figure 4.5: LFM Radar Waveform Embedded in 2.2 dB SINR Communications Interference.

communications signal and the the radar transmit signal coexist in the same time-frequency space.

The SINR threshold for the LFM in (4.12) was computed as a function of its duration and time-bandwidth product (TBP) as well as the asymptotic MSE for high SINR. The result is shown in Figure 4.6. We notice that there exists an inverse relationship between SINR threshold and asymptotic variance for this particular signal model. This inverse relationship has been pointed out for a few different applications such as direction-of-arrival vector array estimation for the spacing between the elements [63]. A few other cases where this effect occurs is discussed in [46, 56] for other applications.

We expect that the SINR threshold affects the tracking algorithm when the transmitted waveform is not designed for low SINR situations. We know from the previous section that the SINR threshold occurs at a higher SINR for higher resolution waveforms. For example, if we consider a TBP of 100 and a duration of $\lambda = 10$ μs for the HFM and LFM, for which we know that the HFM is a higher resolution waveform

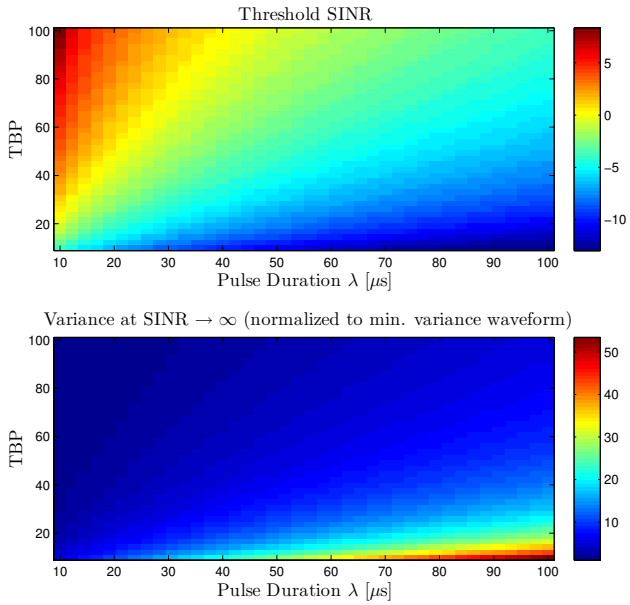

Figure 4.6: SINR Threshold as a Function of the LFM Signal Duration and TBP, Demonstrating an Inverse Relationship Between SINR Threshold and Asymptotic MSE Performance for Each Waveform.

then we expect that the threshold SINR is higher. Indeed, this is the case as can be seen in both the BB and CRLBs shown in Figure 4.7 and the corresponding threshold SINRs shown in Figure 4.13.

Barankin Bound Based Waveform Design

As we are considering very low SINR tracking scenarios due to the presence of high power interference, the measurement model in (4.6) can greatly affect the estimation performance of the targets position and velocity. We propose to select the radar transmit waveform using the deviation of the BB from the CRLB. Specifically, at each time step k, we compute the deviation in (4.9) for a dictionary of J available waveforms $s(t;\mathbf{p}_k^{(j)})$ in (4.11), $j = 1,\ldots,J$, with phase function $\xi_k(t/t_r)$ and varying parameter vector $\mathbf{p}_k^{(j)} = [\lambda_k^{(j)}\ b_k^{(j)}]^T$. Emphasizing its dependence on the jth dictionary waveform with parameter vector $\mathbf{p}_k^{(j)}$, the corresponding SINR threshold $\eta_{\text{thr}}(\mathbf{p}_k^{(j)})$ can be com-

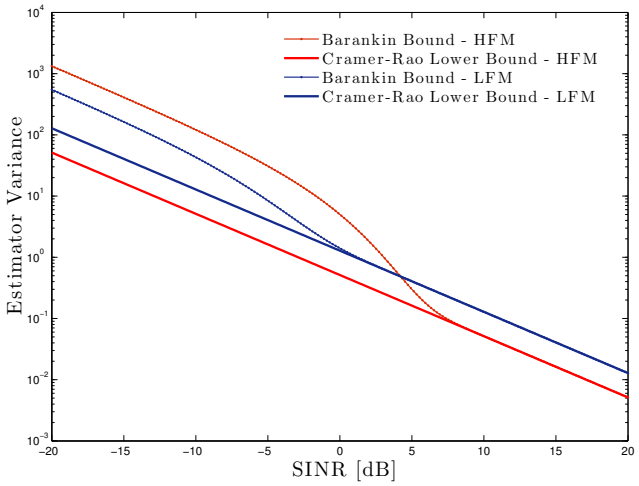

Figure 4.7: BB and CRLB for a Fixed 100 TBP and 10 μs Duration for the HFM and LFM Waveforms.

puted for all waveforms in the dictionary using (4.10). Then, the selected transmit waveform $s(t;\hat{\mathbf{p}}_k)$ is the one with the minimum SINR threshold value. Specifically,

$$s(t;\hat{\mathbf{p}}_k) = \arg \min_{j=1,\ldots,J} \ \eta_{\text{thr}}(\mathbf{p}_k^{(j)}) \,. \tag{4.14}$$

4.3 Low SINR Target Tracking

4.3.1 Target Tracking Formulation

The overall measurement equation for the target tracking formulation includes the measurement in (4.6) with waveform parameter vector $\hat{\mathbf{p}}_k$ in (4.14) and a bearing angle measurement from a noisy linear observation. Assuming a single target moving at a constant velocity in two dimensions, the unknown target state vector $\mathbf{x}_k = [x_k \ y_k \ \dot{x}_k \ \dot{y}_k]^T$ consists of the Cartesian coordinates for the target's position and velocity are (x_k, y_k) and $(\dot{x}_k, \dot{y}_k)$, respectively. The state equation is thus linear and given by $\mathbf{x}_k = \mathbf{F}\,\mathbf{x}_{k-1} + \mathbf{u}_{k-1}$, where $\mathbf{F}$ describes the state transition following the constant velocity model and $\mathbf{u}_k$ is a modeling error random process.

The AF resolution cell measurement model at time step k is given in (4.6). In

addition to the time-delay and Doppler, we also include a bearing angle measurement given by

$$a_k = \phi_k + \beta_k \tag{4.15}$$

where ϕ_k is a linear observation and β_k is zero-mean AWGN with variance σ_β^2. The overall measurement model is given by

The measurements are related to the unknown state vector $\mathbf{x}_k$ using

$$\begin{aligned} \tau_k &= \frac{2}{c_0}\sqrt{x_k^2 + y_k^2} && (4.16)\\ \nu_k &= \frac{2f_c\left(x_k\dot{x}_k + y_k\dot{y}_k\right)}{c_0\sqrt{x_k^2 + y_k^2}} && (4.17)\\ \phi_k &= \arctan\left(y_k/x_k\right) && (4.18) \end{aligned}$$

where $c_0 = 3 \times 10^8$ m/s is the speed of electromagnetic propagation in free space and f_c is the signal carrier frequency in Hz. For the purposes of tracking, we process the joint measurement of the AF and the bearing measurement as the combined vector

$$\begin{aligned} \begin{bmatrix} \mathbf{z}_k \\ b_k \end{bmatrix} &= \begin{bmatrix} \sqrt{P_r}\mathbf{a}_{\boldsymbol{\theta}_k;\mathbf{p}_k} + \mathbf{v}_k \\ \phi_k + \beta_k \end{bmatrix} \\ &= \mathbf{h}(\mathbf{x}_k, \mathbf{p}_k, \mathbf{v}_k, \beta_k). \end{aligned}$$

where the state $\mathbf{x}_k$ has been mapped through the nonlinear relationships in (4.16)-(4.18) via the AF and the bearing measurement equation in (4.15). It is assumed that the state transition matrix for the target motion is given by

$$\mathbf{F} = \begin{bmatrix} 1 & 0 & T_{\text{CPI}} & 0 \\ 0 & 1 & 0 & T_{\text{CPI}} \\ 0 & 0 & 1 & 0 \\ 0 & 0 & 0 & 1 \end{bmatrix}$$

where T_{CPI} representing the coherent processing interval (CPI) of the radar at CPI time step k and $k-1$ and the process noise $\mathbf{u}_k$ is assumed to follow a zero mean Gaussian noise acceleration model [90] with covariance matrix

$$\boldsymbol{\Sigma}_u = i_p \begin{bmatrix} \frac{T_{\text{CPI}}^3}{3} & 0 & \frac{T_{\text{CPI}}^2}{2} & 0 \\ 0 & \frac{T_{\text{CPI}}^3}{3} & 0 & \frac{T_{\text{CPI}}^2}{2} \\ \frac{T_{\text{CPI}}^2}{2} & 0 & T_{\text{CPI}} & 0 \\ 0 & \frac{T_{\text{CPI}}^2}{2} & 0 & T_{\text{CPI}} \end{bmatrix}$$

and i_p denotes the process noise intensity.

4.3.2 Measurement Model for Waveforms with Nonlinear Phase

For a given signal $s(t;\mathbf{p})$, it is not always possible to provide a closed form expression of the AF using the integral in (4.2). For the Gaussian windowed linear frequency-modulated (LFM) signal defined as

$$s(t;\mathbf{p}) = \exp\Big(-\frac{t^2}{2T^2}\Big)\,\exp\left(j2\pi b\, t^2\right),$$

with parameter vector $\mathbf{p} = [T\; b]^T$, the AF can be obtained in closed form as

$$A_s(\tau,\nu;\mathbf{p}) = \exp\left(-\frac{\tau^2}{2T^2} - \frac{T^2\left(\nu - 2b\tau\right)^2}{2}\right).$$

For sampled τ and ν values, the AF can be written in matrix form, $\mathbf{A}(\tau,\nu;\mathbf{p})$, to fit the measurement model.

However, the AF cannot be obtained in closed form for the general frequency-modulated signal,

$$s(t;\mathbf{p}) = \psi(t)e^{j2\pi\beta\xi(t/t_r)}, \tag{4.19}$$

that has arbitrary nonlinear phase function $\xi(t/t_r)$. Here, $t_r > 0$ is a reference time point and $\psi(t)$ is a time-varying amplitude modulation function. Some examples of

$\xi(t/t_r)$ in (4.19) include the phase function

$$\xi(t/t_r) = \ln(|t/t_r|)$$

that corresponds to a hyperbolic frequency-modulated (HFM) signal and

$$\xi(t/t_r) = \sum_{\kappa} \alpha_\kappa (t/t_r)^\kappa$$

that corresponds to a power series frequency-modulated (PFM).

The AF of these signals is approximated numerically, following the discrete formulation in (4.4) for some time-delay τ_k and Doppler shift ν_k. In particular, given a discrete-time signal $s[n;\mathbf{p}_k] = s(nT_s;\mathbf{p}_k)$, $n = 1,\ldots,N_s$, where T_s is the sampling period and N_s is the number of signals samples, we compute the AF in matrix form as

$$\mathbf{A}(\tau_k,\nu_k;\mathbf{p}_k) = \boldsymbol{\Omega}\,\boldsymbol{\Xi}(\tau_k,\nu_k;\mathbf{p}_k) \tag{4.20}$$

where the ilth element of matrix $\mathbf{A}(\tau_k,\nu_k;\mathbf{p}_k) \in \mathbb{C}^{N_\tau \times N_\nu}$ is $A_s(i\,\Delta_\tau - \tau_k, l\,\Delta_\nu - \nu_k;\mathbf{p}_k)$, $i = 1,\ldots,N_\tau$ and $l = 1,\ldots,N_\nu$. The discrete Fourier transform (DFT) matrix $\boldsymbol{\Omega} \in \mathbb{C}^{N_\nu \times N_s}$ in (4.20) is given by

$$\boldsymbol{\Omega} = \begin{bmatrix} e^{j2\pi\Delta_\nu} & e^{j2\pi\Delta_\nu 2} & \cdots & e^{j2\pi\Delta_\nu N_s} \\ \vdots & \vdots & \ddots & \vdots \\ e^{j2\pi N_\nu\Delta_\nu} & e^{j4\pi N_\nu\Delta_\nu 2} & \cdots & e^{j2\pi N_\nu\Delta_\nu N_s} \end{bmatrix}.$$

The matrix $\boldsymbol{\Xi}(\tau_k,\nu_k;\mathbf{p}_k) \in \mathbb{C}^{N_s \times N_\tau}$ in (4.20) is given by

$$\boldsymbol{\Xi}(\tau_k,\nu_k;\mathbf{p}_k) = \begin{bmatrix} \cdots \mathbf{s}(\boldsymbol{\theta}_k;\mathbf{p}_k) \odot \mathbf{s}_{i-1}(\mathbf{p}_k) & \mathbf{s}(\boldsymbol{\theta}_k;\mathbf{p}_k) \odot \mathbf{s}_i(\mathbf{p}_k) & \mathbf{s}(\boldsymbol{\theta}_k;\mathbf{p}_k) \odot \mathbf{s}_{i+1}(\mathbf{p}_k) \cdots \end{bmatrix}$$

where $\odot$ represents a Hadamard product (element-wise multiplication), $\mathbf{s}(\boldsymbol{\theta}_k;\mathbf{p}_k) \in$

$\mathbb{C}^{N_s}$ is given by

$$\mathbf{s}(\boldsymbol{\theta}_k; \mathbf{p}_k) = \begin{bmatrix} s(T_s - \tau_k; \mathbf{p}_k)\, e^{-j2\pi\nu_k} \\ s(2T_s - \tau_k; \mathbf{p}_k]\, e^{-j2\pi\nu_k 2} \\ \vdots \\ s(N_s T_s - \tau_k; \mathbf{p}_k)\, e^{-j2\nu_k N_s} \end{bmatrix}.$$

and $\mathbf{s}_i(\mathbf{p}_k) \in \mathbb{C}^{N_s}$ is given by

$$\mathbf{s}_i(\mathbf{p}_k) = \begin{bmatrix} s(T_s - i\Delta(\tau); \mathbf{p}_k) \\ s(2T_s - i\Delta(\tau); \mathbf{p}_k) \\ \vdots \\ s(N_s T_s - i\Delta(\tau); \mathbf{p}_k) \end{bmatrix}.$$

We implemented the AF using (4.20) for an Gaussian windowed LFM signal and a rectangular windowed HFM signal; the corresponding AF plots for comparison are shown in Figure 4.8 and Figure 4.9, respectively. The two signals show a trade off in resolution in the (τ, ν) plane. In general, the AF resolution increases with the number of AF side-lobes for a particular signal. In this example, the HFM signal is shown to have higher estimation performance for the time-delay and Doppler shift parameters at high SINR than the LFM signal. Based on design considerations, a signal experiences these trade-offs in different ways based on its amplitude modulation, duration, FM rate and phase function.

4.3.3 Integration of Waveform Design With Track-Before-Detect

Due to the low SINR conditions, we use a TBD tracker is implemented using a PF that was discussed in Section 2.3.2 using Equations (2.66)-(2.73). The TBD-PF initiates tracking iterations by a set of possible tracks that depend on the unthresholded AF measurement. For the single target, we assumed a two-state Markov chain of order one to describe the probability of the target entering or leaving the field-of-view

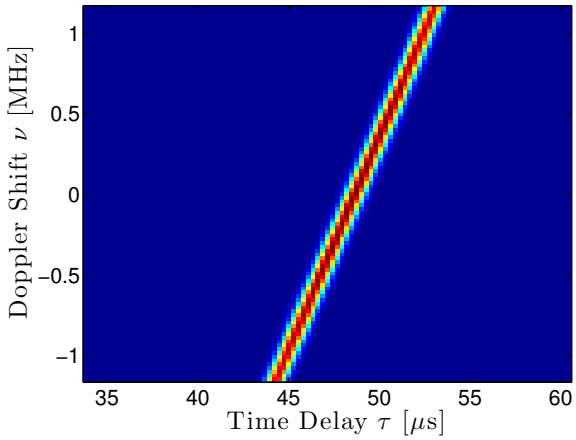

Figure 4.8: AF for a Gaussian Windowed LFM Signal.

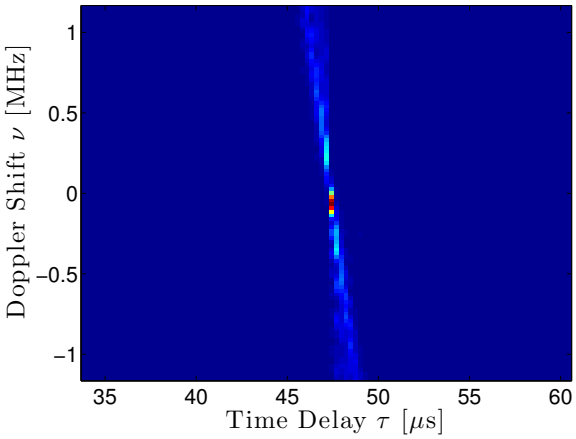

Figure 4.9: AF for a Rectangular Windowed HFM Signal.

(FOV) at each time step k [90]. Using the selected waveform $s(t; \hat{\mathbf{p}}_k)$ and integrating with a TBD-PF tracker, we were able to improve the SINR limit of applicability from -6 dB to -8 dB.

In order to demonstrate the estimation performance for the Gaussian windowed LFM and the rectangular windowed HFM we simulate them at high SINR (6 dB) and use them to track a target using the TBD-PF. Both signals have the same duration of 10 μs and time-bandwidth product (TBP) of 100. The resulting MSE performance is shown in Figure 4.10 as a function of the actual time step. As it can be seen, the MSE is lower for the HFM at every time step.

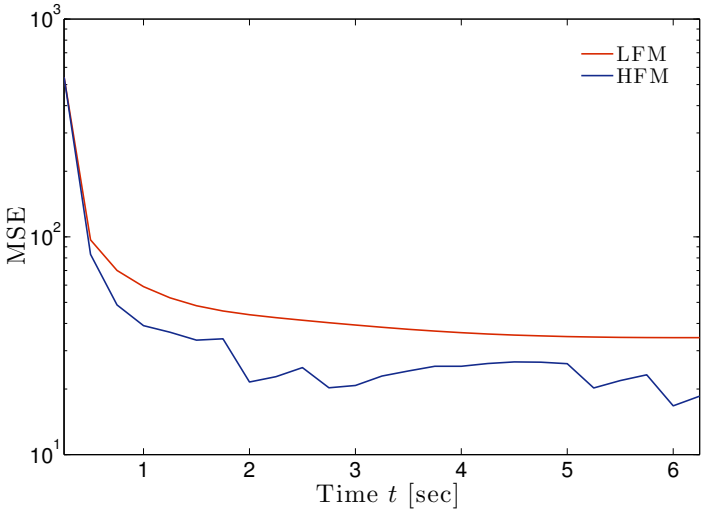

Figure 4.10: MSE Performance of TBD-PF for an HFM and LFM; Both signals have a 10 μs duration and 100 TBP.

We also demonstrated the TBD-PF performance when using only LFM signals but with different parameters. Figures 4.11 and 4.12 show the effect of the particle spread when estimating the target track in the (x, y)-plane using the TBD-PF algorithm and an LFM signal with TBP 10 and 100, respectively; both signals have the same 10 μs duration.

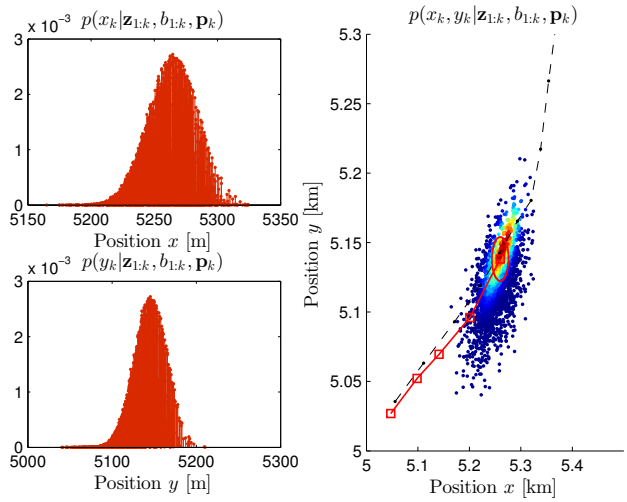

Figure 4.11: Effect on the Tracker Particle Spread in the TBD-PF Algorithm with a Gaussian Windowed LFM Simulated Transmit Waveform With 10 μs duration and 10 TBP.

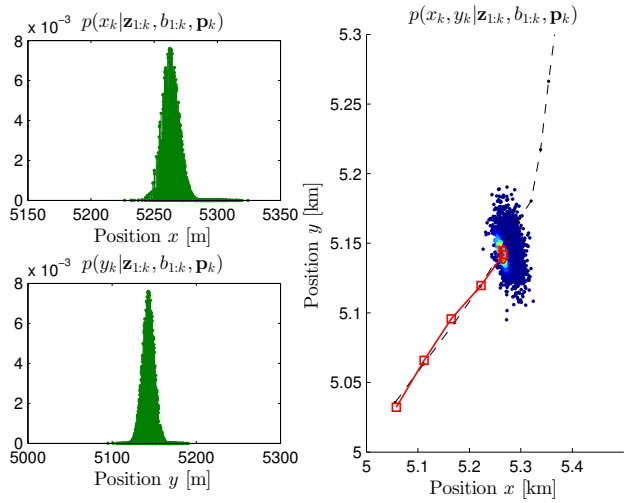

Figure 4.12: Effect on the Tracker Particle Spread in the TBD-PF Algorithm with a Gaussian Windowed LFM Simulated Transmit Waveform With 10 μs duration and 100 TBP.

Before, we saw intuitively from the AF that the HFM has a higher resolution compared to the LFM, so we naturally expect that the CRLB will predict the MSE to be lower for the HFM and higher for the LFM. However, due to the inverse relationship with the SINR threshold, if the HFM is operated below its SINR threshold then the MSE should not be expected to be the best. We now demonstrated this with an example using the TBD-PF algorithm. If we apply this to the TBD-PF algorithm and simulate the tracker at an SINR of 3 dB which is below the HFM's threshold SINR and we also run the same scenario for the LFM we indeed find that the MSE performance is much worse for the HFM. This is demonstrated in Figure 4.15. We compare this to the MSE performance shown in Figure 4.10 where the HFM performs better when the conditions were slightly better at an SINR of 6 dB which is above the expected SINR threshold. Thus, we have a trade-off between SINR threshold and asymptotic (high SINR) MSE performance for tracking.

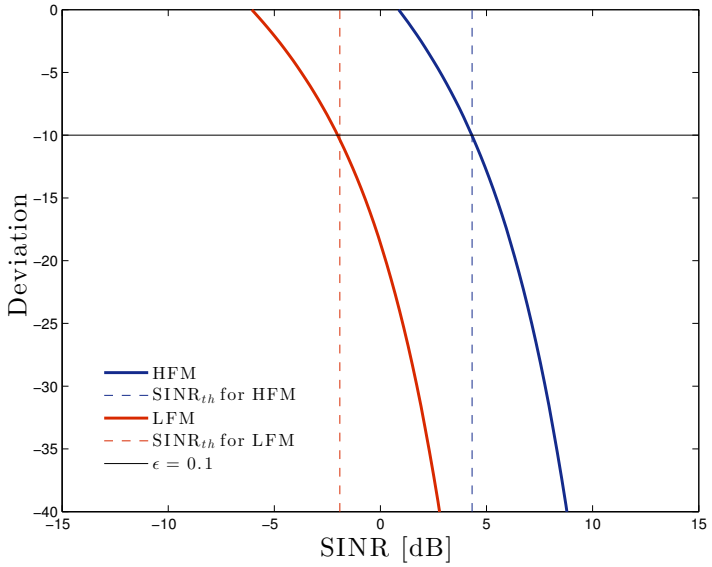

Figure 4.13: Deviations and SINR Threshold for a Fixed TBP of 100 and a Duration of $\lambda = 10$ μs for the HFM and LFM Radar Waveforms.

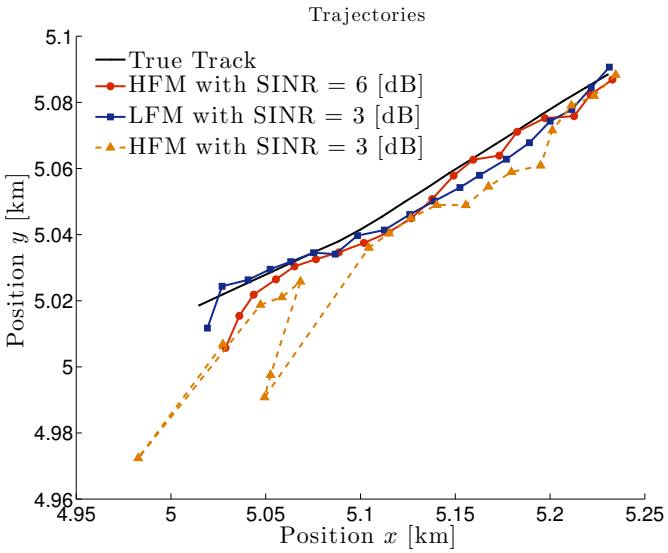

Figure 4.14: Effect of Chosen Waveform Depends on the Operating SINR. Here the HFM SINR Threshold is Higher Than the Current Tracking Operating Point so Performance Starts to Deteriorate.

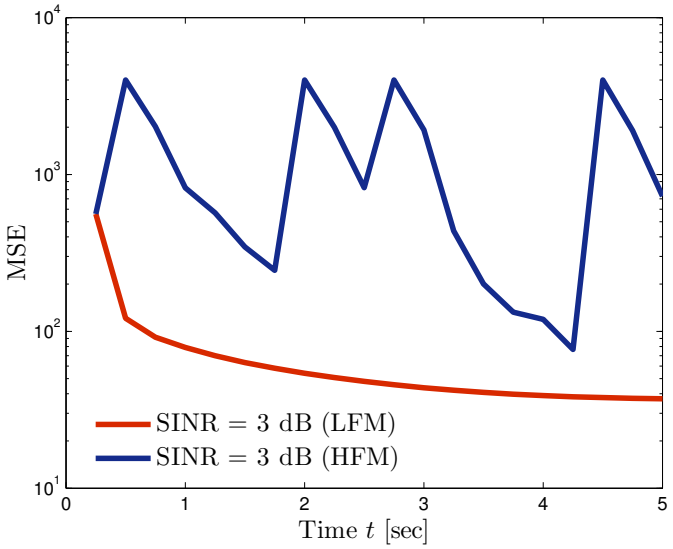

Figure 4.15: Effect of Selected Waveform Depends on the Operating SINR. Here We Show the MSE for the HFM Below its SINR Threshold and the LFM MSE at the Same SINR.

Chapter 5

JOINT WAVEFORM CO-DESIGN FOR COMMUNICATIONS AND RADAR

5.1 Design of Waveforms with Nonlinear Frequency-Modulation

One possible method for radar and communications systems to share the same spectrum is to also share the same type of signaling scheme. The co-design can involve waveforms with the same phase function but varying parameters that can be designed to minimize the interference between the two systems or to optimize other system performance metrics. Radar performance metrics can include mean-squared-error (MSE) of target parameter estimation, range resolution, and transmitter blind-zone. For a communications system, metrics can include spectral efficiency or gross bit rate.

We consider first a simple co-design signaling scheme for a pulse-Doppler radar system that emits a single pulse and a communications system with a single user. Both systems share the same bandwidth B. In complex baseband, we assume that the radar signal $s_{r,B}(t)$ and the communications signal $s_{c,B}(t)$ are both nonlinear frequency-modulated (NLFM) signals given by

$$s_{r,B}(t) = a_r(t)\, e^{j2\pi b_r\, \xi(t/t_r)}$$

$$s_{c,B}(t) = a_c(t)\, e^{j2\pi b_c\, \xi(t/t_r)}$$

where $a_r(t) \in \mathbb{R}$ and $a_c(t) \in \mathbb{R}$ are potentially time-varying amplitude modulation functions, and both signals have the same phase function $\xi(t/t_r)$, with normalizing time constant $t_r > 0$. The radar signal is assumed to have duration T_r and frequency-modulation (FM) rate b_r, whereas the communications signal has duration T_c and FM rate b_c; both signals are also assumed to have unit energy.

The NLFM phase function $\xi(t/t_r)$ can simplify to a variety of signals, including a complex sinusoid with $\xi(t/t_r) = t/t_r$, a linear frequency-modulated (LFM) signal with $\xi(t/t_r) = (t/t_r)^2$, a hyperbolic frequency-modulated (HFM) signal with $\xi(t/t_r) = \ln|t/t_r|$, a power frequency-modulated signal $\xi(t/t_r) = (t/t_r)^k$ $(k \in \mathbb{R})$, and a polynomial frequency-modulated (PFM) signal with $\xi(t/t_r) = \sum_{l=0}^{L-1} \alpha_l (t/t_r)^l$. Such classes of waveforms are found in numerous applications such as sonar, radar, acoustics, biomimetics, and underwater communications [97–101].

5.2 Formulation of Coexistence Systems

5.2.1 Pulse-Doppler Radar Signal Processing

We consider a deterministic non-fluctuating target (Swerling-0 target model) [34, 35]. For a monostatic radar employing pulse-Doppler signal processing, N_p pulses $s_r(t)$ are transmitted during a coherent processing interval (CPI). The received baseband signal corresponding to the mth transmitted pulse, $m = 1, \ldots, N_p$, can be modeled as

$$z_m(t) = \sqrt{P_{\mathrm{r}}} s_r(t - \tau_0 - mT_{\mathrm{PRI}}) e^{-j2\pi\nu_0 mT_{\mathrm{PRI}}} + x_{c,m}(t) + w_m(t),\ 0 \le t \le T_{\mathrm{PRI}} \quad (5.1)$$

where τ_0 and ν_0 correspond to the time-delay and frequency shift respectively, that are assumed to be constant over the CPI, $x_{c,m}(t)$ is the communications interference signal, and $w_m(t)$ is additive white Gaussian noise (AWGN).

Assuming a sampling period of T_s and a pulse repetition interval (PRI) of length T_{PRI}, the discrete-time received signal $z_m[n] = z_m(nT_s)$ is given by

$$z_m[n] = \sqrt{P_{\mathrm{r}}} s_r\left(nT_s - \tau_0 - mT_{\mathrm{PRI}}\right) e^{-j2\pi\nu_0 mT_{\mathrm{PRI}}} + x_{c,m}[n] + w_m[n] \quad (5.2)$$

for $n = 1, \ldots, N_s$, where $N_s = T_{\mathrm{PRI}} F_s$ and $F_s = 1/T_s$. In vector form, the received

signal $\mathbf{z}_m = [z_m[1] \ \cdots \ z_m[N_s]]^T$ can be expressed as

$$\mathbf{z}_m = \sqrt{P_{\mathrm{r}}}\mathbf{s}_r(\tau_0; m)e^{-j2\pi\nu_0 m T_{\mathrm{PRI}}} + \mathbf{x}_{c,m} + \mathbf{w}_m$$

where the target reflected signal from the mth radar transmission is given by

$$\mathbf{s}_r(\tau_0; m) = \begin{bmatrix} s_r(T_s - \tau_0 - mT_{\mathrm{PRI}}) \\ s_r(2T_s - \tau_0 - mT_{\mathrm{PRI}}) \\ \vdots \\ s_r(N_s T_s - \tau_0 - mT_{\mathrm{PRI}}) \end{bmatrix} \in \mathbb{C}^{N_s}$$

and $\mathbf{x}_{c,m}$ and $\mathbf{w}_m$ are similarly defined. Considering N_p pulses over the CPI, the overall received signal is given by

$$z_{\mathrm{CPI}}[n] = \sum_{m=1}^{N_p} \left(\sqrt{P_{\mathrm{r}}} s_r(nT_s - \tau_0 - mT_{\mathrm{PRI}})e^{-j2\pi\nu_0 m T_{\mathrm{PRI}}} + x_{c,m}[n] + w_m[n] \right). \quad (5.3)$$

In matrix form, the N_p received signals can be concatenated to obtain the matrix $\mathbf{Z} \in \mathbb{C}^{N_s \times N_p}$ constructed as

$$\mathbf{Z} = [\mathbf{z}_1 \ \mathbf{z}_2 \ \cdots \ \mathbf{z}_{N_p}]$$

where $\mathbf{z}_m$, $m = 1, ..., N_p$, is defined in (5.2). If we define

$$\mathbf{d}(\nu_0) = \left[e^{j2\pi\nu_0 T_{\mathrm{PRI}}} \ e^{j2\pi\nu_0 2T_{\mathrm{PRI}}} \ \cdots \ e^{j2\pi N_p \nu_0 T_{\mathrm{PRI}}} \right]$$

then the matrix $\mathbf{Z}$ over all PRIs can be written as

$$\mathbf{Z} = \sqrt{P_{\mathrm{r}}}\mathbf{s}_r(\tau_0)\mathbf{d}^H(\nu_0) + \mathbf{X}_c + \mathbf{W} \quad (5.4)$$

where $\mathbf{X}_c = [\mathbf{x}_{c,1} \ \cdots \ \mathbf{x}_{c,N_p}]$ is a matrix whose columns consist of the communications interference symbols over each PRI and $\mathbf{d}^H$ denotes vector Hermitian (complex conjugate transpose) of a complex valued vector $\mathbf{d}$. Note that, with this notation, we can represent the time-domain received signal over the CPI in (5.3) as the column vector

$$\mathbf{z}_{\mathrm{CPI}} = \mathrm{vec}\,(\mathbf{Z}) \in \mathbb{C}^{N_s N_p \times 1}.$$

Here, vec($\mathbf{Z}$) denotes vectorization of matrix $\mathbf{Z}$ by stacking the matrix columns into a single column vector.

The first step in pulse-Doppler processing involves the correlation of the received signal at the mth PRI in (5.1) with a time-delayed version of the transmitted signal to estimate the corresponding target range. Note that the PRI time step m, $m = 1, \ldots, N_p$, denotes slow-time processing, whereas the time sample n, $n = 1, \ldots, N_s$, denotes fast-time processing [34, 35]. Thus, at the mth slow-time PRI time step, we compute the correlation

$$a_{\ell,m} = \sum_{n=1}^{N_s} z_m[n] s_r^*(nT_s - \tau_\ell - mT_{\text{PRI}}) = \mathbf{z}_m^H \mathbf{s}_r(\tau_\ell; m)$$

where τ_ℓ, $\ell = 1, ..., N_\tau$ denotes the ℓth time-delay or range bin. The domain of τ_ℓ is $[T_r, T_{\text{PRI}}]$, and it represents the domain for unambiguous target returns, where T_r is the duration of the transmit radar signal $s_r(t)$. In essence, for a speed of propagation c_{ϵ_0}, targets that are in range bins less then $r_{\text{BZ}} = c_{\epsilon_0} T_r/2$ are not observable since during these bins, the transmitter is on and the receiver is not processing. On the other end, any pulse that is received after $r_{\text{UR}} = c_{\epsilon_0} T_{\text{PRI}}/2$ is considered *ambiguous* as these range bins are processed in the next PRI to estimate a target position that is closer than the actual position [34, 35].

If we assemble a correlation matrix over all time delay (or correspondingly range) bins as

$$\mathbf{\Xi} \triangleq [\mathbf{s}_r(\tau_1)\ \mathbf{s}_r(\tau_2)\ \cdots\ \mathbf{s}_r(\tau_{N_\tau})] \in \mathbb{C}^{N_s \times N_\tau}$$

then, over the set of measurements defined in (5.4), we can define the range correlation matrix $\mathbf{A} = \mathbf{Z}^H \mathbf{\Xi} \in \mathbb{C}^{N_p \times N_\tau}$. Note that slow-time is represented by the rows and fast-time correlation is represented by the columns.

The final output from the pulse-Doppler radar after N_p pulses are received is computed by taking the discrete Fourier transform (DFT) across the rows of the

matrix $\mathbf{A} \in \mathbb{C}^{N_p \times N_\tau}$. Thus, the overall correlation output matrix $\mathbf{Y} \in \mathbb{C}^{N_\nu \times N_\tau}$ is given by

$$\mathbf{Y} = \mathbf{\Phi A} = \mathbf{\Phi Z}^H \mathbf{\Xi} \tag{5.5}$$

where $N_\nu \geq N_p$ is the size of the slow-time DFT. The slow-time DFT matrix can be written as

$$\mathbf{\Phi} = [\boldsymbol{\phi}_1 \ \boldsymbol{\phi}_2 \ \cdots \ \boldsymbol{\phi}_{N_p}]$$

where $\boldsymbol{\phi}_m = [e^{j2\pi\nu_1 m T_{\text{PRI}}} \ \cdots \ e^{j2\pi\nu_{N_\nu} m T_{\text{PRI}}}]^H$ for $m = 1, \ldots, N_p$ and the domain of the lth Doppler shift bin ν_l, $l = 1, \ldots, N_\nu$, is $[-\frac{1}{2}, \frac{1}{2}]$; this corresponds to the unambiguous Doppler shifts $[-\frac{F_{\text{PRF}}}{2}, \frac{F_{\text{PRF}}}{2}]$, where $F_{\text{PRF}} = 1/T_{\text{PRI}}$. Using (5.4), we can then express the pulse-Doppler output in (5.5) as

$$\begin{aligned}\mathbf{Y} &= \sqrt{P_{\text{r}}}\mathbf{\Phi d}(\nu_0)\mathbf{s}_r^H(\tau_0)\mathbf{\Xi} + \mathbf{\Phi}\left(\mathbf{X}_c^H + \mathbf{W}^H\right)\mathbf{\Xi} \\ &= \sqrt{P_{\text{r}}}\mathbf{X}_r + \mathbf{D}_{\text{comm}} + \mathbf{N}\end{aligned}$$

where

$$\mathbf{X}_r \triangleq \mathbf{\Phi d}(\nu_0)\mathbf{s}^H(\tau_0)\mathbf{\Xi}$$

is in the form of the ambiguity function (AF) of the transmitted signal [34, 81], and

$$\mathbf{D}_{\text{comm}} \triangleq \mathbf{\Phi X}_c^H \mathbf{\Xi}$$

$$\mathbf{N} \triangleq \mathbf{\Phi W}^H \mathbf{\Xi}.$$

In this form, the communications interference present in the processed radar return is given by $\mathbf{D}_{\text{comm}}$, and $\mathbf{N}$ is an integrated noise term.

5.2.2 Wireless Communications Receiver Processing

We assume that a communications user transmits the signal $s_c(t)e^{j\phi_v}$ with duration T_c and V-phase shift keying (PSK) modulation [32] with $v = 1, \ldots, V$. The user can

thus transmit up to $\log_2 V$ bits of information in a signal duration. We also assume that $N_{\text{SPP}} = \lfloor T_{\text{PRI}}/T_c \rfloor$ communications symbols are transmitted by the user over one radar PRI.

The communications signal $s_{c,m}(t)$ is a continuous train of transmitted symbols and is given by

$$s_{c,m}(t) = \sum_{q=0}^{N_{\text{SPP}}-1} s_c(t - qT_c - mT_{\text{PRI}})e^{j\phi_{q,m}}$$

where $\phi_{q,m} = 2\pi(v_{q,m} - 1)/V$ and $v_{q,m} = 1, \ldots, V$ is the phase shift index corresponding to the V-PSK constellation point that represents the information of the user for the qth symbol in the mth PRI.

For an AWGN channel, the communications receiver estimates the qth transmitted symbol q. The received signal for the mth PRI is given by

$$z_m(t) = x_{r,m}(t) + \sqrt{P_{\text{c}}} \sum_{q=0}^{N_{\text{SPP}}-1} s_c(t - qT_c - mT_{\text{PRI}})e^{j\phi_{q,m}} + w_m(t),\ 0 \le t \le T_{\text{PRI}}$$

where $x_{r,m}(t) = \sqrt{P_{\text{r}}} s_r(t - \tau_0 - mT_{\text{PRI}})e^{-j2\pi\nu_0 mT_{\text{PRI}}}$ is the radar return discussed in the previous section. At the communications receiver, to determine the qth symbol transmitted in the mth PRI, we compute the correlation

$$T_{v,q,m} = \Re e \left\{ \int_{qT_c}^{(q+1)T_c} z_m(t) s_c(t - qT_c - mT_{\text{PRI}}) e^{j\phi_v} dt \right\},\ q = 0, \ldots, N_{\text{SPP}} - 1 \quad (5.6)$$

and the PSK modulation index is estimated by finding the symbol that maximizes the correlation in (5.6) as [32, 99–101]

$$\hat{v}_{q,m} = \arg \max_{v=1,\ldots,V} \{T_{v,q,m}\}.$$

5.3 Optimization of Waveform Parameters for Minimum Interference

In the multiuser communications systems, the user signaling scheme must be designed to minimize the interference between users or multiple access interference

(MAI) . This is achieved by minimizing the correlation between each user's signal and thus increasing the bit-error-rate (BER) performance of each user [32, 99–101]. As the communications system shares the same bandwidth with the radar, it is also necessary to minimize the interference between the radar and communications systems.

We assume that the n communication user is assigned a unique LFM signal with duration T and FM rate b_n. The signal is given by

$$s_{c,n}(t) = \sqrt{2t}\, e^{j2\pi b_n t^2}, \quad t > 0.$$

The correlation between the signals used by the nth and mth, $n \neq m$ and $m, n \in \mathbb{Z}_{++}$, communications users is given by

$$\phi_{m,n}(\tau, \tau') = |\langle s_{c,m}(t-\tau), s_{c,n}(t-\tau')\rangle_{L^2(\mathbb{R})}|^2$$

where the users have associated time delays τ and τ'. If we assume that the communication user symbols are time synchronized relative to each user, then we can set $\tau = \tau' = 0$. In order to reduce interference between these two users, we need to find the FM rates b_n and b_m to satisfy the constraint

$$\phi_{m,n}(0,0) = |\langle s_{c,m}(t), s_{c,n}(t)\rangle_{L^2(\mathbb{R})}|^2 \tag{5.7}$$

$$= \left| \int_{\mathbb{R}} s_{c,m}(t) s^*_{c,n}(t) dt \right|^2 = \delta_{m,n} \tag{5.8}$$

where $\delta_{m,n} = \delta[m-n]$ is the Kronecker delta function.

In order to solve for the FM rates, we simplify (5.8) to obtain

$$\begin{aligned}
\phi_{m,n}(0,0) &= \left| \int_0^T 2t\, e^{j2\pi b_m t^2} e^{-j2\pi b_n t^2} dt \right|^2 \\
&= \left| \int_0^T 2t e^{j2\pi (b_m - b_n) t^2} dt \right|^2 \\
&= \left| \int_0^{T^2} e^{j2\pi (b_m - b_n) u} du \right|^2 \\
&= \left| T^2 \text{sinc}\left[(b_m - b_n) T^2 \right] \right|^2
\end{aligned}$$

where $\text{sinc}(x) \triangleq \sin(\pi x)/\pi x$. Note that this simplification is only possible by constraining the AM of the LFM signal to be $a_c(t) = \sqrt{2t}$, $t > 0$. Also note that the signals are assumed to be modulated by the same carrier frequency, but the modulation term cancels when the correlation is computed. It is then clear from the definition of $\text{sinc}(x)$ that the correlation between the nth and mth users is minimized when

$$b_m \pm b_n = \frac{l}{T^2}, \text{ where } l \in \mathbb{Z}\,. \tag{5.9}$$

As a result, selecting the FM rate assigned to each communications user to satisfy the condition in (5.9) is expected to reduce MAI [32, 99–101].

Given that the allocated bandwidth is B_a, the maximum possible FM rate is given by

$$b_{\max} = \frac{B_a}{2T},$$

and the maximum number of communications users to be accommodated is given by

$$N_{\max} = \left\lfloor \frac{TB_a}{2} \right\rfloor.$$

Using this information, the FM rate of the nth user, $n = 1, 2, \ldots, N_{\max}$, for minimizing MAI is given

$$b_n = \frac{B_a}{2T} - \frac{N_{\max} - n}{T^2}\,.$$

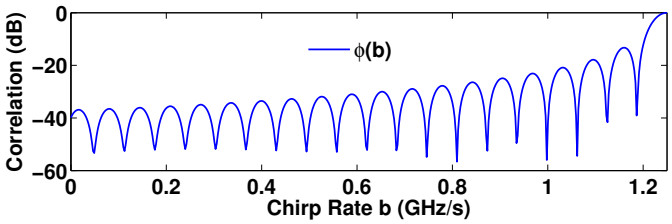

Figure 5.1: Plot of Correlation Function for a Fixed Pulse Duration T as a Function of the FM Rate b.

For the radar transmit waveform, we want to select an LFM signal that results in minimum interference with the LFM signal of the nth communications user, $n = 1, 2, \ldots, N_{\max}$. Thus, we want to minimize the correlation between the transmitted radar signal and all communications users signals [34, 35]. As the radar return has an unknown time-delay τ_0, the resulting correlation to be reduced is given by

$$\begin{aligned}\phi_{r,(c,m)}(\tau_0, 0) &= \left| \langle s_r(t-\tau_0), s_{c,m}(t) \rangle_{L^2(\mathbb{R})} \right|^2 \\ &= \left| \int_{\mathbb{R}} 2\sqrt{t(t-\tau_0)} e^{j2\pi(f_{s,r}(t-\tau_0)+b_r(t-\tau_0)^2)} e^{j2\pi(f_{s,c}t+b_m t^2)} dt \right|^2\end{aligned}$$

where $s_r(t) = \sqrt{2t}\, e^{j2\pi b_r t^2}, \quad t > 0$. This integration is not possible to compute in closed form, but we can evaluate it numerically. Assuming that $f_{s,r} = -B_a/2$, $f_{s,c} = B_a/2$, and letting $b_n = B_a/(2T)$, the correlation as a function of τ_0 and b_r is shown in Figure 5.1. We see from this figure that the correlation is minimized when the FM rate of the radar signal is the negative of the FM rate of the communications user signal [29, 30, 99–101].

5.4 Signal Design Trade-off Analysis

In order to determine the effect of the different communications system operation parameters on the maximum number of users, we consider Figure 5.2. The top left figure shows $N_{\max}$ as a function of time-bandwidth product (TBP), and as it can be seen, at the TBP increases, the maximum number of serviceable users also increases. The bottom left figure shows the maximum number of users for three fixed allocated

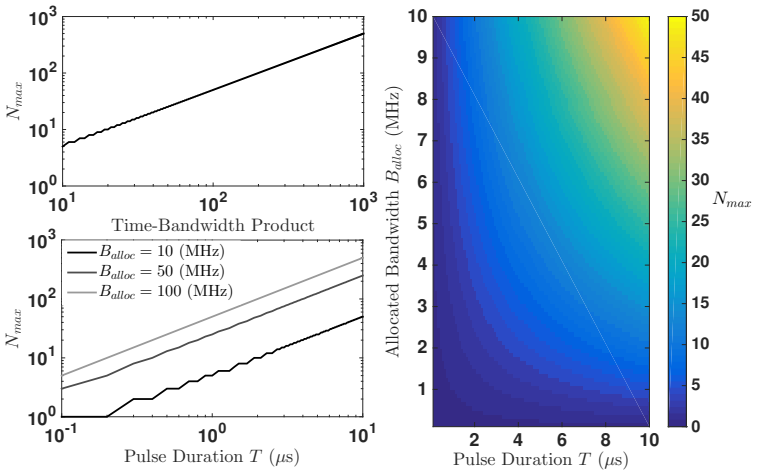

Figure 5.2: Maximum Number of Servicable Users $N_{\max}$ as a Function of Signal Duration T, Allocated Bandwidth B_{a}, and TBP.

bandwidths, $B_{\mathrm{a}} \in \{10, 50, 100\}$ MHz. The right figure shows a 2-D surface of the maximum number of users as a function of signal duration and bandwidth.

We also consider the effect of bit rate on the communications systems performance [32]. We assume that the communications system employs V-PSK modulation with symbol duration T. Then the modulating signal for the symbol is given by

$$s_c(t) = \sqrt{2t} e^{j(2\pi b_c t^2 + \theta_c)}, t \in (0, T)$$

where

$$\theta_c = \frac{2\pi(v-1)}{V}, v = 1, \ldots, V$$

and v is an index corresponding to a unique constellation point representing a sequence of binary digits of length $\log_2 V$. The gross bit rate can then be computed as [32]

$$R_b = \frac{\log_2 V}{T}$$

which is plotted in Figure 5.3. As it can be seen, for a fixed PSK modulation order V, the data rate increases as the symbol duration T decreases. Thus, for a given B_{a}, in

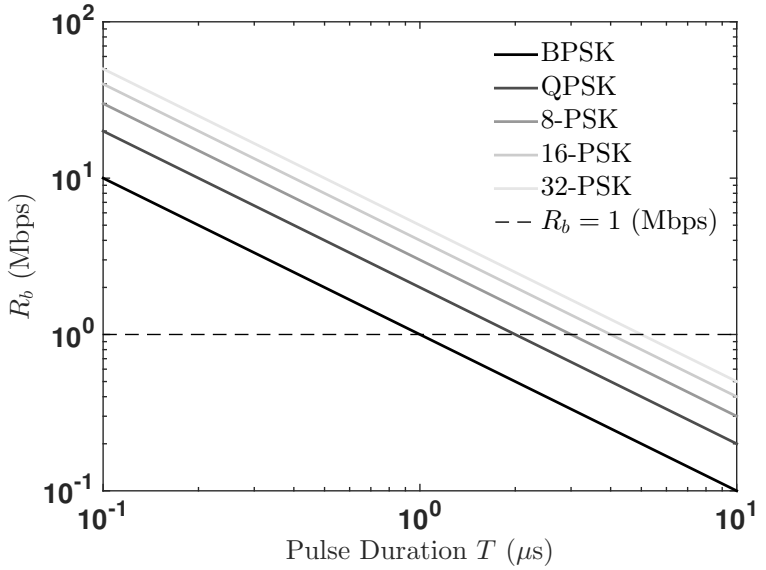

Figure 5.3: Feasible Bit Rate R_b as a Function of Symbol Duration T for V-PSK Modulation, for V Equal to 2, 4, 8, 16, and 32.

order to maximize the number of users $N_{\max}$, the LFM communications signals must have longer durations. As a trade-off, to maximize the data rate, the durations should be shorter. This intuitively makes sense as, the more complicated the communications scheme is, the more susceptible it is to MAI as the channel becomes more crowded.

For the designed communications signaling scheme with V-PSK modulation and an AWGN channel, Figure 5.4 shows a plot of the bit error rate (BER) performance as a function of E_b/N_0, where E_b is the energy per bit and N_0 is the variance of the noise samples. Note that the BER was obtained theoretically as well as using Monte-Carlo (MC) simulations. Note that this plot requires higher signal-to-noise-ratio (SNR) to reliably demodulate higher order modulations.

If we assume that $N_{\text{cu}} \leq N_{\max}$ users occupy the communications channel, then N_{cu} waveforms are transmitted over the same bandwidth as the radar waveform. If the radar receiver has knowledge of the number of users transmitting at each time step, then the radar waveform can be designed to improve range resolution that is given by $\sigma_r = c_{\epsilon_0}/(2B_a)$ [34, 35]. Note that the range resolution as a function of bandwidth

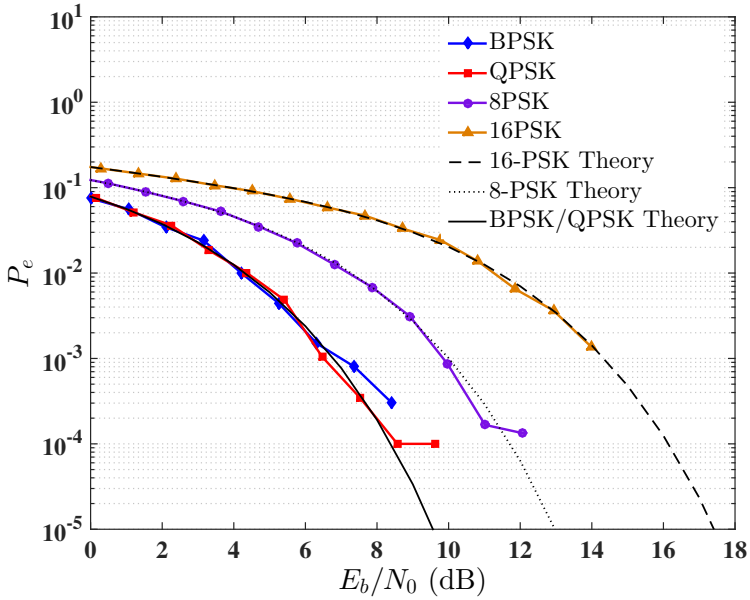

Figure 5.4: BER Performance as a Function of E_b/N_0 for Various V-PSK Modulation Orders Using LFM signals in an AWGN Channel with No Radar Signal Present.

is shown in Figure 5.5. If we assume that the rate of the LFM signal assigned to the radar is given by b_r, then the relationship between the range resolution and the FM rate is given by

$$\sigma_r(T, b_n) = \frac{c_{\epsilon_0}}{4b_r T}\,.$$

As a result, for a fixed duration T and considering the FM rates $b_1, \ldots, b_{N_{\text{cu}}}$ designed for the communications users, then in order to minimize the range resolution, the FM rate of the radar must be chosen as $b_r = b_{N_{\max}}$. Thus, if the objective of the radar system is to minimize the range resolution, then the radar waveform must be chosen as

$$s_{r,\text{opt}}(t) = \sqrt{2t}e^{-j2\pi b_{N_{\max}}t^2}, t \in (0, T)\,.$$

For the following results, we assume that the allocated bandwidth is $B_a = 10$ MHz, the pulse duration for both radar and communications signals is $T = 4$ μs, and the maximum number of users is $N_{\max} = 20$. In Table 5.1, we list four possible

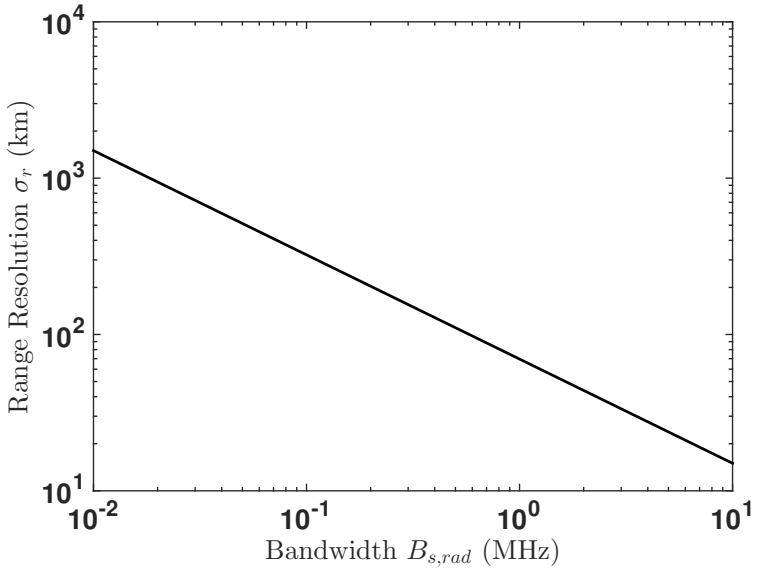

Figure 5.5: Radar Range Resolution as a Function of Transmitted Radar Signal Bandwidth B_a.

schemes when $N_{cu} = 3$ communications users are transmitting. Note that b_{u_i} is the FM rate assigned to the ith user, $i = 1, 2, 3$ and b_r is the FM rate of the radar signal. Figures 5.6-5.8 show the BER performance for the various schemes. It is clear that no single scheme is best overall for the communications system. In Figure 5.9, the radar performance in the various schemes is shown. While the SINR threshold for the different radar waveforms is different in the different schemes, we need to consider a way to also simultaneously minimize the MSE performance.

Table 5.1: FM Rate Selection Schemes

Scheme 1	$b_1 = -b_{20}$	$b_{u_1} = b_{17}$	$b_{u_2} = b_{18}$	$b_{u_3} = b_{19}$
Scheme 2	$b_1 = b_{20}$	$b_{u_1} = b_{17}$	$b_{u_2} = b_{18}$	$b_{u_3} = b_{19}$
Scheme 3	$b_r = -b_{20}$	$b_{u_1} = b_1$	$b_{u_2} = b_4$	$b_{u_3} = b_8$
Scheme 4	$b_r = -b_{20}$	$b_{u_1} = b_{18}$	$b_{u_2} = b_{19}$	$b_{u_3} = b_{20}$

The BB SINR threshold analysis considered in Chapter 4 demonstrated the trade-off in performance as a result of reducing the LFM rate at low SINR, assuming same energy waveforms. Figures 5.10 and 5.11 show the tracking MSE for range and range-

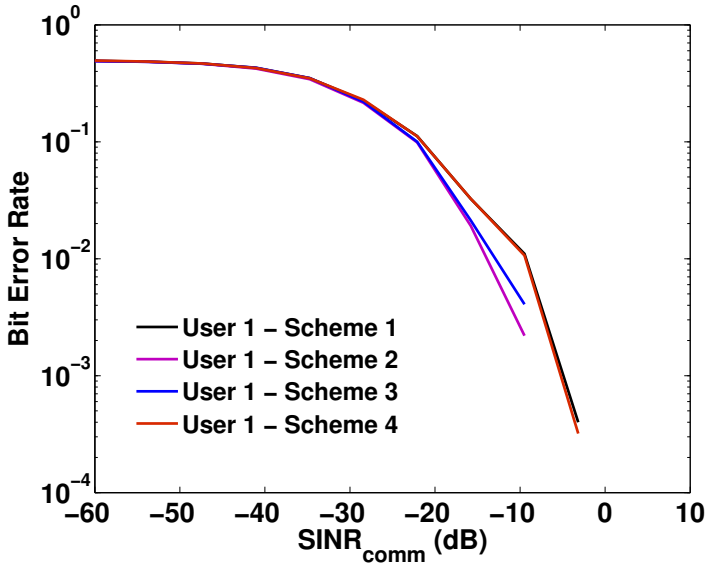

Figure 5.6: BER Performance as a Function of $\text{SINR}_{\text{comm}}$ From the Communications Receiver Perspective for User 1 and Various FM Rate Selection Schemes.

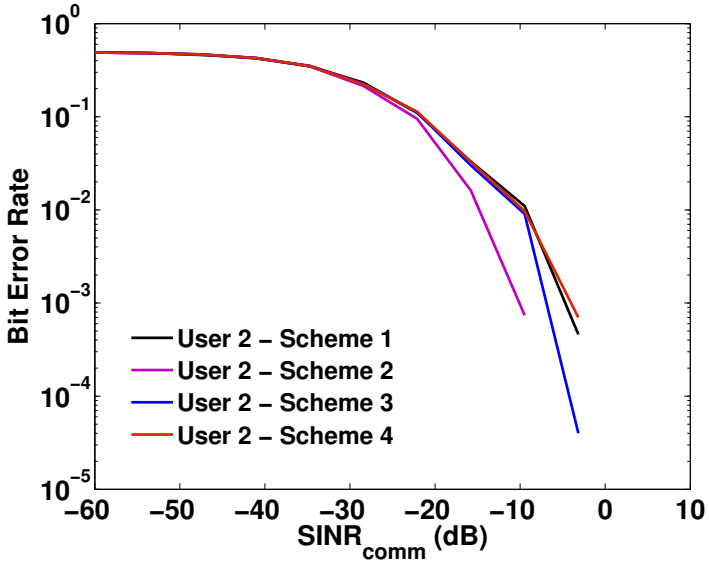

Figure 5.7: BER Performance as a Function of $\text{SINR}_{\text{comm}}$ From the Communications Receiver Perspective for User 2 and Various FM Rate Selection Schemes.

rate at -18 dB and -34 dB SINR_{rad}, respectively, using Kalman filtering [90]. As it can be seen, the lower FM rate waveform in blue results in a lower MSE than the higher FM rate waveform in red when the SINR is lower. Note, however, than for higher SINR, the blue waveform has a higher detection rate and the sidelobe selection

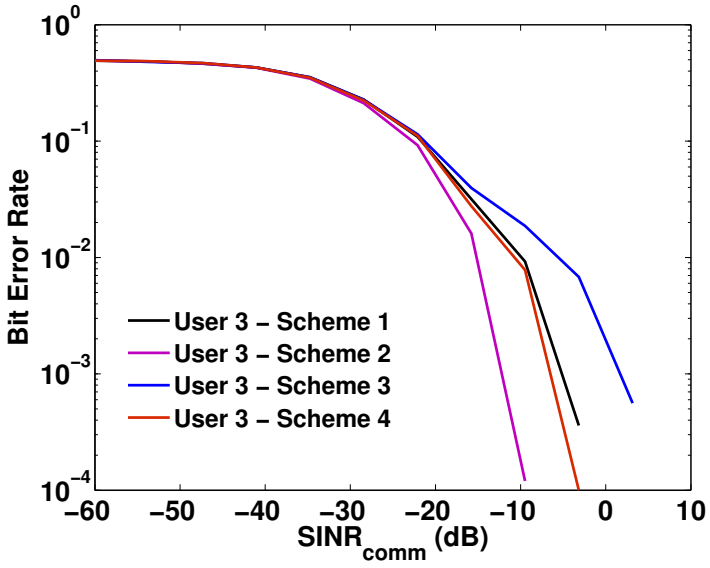

Figure 5.8: BER Performance as a Function of $\text{SINR}_{\text{comm}}$ From the Communications Receiver Perspective for User 3 and Various FM Rate Selection Schemes.

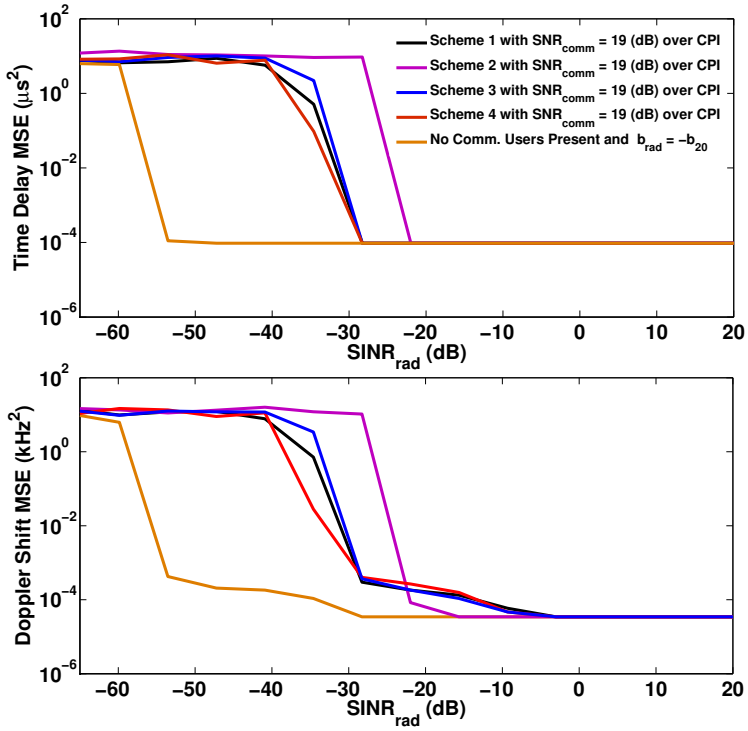

Figure 5.9: Radar Time-Delay and Doppler Shift MSE Performance as a Function of SINR_{rad} From the Radar Receiver Perspective for Various FM Rate Selection Schemes.

probability is lower.

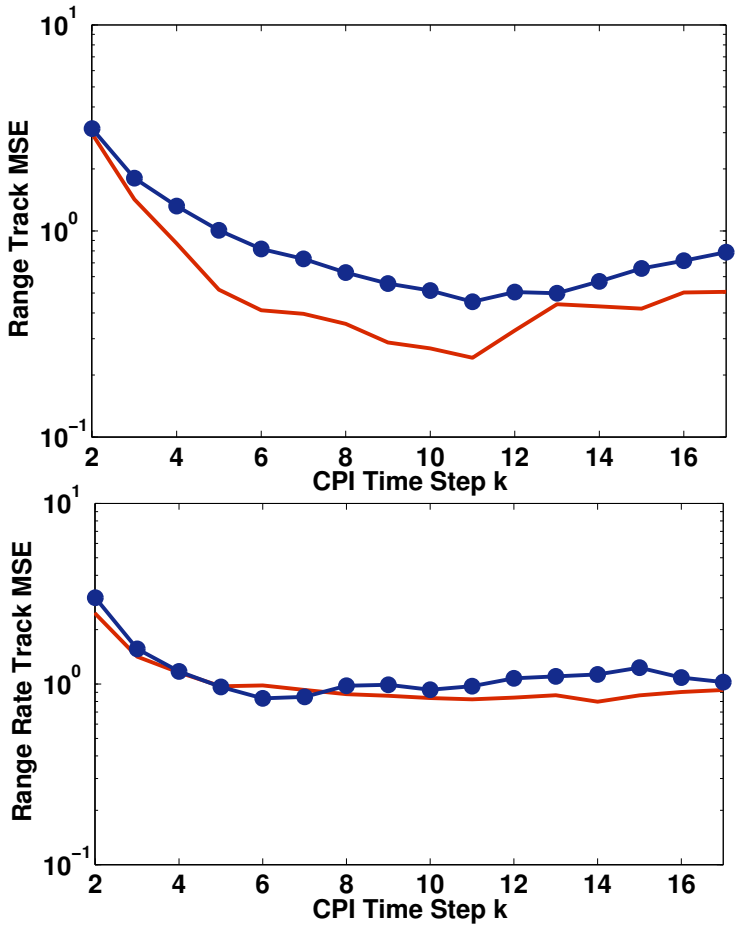

Figure 5.10: MSE for Range and Range-Rate Estimation for $(b_r, b_{u_1}, b_{u_2}, b_{u_3}) = (-b_{20}, b_{18}, b_{19}, b_{20})$ in Red and $(b_r, b_{u_1}, b_{u_2}, b_{u_3}) = (-b_1, b_{18}, b_{19}, b_{20})$ in Blue, at SINR_{rad} of -18 dB.

5.5 Multi-Objective Optimization for Joint Waveform Co-Design

In general, the objectives associated with optimizing both radar and communications systems performance do not have the same joint optimal design. For example, the optimal radar waveform in terms of minimizing range resolution may not necessarily correspond to the radar waveform in terms of optimizing gross bit rate for the communications system.

If the actual number of communications users N_u is less than the maximum number of possible users $N_{\max}$, then the signaling scheme for the users can be revised in

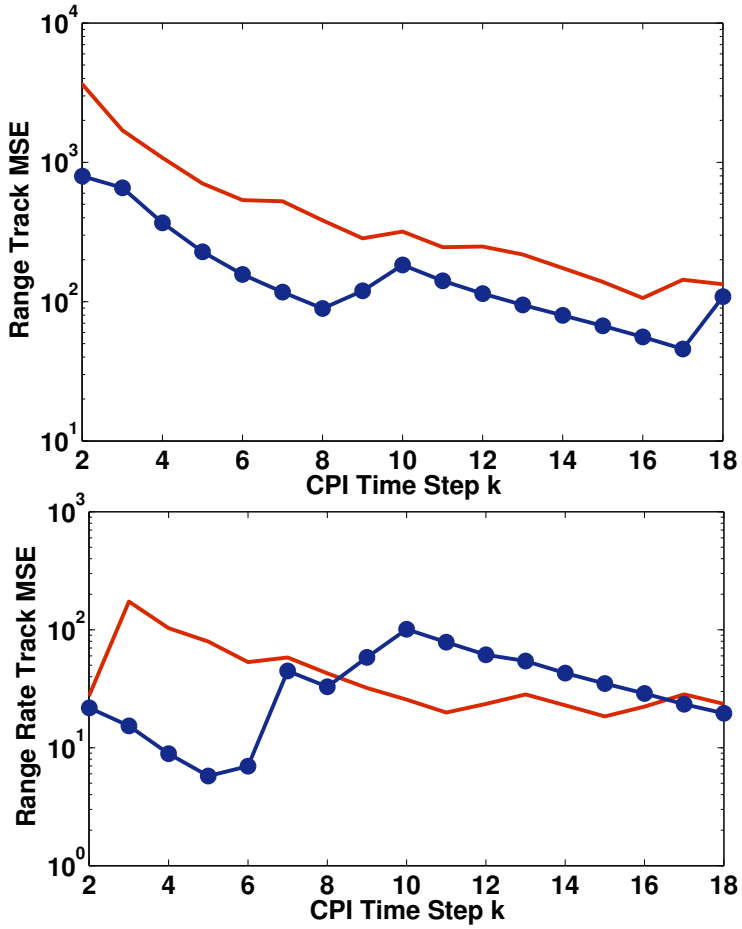

Figure 5.11: MSE for Range and Range-Rate Estimation for $(b_r, b_{u_1}, b_{u_2}, b_{u_3}) = (-b_{20}, b_{18}, b_{19}, b_{20})$ in Red and $(b_r, b_{u_1}, b_{u_2}, b_{u_3}) = (-b_1, b_{18}, b_{19}, b_{20})$ in Blue at SINR_{rad} of -34 dB.

order to increase each user's BER performance. In particular, we want the N_u users to have the best combination of FM rates so as to minimize MAI. If we consider in a received signal that only consists of N_u communications users as

$$z(t) = s_{c,1}(t) + \cdots + s_{c,N_u}(t)$$

and we know that the received signal $z(t)$ is correlated using a matched filter to obtain the estimates of the transmitted bits for each symbol, then it is reasonable to consider an optimization that aims to minimize the correlation between each user, for all users

combinations. This optimal combination can be found as

$$\left\{b_1^*, \ldots, b_{N_u}^*\right\} = \arg \min_{\{b_u\}_{u=1}^{N_u \leq N_{\max}} \in \mathcal{F}_c(T_c)} \left\{ \sum_{\{i,j:i\neq j \text{ unique}\}} \left|\left\langle s_{u_i}, s_{u_j} \right\rangle\right|^2 \right\} \tag{5.10}$$

where

$$\mathcal{F}_c(T_c) = \left\{ b \in \mathbb{R} : \left| \text{sinc}\left[(b_n - b_m)\, T_c^2 \right] \right|^2 \approx 0 \right\}$$

is the set of orthogonal FM rates and $T_c \leq \log_2(V)/R_b$ for V-PSK with desired bit rate R_b.

This is a combinatorics optimization problem that becomes increasingly difficult to solve as N_u increases. For small numbers of users such as $N_u = 3$, it is possible to solve the problem by a brute force search approach. If N_u is larger, the computation becomes very intensive. Thus, in order to solve this combinatorics optimization problem, we employ the simulated annealing (SA) stochastic optimization method [102].

We consider a subsystem optimization using $N_u \leq N_{\max}$ active users with FM rates assigned according to Equation (5.10). This communications signaling scheme is assumed known at the radar receiver. The design of the radar waveform is not obvious is the performance objective function is the estimation MSE. Normally, the radar waveform is selected to have large bandwidth in order to reduce the time-delay estimation MSE and thus improve range resolution [34, 35] However, it is not clear how the large bandwidth radar waveform affects the interference between the radar and communications systems. In order to jointly consider both the MSE and systems interference objectives, we consider the communications interference component at the radar receiver that was given in Section 5.2, Equation (5.5) as

$$\mathbf{D}_{\text{comm}} = \mathbf{\Phi C}(b_1^*, \ldots, b_{N_u}^*, T_c^*)^H \mathbf{\Xi}(b_r, T_r) \tag{5.11}$$

where $\mathbf{C}(b_1^*, \ldots, b_{N_u}^*, T_c^*)$ is the communications signaling scheme over the radar CPI where it is assumed that the N_u users are always transmitting in the worst case. With the assumption that the communications system shares signaling scheme information with the radar then (5.11) can be computed at the radar transmitter to predict what kind of interference to expect from the communications system and attempt to optimize the transmitted radar waveform to minimize the correlation.

Note that this notation emphasizes that the communications interference component depends on the FM rate b_r and pulse duration T_r of the radar waveform. We can minimize the correlation over a set of feasible radar waveforms by considering the following optimization problem of

$$\{b_r^*, T_r^*\} = \arg \max_{(b_r, T_r) \in \mathcal{F}_r} \left\{ ||\mathbf{D}_{\text{comm}}||_F^2 \right\}$$

where $||\mathbf{D}_{\text{comm}}||_F^2 = \text{ tr} \left\{ \mathbf{D}_{\text{comm}}^H \mathbf{D}_{\text{comm}} \right\}$ is the Frobenius norm of the communications disturbance over all time-delay and Doppler cells in $\mathcal{F}_r$ for a given radar waveform. The feasible region for radar waveforms is given by

$$\mathcal{F}_r = \left\{ (b_r, T_r) \in \mathbb{R}^2 : T_{\min} \leq T_r \leq T_{\max}, b_r(T_r; B_{\min}) \geq \frac{B_{\min}}{2T_r}, b_r(t_r; B_{\max}) \leq \frac{B_{\max}}{2T_r} \right\}.$$

An example of this cost function is shown in Figure 5.12 for a B_a of 10 MHz and a minimum sweep rate of 3 MHz.

This optimization is essentially computing the correlation of a radar waveform over any possible time delay and Doppler shift given the known signaling of the communications users, but without knowledge of the users transmitted information. Note that, as the term minimized is the correlation between radar and communications systems, it affects the performance of both systems. However, the trade-off is that, in general, the minimum correlation radar waveform does not provide the best MSE performance.

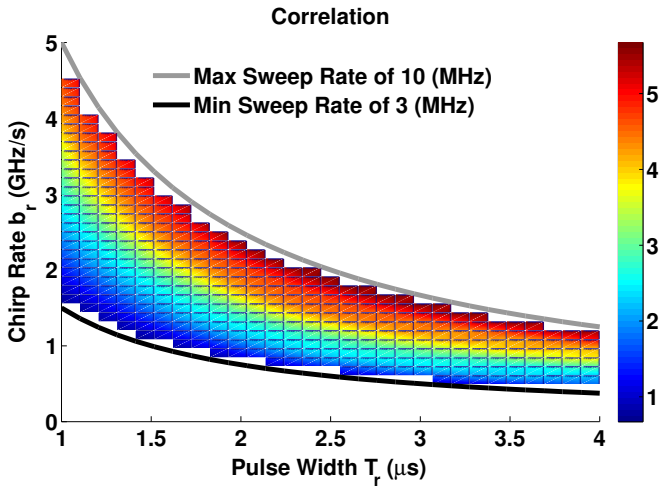

Figure 5.12: Radar and Communications System Correlation Cost Function Example.

In order to examine the performance trade-offs, we formulate the optimization as a multi-objective or Pareto optimization [103]. Consider the problem of optimizing a set of k objective functions $f_l(\mathbf{p})$, $l = 1, \ldots, k$, $k \geq 2$, for a given set of waveform parameters $\mathbf{p}$. We also assume that there exists a set of waveforms $\mathcal{P}$ for which the only feasible solutions to the multi-objective optimization problem exist $\forall \mathbf{p} \in \mathcal{P}$. Then the optimization problem can be written as

$$\begin{aligned} \min \quad & [f_1(\mathbf{p}), \ldots, f_k(\mathbf{p})] \\ & \text{such that } \mathbf{p} \in \mathcal{P} \end{aligned}$$

or equivalently [103] as

$$\begin{aligned} & \min \ \mathbf{f}(\mathbf{p}) \\ & \text{such that } \ \mathbf{p} \in \mathcal{P} \end{aligned}$$

where $\mathbf{f}(\mathbf{p}) = [f_1(\mathbf{p}) \ \ldots \ f_k(\mathbf{p})]^T$. Consider the case where $\mathbf{p} = [b_r, T_r, b_1, b_2, \ldots, b_{N_u}, T_c]^T$ is the vector containing the radar waveform FM rate b_r and duration T_r, and the communications users parameters $b_1, \ldots, b_{N_u}$ and T_c are the for $N_u \leq N_{\max}$ users.

We consider a optimization case where there are $k = 2$ objective functions. We assume that the communications users are first optimized following Equation (5.10) to obtain $b_1^*, b_2^*, \ldots, b_{N_u{}^*}, T_c^*$. The first objective function $f_1(b_r, T_r, b_1^*, b_2^*, \ldots, b_{N_u{}^*}, T_c^*)$ represents the radar time-delay MSE from the simulated asymptotic performance. The second objective function $f_2(b_r, T_r, b_1^*, b_2^*, \ldots, b_{N_u}^*, T_c^*)$ is the correlation between the transmit waveforms of the radar and communications systems. The feasible sets of parameters are those that satisfy $\mathcal{F}_r$ and $\mathcal{F}_c(T_c)$. As a example, we consider $N_u = 4$, shared bandwidth $B_a = 10$ MHz, $T_c^* = 4$ μs, and 16-PSK modulation. The optimal communications rates were found using SA [102]. We constrain the radar signal sweep bandwidth $\Delta_f = 2b_r T_r$ between 3 and 10 MHz and the pulse duration is selected between 1 and 4 μs. In Figure 5.13, we plot the solutions of the two objective functions for a variety of radar waveforms within the $\mathcal{F}_r$ region. The Pareto efficient solutions are connected with the Pareto frontier (shown in gray on the figure). These are solutions that are not dominated by any other outcome from the multi-objective optimization problem. If we examine the Pareto efficient parameter sets in Figures (5.14)-(5.17), we can see the effect of the second objective function on the BER performance for $N_u = 4$ users. It can be seen that the minimum correlation radar waveform of Pareto design case 2 provides the best BER performance. We note that there exists a trade-off in terms of radar time-delay MSE performance in Figure 5.18. In this figure, we see that the MSE performance for the Pareto design case 2 is slightly higher than the MSE performance of the other three Pareto efficient design cases.

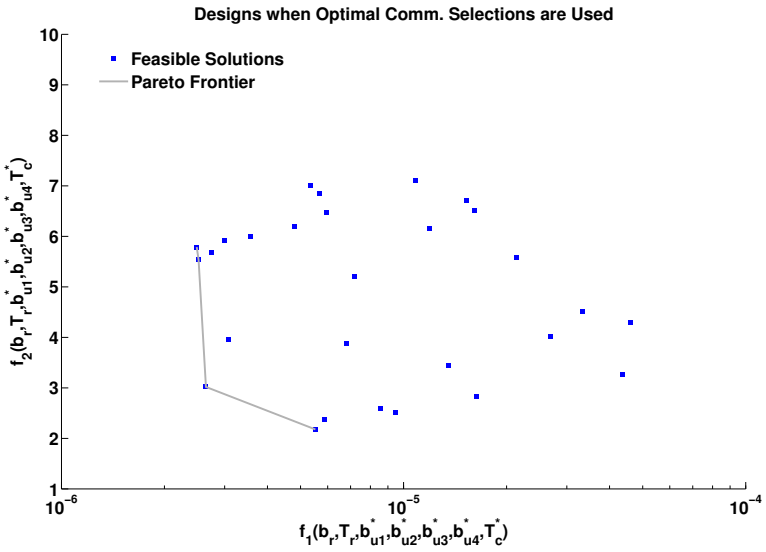

Figure 5.13: Plot of feasible outcomes from the multi-objective optimization problem with Pareto efficient solutions.

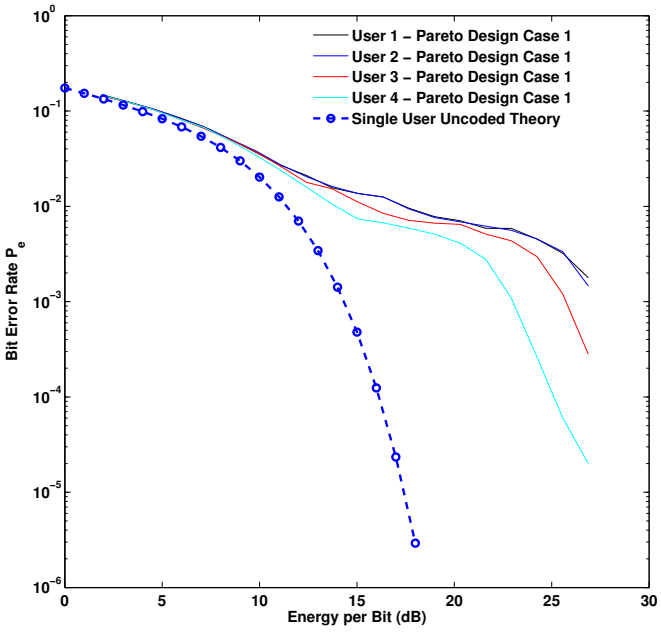

Figure 5.14: BER Performance for Pareto design case 1.

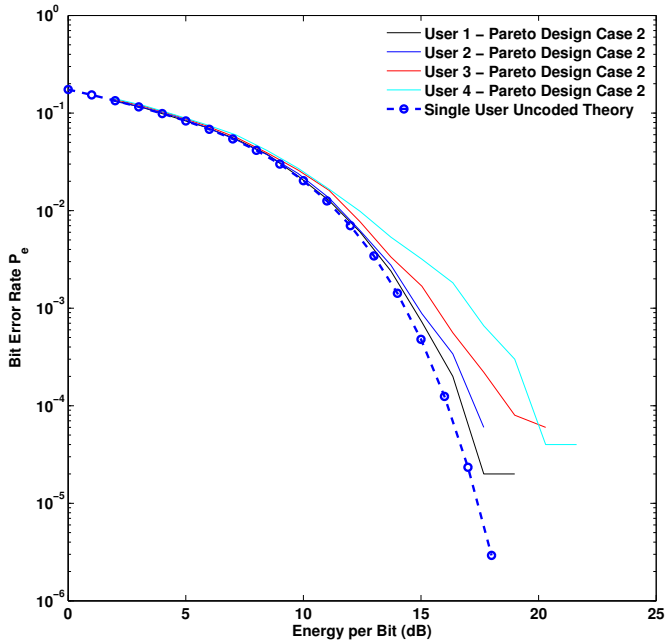

Figure 5.15: BER performance for Pareto design case 2.

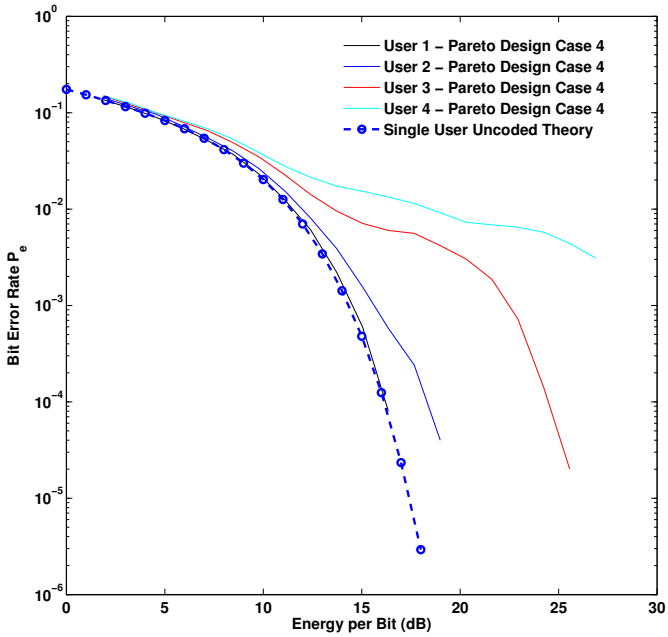

Figure 5.16: BER performance for Pareto design case 4.

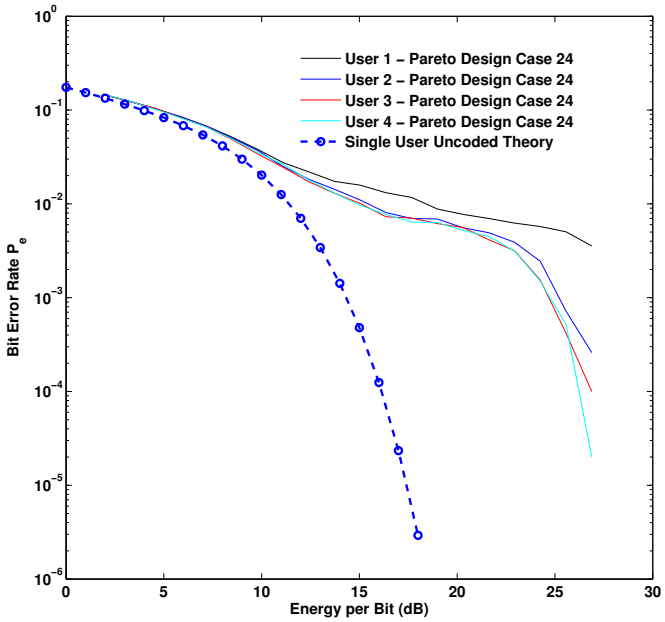

Figure 5.17: BER performance for Pareto design case 24.

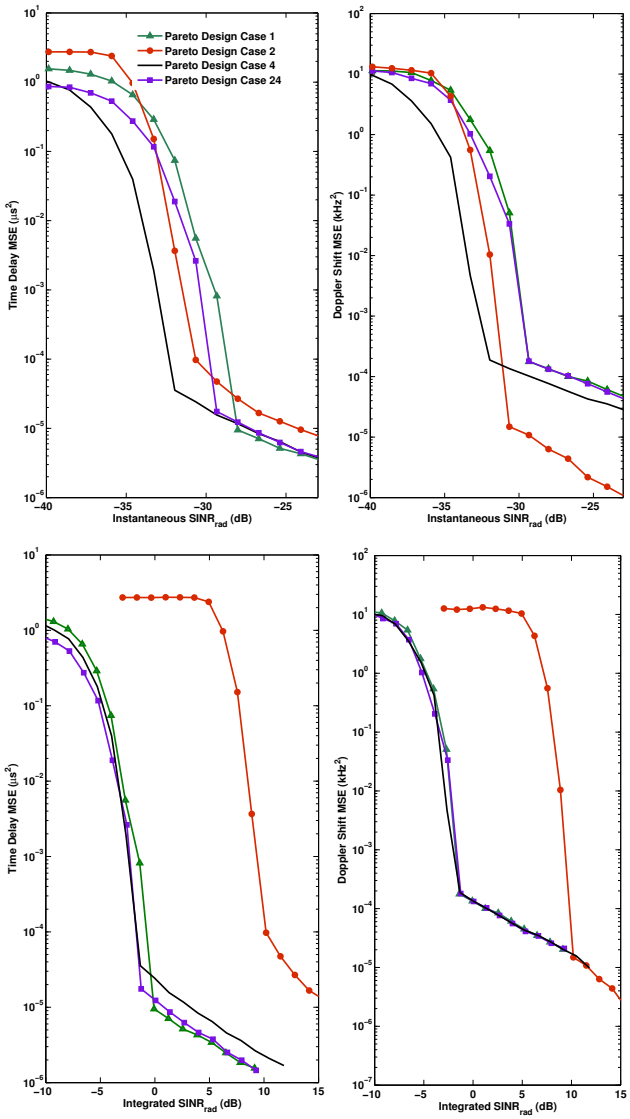

Figure 5.18: Radar MSE performance for all Pareto design cases.

Chapter 6

CONCLUSIONS AND FUTURE WORK

6.1 Conclusion

This thesis proposed tow main statistical signal processing methods to address the radar and communications spectrum coexistence problem. The first method used the use of the Barankin bound (BB) signal-to-interference-plus-noise-ratio (SINR) threshold prediction for radar waveform design in low SINR settings. The second method developed a joint radar and communications waveform co-design for a multi-user communications system and a pulse-Doppler radar.

6.1.1 Radar and Communications Coexistence

We proposed a method for designing radar waveforms that has a useful application when tracking a target operating under low SINR conditions. The method integrates the use of track-before-detect filtering that is based on unthresholded ambiguity function measurements and a new adaptive waveform design algorithm based on the BB. Specifically, we obtain the SINR threshold by computing the deviation of the Barankin bound from the Cramér-Rao Lower Bound (CRLB) and we optimally select the waveform with the minimum SINR threshold. For a set of waveforms with varying parameters we showed that there exists an inverse relationship between the performance of a waveform under high SINR conditions in terms of tracking estimation variance and the waveform's SINR threshold. We demonstrated the applicability of this adaptive waveform design for a radar and communications coexistence problem using waveforms with logarithmic and quadratic phase functions.

Using simulations, we demonstrated that linear frequency-modulated (LFM) waveforms result in lower mean-squared-error (MSE) performance for target parameter estimation than hyperbolic frequency-modulated (HFM) signals. The HFM waveforms, however, perform better than the LFM ones at higher SINR values. This trade-off allows for radar waveform design for the radar and communications coexistence problem when strong communications interference with varying power is assumed to be present at the radar receiver.

6.1.2 Joint Radar and Communications Co-design

We proposed a waveform co-design method for radar and communications systems that share the same allocated bandwidth. Utilizing the LFM waveform for both systems, we showed that it is possible to design a common signaling scheme for radar and communications systems for each system. We optimally designed the LFM rates assigned to each communications user to reduce multiple access interference (MAI) as well as interference between the two systems. We examined performance for each system by developing a multi-objective optimization scheme that minimizes the interference between systems and radar time-delay MSE performance..

Using simulations, we demonstrated that it is feasible to jointly design the transmit waveform for both a pulse-Doppler radar and multi-user communications system when the radar has cooperative knowledge of the communications system signaling scheme information. In order to obtain desirable performance characteristics, it was demonstrated that there exists Pareto trade-offs between optimal design for the radar and optimal design for the communications users. We investigated different Pareto radar waveform designs and examined the effect of a selected radar waveform on the joint system.

6.1.3 SINR Threshold Prediction with BB Kernel Rank

A novel SINR threshold prediction method was proposed based on the effective matrix rank of the BB kernel matrix. Using singular value decomposition (SVD) as a means of computing the effective rank relative to machine precision we demonstrated to have a connection to the exponential decrease in the probability of sidelobe selection over the true mainlobe in maximum likelihood estimator (MLE) computations for nonlinear estimation problems.

Using simulations, we demonstrated the proposed SINR threshold prediction method is demonstrated for estimating frequency, angle, and time-delay parameters from noisy measurements. The kernel effective rank method provides an accurate prediction of the MLE SINR threshold for a variety of unknown parameters, and the performance was compared to other bounds and SINR threshold prediction methods.

6.2 Future Work

A future direction for the radar and communications coexistence problem includes extending our proposed BB SINR threshold approach to tracking multiple targets. For low SINR conditions and multiple targets, the track-before-detect tracking can be combined with random finite set analysis and the multi-Bernoulli multi-target tracker. Our proposed framework can also be extended to consider targets in clutter or in wideband environments and develop design trade-offs for different radar scenes.

For the radar and communications systems joint co-design problem, it is possible to extend our signaling scheme to include other waveforms with nonlinear phase functions such as HFM or power frequency-modulated (PFM) signals with time-varying amplitude modulation. Although our approach assumed transmission in fading channels for the communications systems it can be extended to include frequency selec-

tive and time-frequency fading channels. The Pareto optimization design can also be extended to include more objective functions, such as user capacity, bit rate, and spectral efficiency to further improve the joint waveform designs. Another possible extension is to employ multiple chirp rates for single users when the number of users is less than the maximum allowable in the design. Such an approach could improve the spectral efficiency for each user as more information would be able to be transmitted simultaneously, allowing for higher achievable data rates.

REFERENCES

[1] S. Berger, "Spectrum congestion - is it a technical problem?," in *United States National Committee of URSI National Radio Science Meeting*, p. 1, 2014.

[2] D. Jokanovic and M. Josipovic, "RF spectrum congestion: Resolving an interference case," in *IEEE International Conference on Microwaves, Communications, Antennas and Electronics Systems*, pp. 1–4, 2011.

[3] J. R. Krier, J. T. R. Marissa C. Norko, R. J. Baxley, A. D. Lanterman, X. Ma, , and J. R. Barry, "Performance bounds for an OFDM-based joint radar and communications system," in *IEEE Military Communications Conference*, pp. 511–516, 2015.

[4] A. R. Chiriyath and D. W. Bliss, "Joint radar-communications performance bounds:data versus estimation information rates," in *IEEE Military Communications Conference*, pp. 1491–1496, 2015.

[5] A. D. Harper, J. T. Reed, J. L. Odom, and A. D. Lanterman, "Performance of a joint radar-communication system in doubly-selective channels," in *Asilomar Conference on Signals, Systems and Computers*, pp. 1369–1373, 2015.

[6] D. Bliss, "Cooperative radar and communications signaling: The estimation and information theory odd couple," in *IEEE Radar Conference*, pp. 50–55, 2014.

[7] J. R. Guerci, R. M. Guerci, A. Lackpour, and D. Moskowitz, "Joint design and operation of shared spectrum access for radar and communications," in *IEEE Radar Conference*, pp. 761–766, May 2015.

[8] C. Sturm, T. Zwick, and W. Wiesbeck, "An OFDM system concept for joint radar and communications operations," in *IEEE Vehicular Technology Conference*, pp. 1–5, 2009.

[9] D. Garmatyuk, J. Schuerger, K. Kauffman, and S. Spalding, "Wideband OFDM system for radar and communications," in *IEEE Radar Conference*, pp. 1–6, 2009.

[10] R. Cager, D. LaFlame, and L. Parode, "Orbiter Ku-band integrated radar and communications subsystem," *IEEE Transactions on Communications*, vol. 28, no. 11, pp. 1604–1619, 1978.

[11] S. Liu, Z. Huang, and W. Zhang, "A power-efficient radar waveform compatible with communication," in *International Conference on Communications, Circuits and Systems*, vol. 2, pp. 1–4, 2013.

[12] M. R. Bell, N. Devroye, D. E. T. Koduri, and S. R. D. Tuninetti, "Results on spectrum sharing between a radar and a communications system," in *International Conference on Electromagnetics in Advanced Applications*, pp. 826–829, 2014.

[13] A. Turlapaty and Y. Jin, "A joint design of transmit waveforms for radar and communications systems in coexistence," in *IEEE Radar Conference*, pp. 315–319, 2014.

[14] H. Takase and M. Shinriki, "A dual-use radar and communication system with complete complementary codes," in *International Radar Symposium*, pp. 1–4, 2014.

[15] C. Sturm, M. Braun, and W. Wiesbeck, "Deterministic propagation modeling for joint radar and communication systems," in *International Symposium on Electromagnetic Theory*, pp. 942–945, 2010.

[16] J. T. Johnson, C. J. Baker, H. Wang, L. Ye, and C. Zhang, "Assessing the potential for spectrum sharing between communications and radar systems in the L-band portion of the RF spectrum allocated to radar," in *International Conference on Electromagnetics in Advanced Applications*, pp. 331–334, 2014.

[17] A. K. Mishra and M. Inggs, "White space symbiotic radar: A new scheme for coexistence of radio communications and radar," in *IEEE Radar Conference*, pp. 56–60, 2015.

[18] S. Heuel and A. Roessler, "Coexistence of S-band radar and 4G mobile networks," in *International Radar Symposium*, pp. 1–4, 2014.

[19] A. Aubry, A. D. Maio, M. Piezzo, M. M. Naghsh, M. Soltanalian, and P. Stoica, "Cognitive radar waveform design for spectral coexistence in signal-dependent interference," in *IEEE Radar Conference*, pp. 474–478, 2014.

[20] A. Turlapaty and Y. Jin, "A joint design of transmit waveforms for radar and communications systems in coexistence," in *IEEE Radar Conference*, pp. 315–319, 2014.

[21] J. Guerci, *Cognitive Radar: The Knowledge-Aided Fully Adaptive Approach*. Artech House, 2010.

[22] S. Haykin, *Cognitive Dynamic Systems: perception-action cycle, radar, and radio*. Cambridge University Press, 2012.

[23] S. Haykin, "Cognitive radar: A way of the future," *IEEE Signal Processing Magazine*, pp. 30–40, January 2006.

[24] S. Haykin, Y. Xue, and T. N. Davidson, "Optimal waveform design for cognitive radar," in *Asilomar Conference on Signals, Systems, and Computers*, pp. 3–7, October 2008.

[25] N. A. Goodman, P. R. Venkata, and M. A. Neifeld, "Adaptive waveform design and sequential hypothesis testing for target recognition with active sensors," *IEEE Journal of Selected Topics in Signal Processing*, vol. 1, pp. 105–113, June 2007.

[26] U. K. Majumder, M. R. Bell, and M. Rangaswamy, "A novel approach for designing diversity radar waveforms that are orthogonal on both transmit and receive," in *IEEE Radar Conference*, pp. 1–6, 2013.

[27] J. G. Metcalf, C. Sahin, S. D. Blunt, and M. Rangaswamy, "Analysis of symbol-design strategies for intrapulse radar-embedded communications," *IEEE Transactions on Aerospace and Electronic Systems*, vol. 51, pp. 2914–2931, October 2015.

[28] K. Chen, Y. Liu, and W. Zhang, "Study on integrated radar-communication signal of OFDM-LFM based on FRFT," in *IET International Radar Conference*, pp. 1–6, 2015.

[29] G. Saddik, R. Singh, and E. Brown, "Ultra-wideband multifunctional communications/radar system," *IEEE Transactions on Microwave Theory and Techniques*, vol. 55, pp. 1431–1437, July 2007.

[30] M. Roberton and E. Brown, "Integrated radar and communications based on chirped spread-spectrum techniques," in *IEEE MTT-S Digest*, pp. 611–614, 2003.

[31] Z. Zhao and D. Jiang, "A novel integrated radar and communication waveform based on LFM signal," in *International Conference on Electronics Information and Emergency*, pp. 219–223, 2015.

[32] T. S. Rappaport, *Wireless Communications: Principles and Practice*. Prentice Hall, 2002.

[33] D. W. Bliss and S. Govindasamy, *Adaptive Wireless Communications*. Cambridge University Press, 1 ed., 2013.

[34] M. Skolnik, *Radar Handbook*. McGraw Hill, 2008.

[35] M. A. Richards, J. A. Scheer, and W. A. Holm, *Principles of Modern Radar*. SciTech Publising Inc., 2010.

[36] H. T. Hayvaci and B. Tavli, "Spectrum sharing in radar and wireless communications systems: a review," in *International Conference on Electromagnetics in Advanced Applications*, pp. 810–813, 2014.

[37] A. R. Chiriyath, B. Paul, G. M. Jacyna, and D. W. Bliss, "Inner bounds on performance of radar and communications co-existence," *IEEE Transactions on Signal Processing*, vol. 64, pp. 467–474, September 2016.

[38] J. Guerci and R. M. Guerci, "RAST: Radar as a subscriber technology for wireless spectrum cohabitation," in *IEEE Radar Conference*, pp. 1130–1134, 2014.

[39] V. J. Amuso and R. A. Schneible, "Distributed apertures for robustness in radarand communications (DARRC)," in *IEEE Radar Conference*, pp. 111–116, 2015.

[40] C. Shahriar, A. Abdelhadi, and T. C. Clancy, "Overlapped-MIMO radar waveform design for coexistence with communication systems," in *IEEE Wireless Communications and Networking Conference*, pp. 223–228, 2015.

[41] M. Bica, K.-W. Huang, U. Mitra, and V. Koivunen, "Opportunistic radar waveform design in joint radar and cellular communication systems," in *IEEE Global Communications Conference*, pp. 1–7, 2015.

[42] A. Hassanien, M. G. Amin, Y. D. Zhang, and F. Ahmad, "Dual-function radar-communications: Information embedding using sidelobe control and waveform diversity," *IEEE Transactions on Signal Processing*, vol. 64, no. 8, pp. 2168–2181, 2016.

[43] S. S. Bhat, R. M. Narayanan, and M. Rangaswamy, "Bandwidth sharing and scheduling for multimodal radar with communications and tracking," in *IEEE Sensor Array and Multichannel Signal Processing Workshop*, pp. 233–236, 2012.

[44] S. M. Kay, *Fundamentals of Statistical Signal Processing, Volume I: Estimation Theory*. Prentice Hall, 1993.

[45] K. Todros and J. Tabrikian, "General classes of performance lower bounds for parameter estimation - part I: Non-Bayesian bounds for unbiased estimators," *IEEE Transactions on Information Theory*, vol. 56, pp. 5045–5063, October 2010.

[46] D. W. Bliss, K. W. Forsythe, and C. D. Richmond, "MIMO radar: Joint array and waveform optimization," in *Asilomar Conference on Signals, Systems, and computers*, pp. 207–211, November 2007.

[47] D. Meng, W. Xu, and M. Xia, "Understanding the method of interval errors from the information theory perspective," in *IEEE International Conference on Acoustics, Speech and Signal Processing*, pp. 2117–2120, April 2009.

[48] J. M. Cantor, C. D. Richmond, D. W. Bliss, and B. Correll, "Mean-squared-error prediction for Bayesian direction-of-arrival estimation," *IEEE Transactions on Signal Processing*, vol. 61, pp. 4729–4739, August 2013.

[49] C. D. Richmond, "Capon algorithm mean-squared error threshold SNR prediction and probability of resolution," *IEEE Transactions on Signal Processing*, vol. 53, pp. 2748–2764, July 2005.

[50] C. D. Richmond, "Mean-squared error and threshold SNR prediction of maximum-likelihood signal parameter estimation with estimated colored noise covariances," *IEEE Transactions on Signal Processing*, vol. 52, pp. 2146–2164, April 2006.

[51] E. Chaumette, J. Galy, A. Quinlan, and P. Larzabal, "A new Barankin bound approximation for the prediction of the threshold region performance of maximum likelihood estimators," *IEEE Transactions on Signal Processing*, vol. 56, pp. 5319–5333, November 2008.

[52] F. Athley, "Threshold region performance of maximum likelihood direction of arrival estimators," *IEEE Transactions on Signal Processing*, vol. 53, pp. 1359–1373, April 2005.

[53] F. Athley, "Threshold region performance of deterministic maximum likelihood doa estimation of multiple sources," in *Asilomar Conference on Signals, Systems and Computers*, vol. 2, pp. 1283–1287, November 2002.

[54] E. W. Barankin, "Locally best unbiased estimates," *The Annals of Mathematical Statistics*, vol. 20, pp. 447–501, December 1949.

[55] P. Swerling, "Parameter estimation for waveforms in additive Gaussian noise," *Journal of the Society for Industrial and Applied Mathematics*, vol. 7, pp. 152–166, June 1959.

[56] A. Pinkus and J. Tabrikian, "Barankin bound for range and Doppler estimation using orthogonal signal transmission," in *IEEE Conference on Radar*, pp. 94–99, April 2006.

[57] L. Knockaert, "The Barankin bound and threshold behavior in frequency estimation," *IEEE Transactions on Information Theory*, vol. 45, pp. 2398–2401, August 1997.

[58] J. Tabrikian and J. L. Krolik, "Barankin bounds for source localization in an uncertain ocean environment," *IEEE Transactions on Signal Processing*, vol. 47, pp. 2917–2927, November 1999.

[59] M. Morelande and B. Ristic, "Signal-to-noise ratio threshold effect in track before detect," *IET Radar, Sonar & Navigation*, vol. 3, pp. 601–608, April 2009.

[60] A. Zeira and P. M. Schultheiss, "Realizable lower bounds for time delay estimation: Part 2 - threshold phenomena," *IEEE Transactions on Signal Processing*, vol. 42, pp. 1001–1007, May 1994.

[61] R. J. McAulay and L. P. Seidman, "A useful form of the Barankin lower bound and its application to LFM threshold analysis," *IEEE Transactions on Information Theory*, vol. 15, pp. 273–278, March 1969.

[62] J. S. Abel, "A bound on mean-square-estimate error," *IEEE Transactions on Information Theory*, vol. 39, pp. 1675–1680, September 1993.

[63] T. Li, J. Tabrikian, and A. Nehorai, "A Barankin-type bound on direction estimation using acoustic sensor arrays," *IEEE Transactions on Signal Processing*, vol. 59, pp. 431–435, January 2011.

[64] A. Quinlan, E. Chaumette, and P. Larzabal, "A direct method to generate approximations of the Barankin bound," in *IEEE International Conference on Acoustic, Speech, and Signal Processing*, vol. 3, pp. 1520–6149, 2006.

[65] P. Forbter and P. Larzabal, "On lower bounds for deterministic parameter estimation," in *IEEE International Conference on Acoustics, Speech, and Signal Processing*, vol. 2, pp. 1137–1140, May 2002.

[66] K. Todros, R. Winik, and J. Tabrikian, "On the limitations of Barankin type bounds for MLE threshold prediction," *Signal Processing*, vol. 108, p. 622627, March 2015.

[67] K. Todros and J. Tabrikian, "A new lower bound based on weighted Fourier transform of the likelihood ratio function," in *IEEE Sensor Array and Multichannel Signal Processing Workshop*, pp. 428–432, July 2008.

[68] S. G. Zerbo and B. C. Frias, "On a theoretical background for computing reliable approximation of the Barankin bound," *Simposio Argentino de Investigacion Operativa*, vol. 13, pp. 128–142, 2015.

[69] S. K. Chow and P. M. Schultheiss, "Delay estimation using narrowband process," *IEEE Transactions on Acoustics Speech and Signal Processing*, vol. 29, pp. 478–484, June 1981.

[70] R. McAulay and L. P. Seidman, "A useful form of the Barankin lower bound and its application to PPM threshold analysis," *IEEE Transactions on Information Theory*, vol. 15, pp. 273–279, 1969.

[71] M. Morelande and B. Ristic, "Signal-to-noise ratio threshold effect in track before detect," *IET Radar, Sonar & Navigation*, vol. 3, pp. 601–608, April 2009.

[72] R. J. McAulay and E. M. Hofstetter, "Barankin bounds on parameter estimation," *IEEE Transactions on Information Theory*, vol. 7, pp. 669–676, November 1971.

[73] J. Tabrikian and J. L. Krolik, "Barankin bounds for source localization in an uncertain ocean environment," *IEEE Transactions on Signal Processing*, vol. 47, pp. 2917–2927, November 1999.

[74] L. N. Atallah, J.-P. Barbot, and P. Larzabal, "From Chapman-Robbins bound towards Barankin bound in threshold behaviour prediction," *IEEE Electronic Letters*, vol. 40, pp. 279–280, February 2004.

[75] E. Chaumette, J. Galy, A. Quinlan, and P. Larzabal, "A new Barankin bound approximation for the prediction of the threshold region performance of maximum likelihood estimators," *IEEE Transactions on Signal Processing*, vol. 56, pp. 5319–5333, November 2008.

[76] A. Jung, Z. Ben-Haim, F. Hlawatsch, and Y. C. Eldar, "Unbiased estimation of a sparse vector in white Gaussian noise," *IEEE Transactions on Information Theory*, vol. 57, pp. 7856–7876, 2011.

[77] L. Knockaert, "The Barankin bound and threshold behavior in frequency estimation," *IEEE Transactions on Information Theory*, vol. 45, pp. 2398–2401, August 1997.

[78] A. Pinkus and J. Tabrikian, "Barankin bound for range and Doppler estimation using orthogonal signal transmission," in *IEEE Conference on Radar*, pp. 94–99, April 2006.

[79] T. Li, J. Tabrikian, and A. Nehorai, "A Barankin-type bound on direction estimation using acoustic sensor arrays," *IEEE Transactions on Signal Processing*, vol. 59, pp. 431–435, January 2011.

[80] J. Kota, N. Kovvali, D. W. Bliss, and A. Papandreou-Suppappola, "Waveform selection for range and Doppler estimation via Barankin bound signal-to-noise ratio threshold," in *IEEE International Conference on Acoustic, Speech, and Signal Processing*, pp. 4658–4662, May 2014.

[81] H. L. V. Trees, *Detection, Estimation, and Modulation Theory, Radar-Sonar Signal Processing and Gaussian Signals in Noise*, vol. III. Wiley-Interscience, October 2001.

[82] E. L. Lehmann, "A general concept of unbiasedness," *The Annals of Mathematical Statistics*, vol. 22, no. 4, pp. 587–592, 1951.

[83] K. Todros and J. Tabrikian, "A new lower bound on the mean-square error of unbiased estimators," in *IEEE International Conference on Acoustics, Speech and Signal Processing*, pp. 3913–3916, March 2008.

[84] J. Albuquerque, "The Barankin bound: A geometric interpretation," *IEEE Transactions on Information Theory*, vol. 19, pp. 559–561, July 1973.

[85] E. Parzen, "Statistical inference on time series by Hilbert space methods, part 1," Tech. Rep. 23, Stanford University, 1959.

[86] S. Schmutzhard, A. Jung, and F. Hlawatsch, "Minimum variance estimation for the sparse signal in noise model," in *IEEE International Symposium on Information Theory*, pp. 124–128, July 2011.

[87] D. L. Duttweiler and T. Kailath, "RKHS approach to detection and estimation problems-part V: Parameter estimation," *IEEE Transactions on Information Theory*, vol. 19, pp. 29–37, January 1973.

[88] R. J. McAulay and E. M. Hofstetter, "Barankin bounds on parameter estimation," *IEEE Transactions on Information Theory*, vol. 7, pp. 669–676, November 1971.

[89] L. N. Atallah, J.-P. Barbot, and P. Larzabal, "From Chapman-Robbins bound towards Barankin bound in threshold behaviour prediction," *IEEE Electronic Letters*, vol. 40, pp. 279–280, February 2004.

[90] B. Ristic, S. Arulampalam, and N. Gordon, *Beyond the Kalman Filter - Particle Filters for Tracking Purposes*. Artech House, 2004.

[91] M. S. Arulampalam, S. Maskell, N. Gordon, and T. Clapp, "A tutorial on particle filters for online nonlinear/non-Gaussian Bayesian tracking," *IEEE Transactions on Signal Processing*, vol. 50, pp. 174–188, February 2002.

[92] H. L. V. Trees, *Bayesian Bounds for Parameter Estimation and Nonlinear Filtering/Tracking*. Wiley-IEEE Press, August 2007.

[93] G. Strang, *Linear Algebra and Its Applications*. Brooks Cole, 4 ed., 2006.

[94] L. Trefethen and D. B. III, *Numerical Linear Algebra*. Society for Industrial and Applied Mathematics, 1 ed., 1997.

[95] A. Papandreou-Suppappola, *Applications in Time-Frequency Signal Processing*. CRC Press, 2002.

[96] J. J. Zhang, Q. Ding, S. Kay, A. Papandreou-Suppappola, and M. Rangaswamy, "Agile multi-modal tracking with dependent measurements," in *Asilomar Conference on Signals, Systems, and Computers*, pp. 1653–1657, November 2010.

[97] S. P. Sira, Y. Li, A. Papandreou-Suppappola, D. Morrell, D. Cochran, and M. Rangaswamy, "Waveform-agile sensing and processing," *IEEE Signal Processing Magazine*, vol. 26, pp. 53–64, January 2009.

[98] S. P. Sira, A. Papandreou-Suppappola, and D. Morrell, "Dynamic configuration of time-varying waveforms for agile sensing and tracking in clutter," *IEEE Transactions on Signal Processing*, vol. 55, pp. 3207–3217, July 2007.

[99] H. Shen, S. Machineni, C. Gupta, and A. Papandreou-Suppappola, "Time-varying multichirp rate modulation for multiple access systems," *IEEE Signal Processing Letters*, vol. 11, pp. 497–500, May 2004.

[100] H. Shen and A. Papandreou-Suppappola, "Diversity and channel estimation using time-varying signals and time-frequency techniques," *IEEE Transactions on Signal Processing*, vol. 54, pp. 3400–3413, September 2006.

[101] S. Machineni, H. Shen, and A. Papandreou-Suppappola, "Multi-user schemes using nonlinear time-varying modulation," in *IEEE International Conference on Acoustics Speech and Signal Processing*, pp. 941–944, 2004.

[102] D. Bertsimas and J. Tsitsiklis, "Simulated annealing," *Statistical Science*, vol. 8, no. 1, pp. 10–15, 1993.

[103] S. Boyd and L. Vandenberghe, *Convex Optimization*. Cambridge University Press, 2004.